Pharmacological and Electroceutical Modulations of Local Field Potentials in Parkinson's Disease

by
Musa Ozturk

A dissertation submitted to the
Biomedical Engineering Department of Cullen College of Engineering
in partial fulfillment of the requirements for the degree of

Doctor of Philosophy
in Biomedical Engineering

Chair of Committee: Nuri F. Ince, PhD

Committee Member: Ashwin Viswanathan, MD

Committee Member: Joseph T. Francis, PhD

Committee Member: Rose T. Faghih, PhD

Committee Member: Yingchun Zhang, PhD

University of Houston
May 2020

Dedicated to the ONE,

to whom all belong and to whom all return

Acknowledgments

I am sincerely grateful to all who have contributed to completion of my dissertation, which was an immensely cultivating experience. I would like to acknowledge my graduate advisor Dr Nuri Ince, for his guidance, feedback and support throughout this journey, including late night stays and lab dinners. I am grateful to Dr Ashwin Viswanathan not only for his clinical contributions to the projects but his continuous kindness throughout our collaboration. I would also like to thank the rest of my dissertation committee, Drs Rose Faghih, Joseph Francis and Yingchun Zhang, for their valuable time and timely feedback.

I have had many lab-mates and colleagues during graduate school, and I am thankful to all for their personal and professional help. Additionally, I have had a chance to work with many institutions in the Texas Medical Center. I am truly grateful to all the staff, nurses and the trainees who have indirectly helped with my dissertation without any expectations and sincerely appreciate the irreplaceable contribution from participating patients.

Most importantly, I would not be able to be where I am without continuous support of my beloved family members and friends. I will appreciate their unconditional love and sacrifices forever.

The financial support during my graduate studies was provided by National Institutes of Health (NIH), Abbott, Medtronic, Biomedical Engineering Department of University of Houston and The National Scientific Research Council of Turkey (TUBITAK).

Abstract

Parkinson's disease (PD) is a complex neurodegenerative disorder with motor and cognitive symptoms caused by loss of dopaminergic neurons in the basal ganglia. There is no cure but treatment options such as dopaminergic medication and deep brain stimulation (DBS) can help relieve the symptoms. Despite decades of clinical use, the underlying electro-pathophysiology of these treatments are still not clear.

In this dissertation, we have investigated the modulations of local field potentials (LFPs) recorded from the subthalamic nucleus (STN) of patients with PD. To do so reliably, we first presented an online processing pipeline that helps refine the targeting of STN intraoperatively. We benchmarked this system against the gold-standard clinical practice involving single unit activity (SUA) with a randomized and double blinded pilot study. In patients referred for bilateral DBS, we implanted one hemisphere with SUA guidance and the other with LFP randomly. Then, we compared the clinical improvement assessed by a blinded neurologist. Our results suggested that our LFP-based targeting approach performed equally or better at localizing the STN and can be utilized as an additional feedback modality in the operating room, as it does not require any additional hardware or surgical procedures.

Next, with a well-localized STN, we studied the pharmacological modulations of LFPs with dopaminergic medication over unique 24-hour-long recordings from externalized DBS leads. The reasoning behind such long

recordings was that the medications have long wash-in and wash-out times and it is important to replicate observations. Thus, each of our nine patients had a chance to take their medications three times during the recordings. We not only observed power changes in the LFP spectra in the beta (12-30 Hz) and high-frequency (200-400 Hz) bands, as reported previously, but also reported strong non-linear cross-frequency coupling between these bands for the first time in the ON state. Prior to this observation, the coupling in the STN was considered to be purely pathological, as it was consistently reported in the unmedicated state only. However, our observations suggest that the coupling can have impeding or enhancing effects on the normal processes depending on the coupled frequencies.

Finally, we investigated the electroceutical modulations of the LFPs with therapeutic and non-therapeutic DBS. Due to the fast-acting nature of stimulation therapy, we performed the recordings intraoperatively in eight patients. Interestingly, we observed -for the first time- high-frequency (200-400 Hz) activity in the STN only during therapeutic stimulation, similar to medicated patients and healthy non-human primates. The consistent appearance of this activity in healthy and treated basal ganglia with medication and DBS prompts that there may be LFP oscillations specific to the healthy and diseased states, and that these oscillations can further our understanding of the pathophysiology of PD and can be used for the development of novel tools for diagnostic purposes such as target localization, and for treatment purposes such as selection of optimal stimulus parameters and adaptive/closed-loop DBS.

Table of Contents

List of Tables

List of Figures

List of Abbreviations

BG	Basal ganglia
CFC	Cross-frequency coupling
CT	Computed tomography
DBS	Deep brain stimulation
DFM	Depth-frequency map
ECA	Evoked compound activity
EEG	Electroencephalogram
EMG	Electromyogram
EMU	Epilepsy monitoring unit
GABA	Gamma-amino butyric acid
GPe	Globus pallidus externa
GPi	Globus pallidus interna
HFO	High frequency oscillations
HFS	High frequency stimulation
IPG	Implantable pulse generator
LDA	Linear discriminant analysis
L-DOPA	Levodopa
LFP	Local field potential
LID	Levodopa induced dyskinesia
LMS	Least mean square
MDS	Movement Disorders Society
MER	Microelectrode recordings
MPTP	1-methyl-4-phenyl-1,2,3,6-tetrahydropyridine
MRI	Magnetic resonance imaging
PAC	Phase-amplitude coupling
PD	Parkinson’s disease
PSD	Power spectral density
SNc	Substantia nigra pars compacta
SNr	Substantia nigra pars reticulata
SNR	Signal-to-noise ratio
STN	Subthalamic nucleus
SUA	Single unit activity
TF	Time-frequency
UPDRS	Unified Parkinson’s Disease Rating Scale
VIM	Ventralis intermedius nucleus
VTA	Volume of tissue activated

1 Background and Aims

The brain is one of the most complex and mysterious systems known to man. Since it is similar to a black box (i.e., its mechanisms of action not visible to the naked eye, as it would be in the case of heart for instance), understanding of its functions and the diseases originating from its malfunctioning has always been challenging, especially of the structures in the deeper regions such as basal ganglia (Eisinger et al., 2019). However, it is not impossible to infer clues and learn more about these structures. One such opportunity arises from the electrophysiological recordings during surgeries involving open craniotomy for the treatment of neurological disorders. Since the communication in the brain is by means of electrochemical processes (Buzsáki, 2006), electrophysiological signals recorded under controlled conditions present a chance to wiretap and discover the underlying physiological and pathological neural networks and mechanisms. This knowledge not only furthers neuroscience but can also be utilized to develop effective diagnostic tools and novel treatments.

Parkinson's disease (PD) is a well-known neurodegenerative disorder that debilitates its patients with motor and cognitive symptoms (Jankovic, 2008). Unfortunately, there is no cure for PD as of today but, there are treatment options such as medication (Strauss et al., 2014; Jenner, 2013) and electrical stimulation (Benabid et al., 2009; Groiss et al., 2009; Collins et al., 2010). The latter option, referred to as deep brain stimulation (DBS), involves a surgery to implant the stimulus-delivering electrode. This electrode is placed at a target location such as subthalamic nucleus (STN), which is a key basal ganglia

structure in the neural circuitry inducing PD and one of the most commonly targeted structures for stimulation in PD patients (Gross et al., 2006; Benabid et al., 2009). Previous work on the modulations of electrophysiological activity from STN have helped researchers identify neuro-biomarkers for finding the optimal stimulation regions and enhancing DBS therapy through the development of closed-loop systems (Little et al., 2013; Priori et al., 2013; Johnson et al., 2016).

This dissertation focuses on the electro-pathophysiology of STN in PD patients and investigates the modulations of local field potentials (LFP), which originate from the collective activity of populations of neurons (Priori et al., 2004; Gross et al., 2006; Buzsáki et al., 2012). The aim is to characterize the changes in the nature of LFPs during pharmacological and electroceutical intervention, in order to better understand the disease and the mechanisms of its therapies.

The first chapter of this work provides introductory information on PD pathophysiology and electrophysiological modulations reported in patients with PD during treatment. The second chapter presents an online processing system to robustly refine the targeting of STN for the implantation of DBS lead, as the observations for STN-LFP modulations would be invalid with sub-optimal targeting. The third chapter investigates the modulations in the LFP oscillations with Parkinsonian medication through unique 24-hour post-operative monitoring. The fourth chapter characterizes the changes in LFP under different therapeutic and non-therapeutic stimulation conditions through intra-operative recordings. The fifth chapter is a succinct summary of results and their implications for future work.

1.1 Pathophysiology of Parkinson's Disease

PD is a complex neurodegenerative movement disorder with a progressive prognosis (Fahn, 2003; Jankovic, 2008). PD was first described by Dr. James Parkinson in 1817 as "a shaking palsy" (Parkinson, 2002) and then Jean-Martin Charcot refined his description and credited the disease to him almost half a century later (Goetz, 2011). Today, PD is one of the most common neurodegenerative disorders, affecting ten million people worldwide. In the US, nearly one million patients live with PD and approximately 60000 cases are diagnosed each year. Although PD can develop at any age, it is often associated with the elderly since more than 95% of the patients diagnosed are over 50 years old (Parkinson's Foundation, Understanding Parkinson's, Statistics, 2020).

PD encompasses a wide spectrum of motor and non-motor features (Thenganatt and Jankovic, 2014). The four cardinal motor features are resting tremor, rigidity, bradykinesia (or akinesia), and postural instability while the non-motor symptoms include autonomic dysfunction, cognitive and neurobehavioral impairment, sensory abnormalities and sleep disorders (Jankovic, 2008). The clinical criteria for PD determined by the United Kingdom Parkinson Disease Society Brain Bank are the presence of bradykinesia and at least one of the other cardinal symptoms in addition to three supplementary signs (Jankovic, 2008; Thenganatt and Jankovic, 2014). Only the motor symptoms are detailed below due to their relevance to this dissertation.

Bradykinesia/akinesia is the most characteristic clinical manifestation of PD and it refers to loss of amplitude or speed in planning, initiation, and execution of movement (Jankovic, 2008; Rodriguez-Oroz et al., 2009; Massano and Bhatia, 2012). Examples include the long reaction time, slower and smaller handwriting, drooling, loss of facial expression (hypomimia) and decreased blinking (Fahn, 2003; Jankovic, 2008). It is vital to distinguish true bradykinesia from simple slowness, which is frequently seen in elderly patients with loss of muscle power in order to prevent misdiagnosis. Therefore, bradykinesia is assessed clinically by asking the patient to perform repetitive and alternating movements as quickly and widely as possible, to observe not only the slowness but also the decrease in the amplitude of their movement (Jankovic, 2008; Massano and Bhatia, 2012). As in other PD symptoms, bradykinesia fluctuates with emotional state and a bradykinetic patient can move faster with excitement or fear (kinesia paradoxia). Based on this phenomenon, it was proposed that PD patients with bradykinesia have intact motor programs but have difficulty accessing them without an external trigger such as a loud noise or visual stimulus (Jankovic, 2008).

The rest tremor (also called parkinsonian tremor) is a rhythmic involuntary movement that occurs when the affected body part is relaxed (Fahn, 2003; Massano and Bhatia, 2012). The tremor increases or can be triggered by stress and mental tasks such as arithmetic calculation (Fahn, 2003; Rodriguez-Oroz et al., 2009; Massano and Bhatia, 2012) and it stops with the voluntary movement and sleep (Jankovic, 2008; Massano and Bhatia, 2012). The most

distinguishing type of tremor in PD is referred to as “pill-rolling” and occurs between the thumb and index fingers (Jankovic, 2008; Rodriguez-Oroz et al., 2009). The tremors are typically at 4-6 Hz, unlike the typical frequency seen in other movement disorders such as essential tremor with 8-12 Hz (Jankovic, 2008; Rodriguez-Oroz et al., 2009; Schneider and Deuschl, 2015). Rest tremor in PD can also involve the lips, chin, tongue, jaw and lower limbs but unlike essential tremor, rarely involves the neck, head or voice (Jankovic, 2008; Massano and Bhatia, 2012). PD patients might also have resting and action tremor together or postural and kinetic tremor with no resting tremor at all (Fahn, 2003; Camara et al., 2015; Schneider and Deuschl, 2015).

Rigidity in PD refers to increased muscle tone and resistance during examination by passive movements and it is constant throughout the range of movement (Jankovic, 2008; Rodriguez-Oroz et al., 2009; Massano and Bhatia, 2012). Both flexor and extensor muscles are involved, and resistance depends on the velocity of the movement as the maximum resistance is experienced when the passive movements are performed slowly (Rodriguez-Oroz et al., 2009). Moreover, the voluntary movement of contralateral body parts usually amplify rigidity and can be useful when detecting mild cases (Jankovic, 2008; Rodriguez-Oroz et al., 2009; Massano and Bhatia, 2012). When patients have both resting tremor and muscular rigidity, the classical “cogwheel” phenomenon, which is characterized by jerky and ratchet-like movements of joints, can be observed (Jankovic, 2008; Massano and Bhatia, 2012).

Postural instability is characterized by a stooped posture, shuffling gait and decreased arm swing (Fahn, 2003; Jankovic, 2008; Massano and Bhatia, 2012). Postural instability, due to the loss of postural reflexes, together with freezing of gait can have serious impact on quality of life and safety of the patients since they are major causes of falls and injuries (Jankovic, 2008; Spildooren et al., 2010; Massano and Bhatia, 2012). Dual- or multi-tasking is substantially compromised, as walking and turning become difficult or even impossible when the patients are cognitively engaged (Spildooren et al., 2010). Clinically, the posture and gait should be assessed both in an open corridor and while passing through narrow doorways since the freezing often happens in narrow or crowded spaces (Massano and Bhatia, 2012). For the assessment of postural reflexes and stability, the “pull test” is performed, in which the patient is pulled backward/forward from the shoulders to disrupt his/her balance. The absence of postural response or taking more than two steps to regain balance is considered abnormal (Jankovic, 2008; Massano and Bhatia, 2012). Manifestation of instability due to loss of postural reflexes and gait impairment is observed in the late stages of PD and generally occurs after the progression of other clinical features (Jankovic, 2008).

1.2 Basal Ganglia Circuits Concerning Parkinson’s Disease

Manifestations of PD symptoms involve various structures in the basal ganglia (BG), which refers to a group of highly organized subcortical nuclei that are linked to various functions like movement control, attention and emotion

(Wichmann and Delong, 1996; Obeso et al., 2008). The major anatomical BG structures illustrated in Figure 1.1A are the striatum (caudate nucleus and putamen), globus pallidus (interna and externa), substantia nigra (pars compacta and pars reticulata) and the STN (Nambu, 2011). The striatum and the STN serve as input structures of the BG as they receive topographically organized input from the cerebral cortex, whereas the globus pallidus interna (GPi) and the substantia nigra pars reticulata (SNr) are the output structures as they relay the BG output to the thalamus and brainstem (DeLong and Wichmann, 2007). Together with the cortex, thalamus and brainstem, BG forms three functional loops: motor circuit, associative circuit and limbic circuit (Obeso et al., 2008). In each circuit, information originating from different somatotopic regions of the cortex is processed through different components of BG (Figure 1.1B). Since movement disorders represent a major clinical expression of the faulty BG, the motor circuit is the most commonly studied cortico-basal ganglia-thalamo-cortical loop (DeLong and Wichmann, 2007; Obeso et al., 2008).

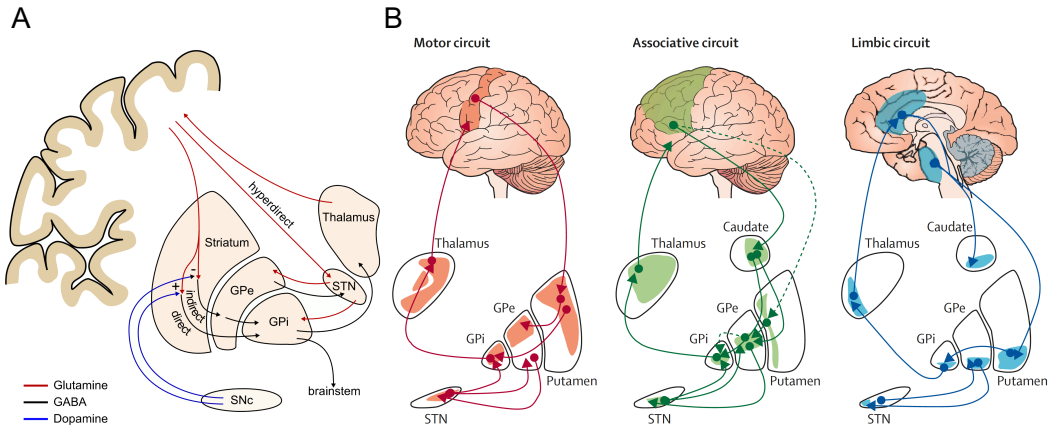

Figure 1.1: *Basal ganglia structures, pathways to (A) the cortex and (B) functional circuits. A is adopted from (Brittain and Brown, 2014) and B is adopted from (Rodriguez-Oroz et al., 2009) and (Obeso et al., 2008)*

The motor circuit functions through three pathways involving various excitatory and inhibitory projections: direct pathway, indirect pathway and hyperdirect pathway (Figure 1.1A) (DeLong and Wichmann, 2007; Obeso et al., 2008; Nambu, 2011). In the direct pathway, striatum receives excitatory inputs (glutaminergic) from cortex and secretes inhibitory neurotransmitter gamma-amino butyric acid (GABAergic) into GPi/SNr directly. Since GPi/SNr has inhibitory projections to thalamus, its inhibition increases firing rate of motor thalamus and brainstem. On the other hand, in the indirect pathway, striatal neurons project to GPi/SNr through globus pallidus externa (GPe) and STN respectively. Indirect pathway causes inhibition on thalamus and thus, a decreased motor activity. Finally, the hyperdirect pathway contains a direct cortical input to the STN which projects to the GPi/SNr. This pathway enables faster cortical excitation on GPi/SNr than the direct and indirect pathways (DeLong and Wichmann, 2007; Obeso et al., 2008; Nambu, 2011).

Differential effect of dopamine on striatum balances the activity between direct and indirect pathways (DeLong and Wichmann, 2007). Dopamine released from substantia nigra pars compacta (SNc) increases activity along the direct pathway (by acting on D1 receptors in striatal neurons) and reduces activity along the indirect pathway (by acting on D2 receptors). In this case, a net reduction in GPi/SNr activity occurs. Conversely, a decrease in the striatal dopamine release increases the inhibitory GPi/SNr output activity (Figure 1.1A).

PD symptoms are manifested when the BG loops do not function properly due to dopamine deficiency caused by the neuron loss in the SNc

(Hornykiewicz, 2006). The death of dopamine-producing neurons causes a decrease in the overall dopamine secretion into the striatum, which reduces the activation of direct, and the inhibition of indirect pathway. Consequently, the dopamine depletion increases the STN-mediated activation and decreases GPe-mediated inhibition of GPi/SNr. The increase in the inhibitory GPi/SNr output, in turn, decreases the activity in the thalamo-cortical neurons resulting in decreased motor activity (DeLong and Wichmann, 2007).

STN, as a vital component of these circuits, plays a critical role in performing motor functions, cognition and emotion (Temel et al., 2005; Benarroch, 2008; Ballanger et al., 2009), and it is one of the most commonly targeted structures for DBS in PD patients (Gross et al., 2006; Benabid et al., 2009). Similar to functional BG loops, STN is somatotopically divided into three different territories: motor, associative and limbic territory (Rodriguez-Oroz et al., 2001; Benarroch, 2008; Obeso et al., 2008). A sizeable portion of the STN in the dorsolateral direction corresponds to the motor territory (Obeso et al., 2008; Nambu, 2011). This territory plays a crucial role in the motor control through direct interaction with cortex, GPe and GPi (Benarroch, 2008) and is considered as the optimal region for DBS (Rodriguez-Oroz et al., 2001; Abosch et al., 2002; Starr et al., 2003; Theodosopoulos et al., 2003; Horn et al., 2017).

1.3 Treatment Options for Parkinson's Disease

The dopamine depletion in the BG due to the death of dopaminergic neurons is considered the pathological hallmark of PD (Hornykiewicz, 2006).

Consequently, the initial treatment of PD involves pharmacological manipulation of striatal dopamine levels through medications such as levodopa (L-DOPA) (Jankovic, 2001; Goetz et al., 2005). L-DOPA is the natural precursor to dopamine and was shown to provide a dramatic improvement of anti-kinetic symptoms in human subjects as early as the 1960s (Goetz, 2011). Though L-DOPA is one of the most effective treatment options for PD symptoms, in the long term (after 3-5 years), the majority of the patients develop motor complications, including fluctuations in the efficacy and dyskinesias (involuntary movements) (Jankovic, 2001).

Depending on the disease duration and patient-specific considerations, surgical and/or supportive therapies might be required for the treatment of PD (Goetz et al., 2005; deSouza et al., 2013). The surgical intervention for movement disorders dates back to early 1900s, even before the L-DOPA treatment and focused on the management of hyperkinetic symptoms (e.g., tremor) through ablation of brain structures such as thalamus (thalamotomy) and pallidum (pallidotomy) (Goetz, 2011). The surgical applications including stereotactic lesioning of BG structures gained popularity, but the success of these approaches were limited, partly because of inaccurate and imprecise targeting and, irreversible impairment in swallowing, speech and cognition caused by the bilateral lesions (Hickey and Stacy, 2016). Although the discovery of therapeutic effects of L-DOPA halted the progress in the surgical intervention, the development of drug-induced motor and cognitive complications such as

dyskinesias and hallucinations revived the interest in the surgical procedures (Hickey and Stacy, 2016).

The serendipitous discovery of therapeutic effects of high frequency stimulation (HFS) by Dr. Benabid and his colleagues in 1987 started a paradigm shift in the treatment of PD and many other neurological disorders. Unlike the ablative techniques, HFS of the ventral-intermedial thalamus (VIM, ventralis intermedius nucleus) was a reversible and adjustable approach for controlling tremor (Benabid et al., 1987). Soon after, a significant reduction in cardinal symptoms of PD (i.e., bradykinesia, rigidity, tremor) was reported in the first PD patients who received HFS in STN (Benabid et al., 1994; Limousin et al., 1995). The therapeutic effect of STN-DBS decreased the L-DOPA doses by an average of 60%, which in turn reduced the medication-induced motor fluctuations and dyskinesias (Limousin et al., 1998). Since then, DBS became an established therapy and rapidly replaced the ablative procedures due to its reversible and programmable nature (Benabid et al., 2009; Mahlknecht et al., 2015; Hickey and Stacy, 2016). STN and GPi are the two common targets for surgical treatment of PD, with STN being more effective in improving both resting tremor and action tremors (Odekerken et al., 2013; Williams et al., 2014; Wong et al., 2019). The STN as the most commonly used target (Benabid et al., 2009) will be the scope of the work presented throughout this dissertation.

Current DBS systems used for movement disorders are referred as “open-loop”, which are manually programmed and exert their effects regardless of the patient’s disease state (Sun and Morrell, 2014; Parastarfeizabadi and Kouzani,

2017; Bouthour et al., 2019). These systems not only have limited efficacy and adverse effects due to under- or over-stimulation, they also require regular clinical visits for tedious iterative adjustments of the stimulation parameters (Bouthour et al., 2019; Hell et al., 2019). By contrast, “closed-loop” DBS systems adapt the stimulation parameters (such as amplitude or frequency) with respect to a suitable biomarker, representing the clinical features of the disease, that can be sensed by the implanted electrodes (Sun and Morrell, 2014; Parastarfeizabadi and Kouzani, 2017; Bouthour et al., 2019; Hell et al., 2019). Although closed-loop stimulators have been used for epilepsy since early 2000s (Osorio et al., 2001), the lack of robust biomarkers for PD (unlike distinct waveform of neural activity during seizures) have hindered development of closed-loop DBS (Parastarfeizabadi and Kouzani, 2017). Therefore, the identification of neuro-biomarkers for PD, describing the motor and cognitive manifestations of the disease, is crucial for robust and reliable operation of chronic closed-loop DBS (Bouthour et al., 2019; Hoang and Turner, 2019).

1.4 Targeting Modalities for DBS Lead Implantation

Accurate localization of the target structure is a vital requirement for achieving optimal outcomes with DBS (Zonenshayn et al., 2000; Sterio et al., 2002; Amirnovin et al., 2006; Gross et al., 2006; Campbell et al., 2019). Otherwise, the stimulation can cause adverse effects arising from unintended activation of regions surrounding the target structures such as STN (Krack et al., 2001; Okun et al., 2003; Deuschl et al., 2006; Guehl et al., 2006; Wojtecki

et al., 2007; Benabid et al., 2009; Groiss et al., 2009; Richardson et al., 2009; Zhang et al., 2016), and/or result in inadequate clinical improvement postoperatively (Okun et al., 2005). Thus, several anatomical and electrophysiological targeting techniques are utilized for the accurate localization of STN.

Anatomical targeting can be divided into two groups: direct and indirect approach. Direct approach uses radiological images of the target in a stereotactic frame to determine the entry point and trajectory to reach the target (Machado et al., 2006; Patel et al., 2008). While advanced magnetic resonance imaging (MRI) technology allows direct visualization of some BG structures (Strauss et al., 2014), potential problems during fusion of MRI and computed tomography (CT) might lead to misinterpretation of the anatomy and result in sub-optimal positioning (Benabid, 2003; Machado et al., 2006). On the other hand, the indirect targeting approach normalizes the stereotactic brain atlases based on the coordinates of major landmarks such as anterior and posterior commissures (AC-PC line) to estimate the location of the target (Machado et al., 2006; Patel et al., 2008). However, the anatomical variations among individuals and the use of average values of the coordinates by clinical teams are major limitations of this technique (Machado et al., 2006; Patel et al., 2008). While MRI-guided asleep DBS is being performed by some centers (Aziz and Hariz, 2017; Brodsky et al., 2017; Chen et al., 2018; Ho et al., 2018; Wang et al., 2019; Liu et al., 2020), intraoperative electrophysiology remains to be an important technique for localizing the STN, to validate or to further improve the

targeting accuracy (Zonenshayn et al., 2000; Sterio et al., 2002; Amirnovin et al., 2006; Gross et al., 2006; Abosch et al., 2013; Campbell et al., 2019).

Electrophysiological targeting involves intraoperative awake recordings from microelectrodes (MER) and clinical testing with acute stimulation for validation of the target structure (Abosch et al., 2013; Strauss et al., 2014). A survey study involving 143 DBS centers worldwide reported that 83% of these centers use single unit activity (SUA) recordings for targeting (Abosch et al., 2013). Typically, up to five microelectrodes are advanced towards the target structure to obtain a 3-dimensional perspective (Gross et al., 2006; Benabid et al., 2009; Abosch et al., 2013). SUA is used to identify cells with firing characteristics consistent with STN neurons (Figure 1.2) and response characteristics confirming the motor sub-territory of the STN based on a variety of visual and auditory cues (Hutchison et al., 1998; Magnin et al., 2001; Rodriguez-Oroz et al., 2001; Abosch et al., 2002; Benazzouz et al., 2002). Yet, the interpretation of the complex waveforms can be subjective and heavily experience-based (Benazzouz et al., 2002; Benabid et al., 2009; Marceglia et al., 2010; Abosch et al., 2013). Aside from difficulties in

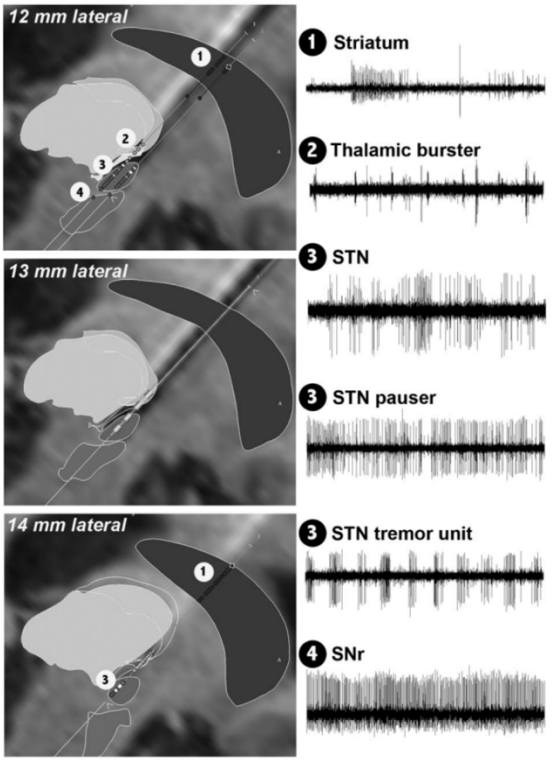

Figure 1.2: *Sample firing characteristics observed during MER mapping en route to STN. Adopted from (Gross et al., 2006)*

interpreting the data and small number of neurons sampled by 1-5 microelectrodes, challenges in interface stability (e.g., necessity of turning lights or other devices off in the operating room) and high bandwidth/sampling frequency requirements may complicate the collection and real-time analysis of SUA (Novak et al., 2011; Rouse et al., 2011; Thompson et al., 2014).

Despite being a useful supplementary tool in determining side effects and therapeutic window, intraoperative acute DBS is also utilized for targeting (without MER) by a small number of centers around the world (Abosch et al., 2013). However, intraoperative factors such as micro-lesion effect, which might suppress the symptoms and prevent the assessment of clinical improvement, as well as the relatively poor spatial resolution of the macroelectrode (DBS lead) are major limitations against the sole use of this technique for an accurate intraoperative targeting (Gross et al., 2006; Wang et al., 2014).

Local field potentials (LFP) representing the aggregated synaptic activity of a population of neurons (Priori et al., 2004; Gross et al., 2006; Buzsáki et al., 2012) can be obtained from the shaft of the same microelectrode used for SUA recordings. Although the use of microelectrode LFPs for the targeting of DBS implantation is currently scarce (Abosch et al., 2013), there is a growing interest (Chen et al., 2006; Telkes et al., 2016; Kolb et al., 2017). Moreover, structural integrity and relatively low impedance of the ring electrode on the shaft (compared to the fragile, high impedance tip used for SUA) can address the shortcomings of the aforementioned techniques and bring the LFPs to the operating room for a more robust and reliable clinical targeting experience.

1.5 Electrophysiological Extracellular Recordings

1.5.1 Single Unit Activity

A fundamental understanding of the origin of neural signals as well as of the effect of measurement conditions on their waveforms is necessary for the interpretation of the electrophysiological recordings. Neuronal transmembrane currents are the basis of the extracellular fields measured from the brain, and the relative position and geometry of the electrode with respect to the neuronal interface determines the recorded waveform. The unit of neural excitation is the action potential propagating along the axon and/or dendrites by the exchange of Na+ and K+ ions between intra and extracellular matrices (Plonsey and Barr, 2007). The movement of ions generates a current loop, in which there is an inward current flow at the action potential site (sink), that travels along the cell core and exits at various places (sources) to return to the sink (Humphrey and Schmidt, 1990). When an electrode is close enough to this loop (100-200 μm) and has adequate impedance (~1 MOhm), as in the case of microelectrode recordings, the single unit discharging activity can be captured (Moffitt and McIntyre, 2005; Cogan, 2008).

Motor symptoms associated with movement disorders such as PD are ascribed to the changes in neural activity that can be observed at the single-unit level. In addition to the firing rate, functional and pathological brain processes are mediated by firing patterns as well (Terman et al., 2002; Wichmann and DeLong, 2006; Kaku et al., 2020). Pathological increases in single-cell activity in the thalamus and basal ganglia (Bergman et al., 1994, 1998; Hua et al., 1998;

Wichmann et al., 1999; Levy et al., 2002) may lead to inferior information processing (Hammond et al., 2007) and motor impairment in movement disorders (Bergman et al., 1998; Wichmann et al., 1999). Explicitly, increased tonic and phasic activity in the basal ganglia promotes the inhibition of thalamo-cortical neurons and leads to akinesia and rigidity in PD (Bergman et al., 1994, 1998). Similarly, cell bursting activity was correlated with EMG measurements during periods of tremor PD patients, and thus, may be involved in pathogenesis of tremor (Lenz et al., 1988; Hua et al., 1998). Consequently, single unit activity (SUA) have been used as a gold standard electrophysiological mapping technique for the clinical targeting of various basal ganglia structures, including STN (Benabid et al., 2009; Przybyszewski et al., 2016; Valsky et al., 2017).

Studies investigating the somatotopic organization of the STN through single-cell recordings have shown that among various spiking profiles (Figure 1.3), dorsal bursting and ventral tonic (regular) firings are associated with the symptoms of PD (Sharott et al., 2014; Kaku et al., 2020). Non-human primate research also shows that the firing rate and pattern changes in STN neurons can be indicative of healthy, PD or treated state (Bergman et al., 1994; Soares et al., 2004; Gilmour et al., 2011). Similarly, single-unit recordings have been shown to modulate with electrical stimulation and study of these changes have helped to elucidate changes in the network activity generated by DBS, which consequently improved our understanding of the mechanisms of action of this therapy (Benazzouz et al., 2000; Anderson et al., 2003; Hashimoto et al., 2003; McIntyre et al., 2004a; Guo et al., 2008; Johnson et al., 2008). Despite high-

fidelity and widespread use in clinical targeting, shortcomings (Figure 1.4) such as the short- (Rouse et al., 2011) and long-term stability issues (Williams et al., 1999) and lack of representation of network-level activity from few neurons (McIntyre and Grill, 2001; McIntyre et al., 2004b) might hamper use of SUA for novel treatments such as closed-loop DBS.

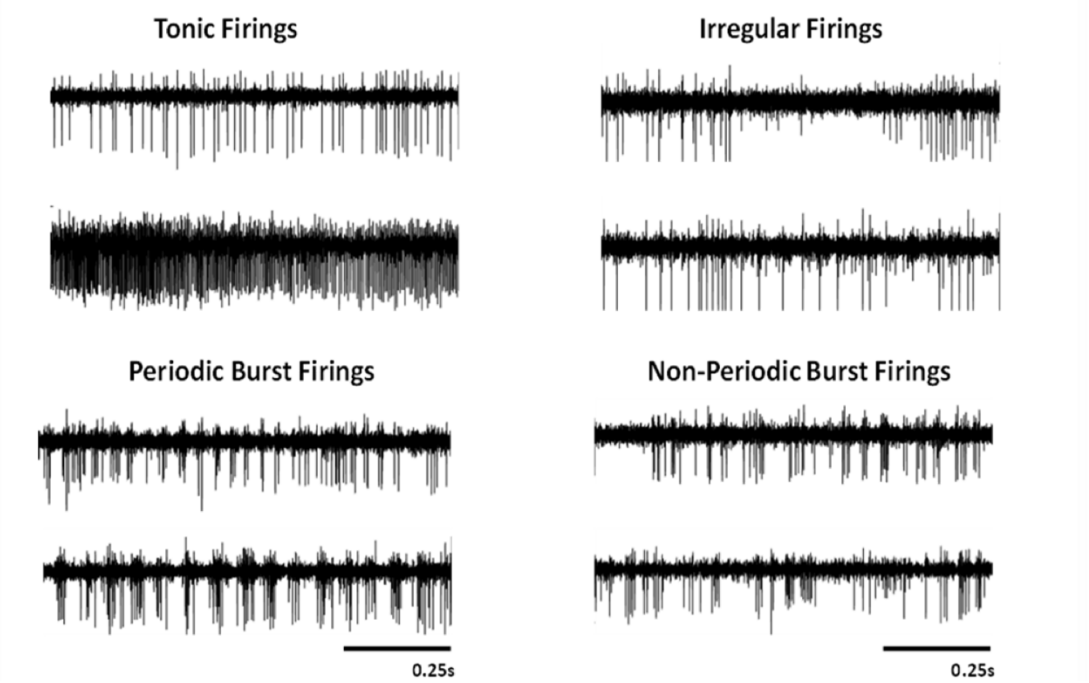

Figure 1.3: *Sample raw traces representing different types of single cell firings observed in the STN. Adopted from (Kaku et al., 2020)*

1.5.2 Local Field Potentials

Spatial alignment of neurons and temporal synchrony of their firing leads to higher amplitude oscillating extracellular potentials (Buzsáki et al., 2012; Lempka and McIntyre, 2013). LFPs represent the sum of these extracellular potentials of numerous neurons in a region (Figure 1.4) (Brown and Williams, 2005; Buzsáki et al., 2012). The volume of this region contributing to the LFP signals may vary according to the size of the electrode and where it is implanted

and can include tens or thousands of neurons (Buzsáki, 2006). Action potentials generate strong currents, but generally lead to smaller field potentials due to temporal dispersion, unless there is synchronous action potential generation in many neurons (Buzsáki et al., 2012). Temporal synchrony is more likely to occur for relatively slow-acting events such as synaptic activity, so LFPs are generally thought to arise from dendritic synaptic currents instead (Buzsáki et al., 2012).

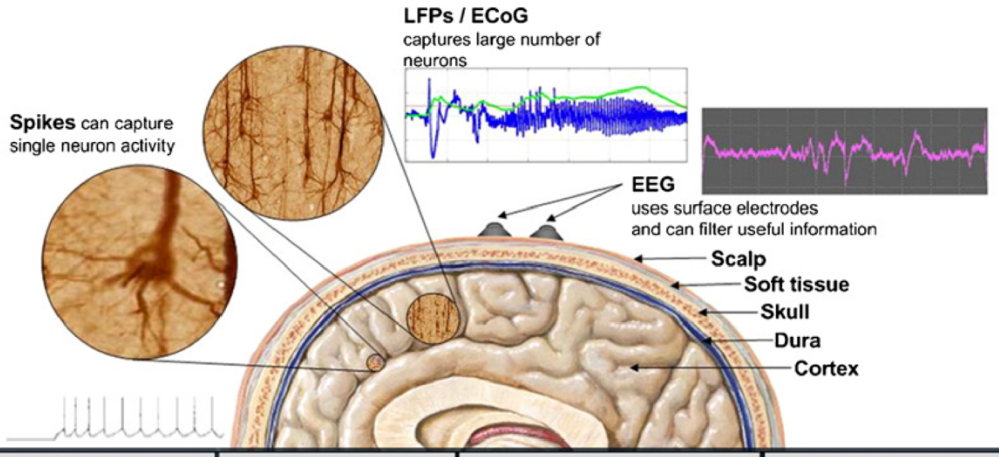

Sensing Methodology	Chronic Recording	Information Coding	System Power
Spike Recording	Challenging Interface Stability	High Fidelity, Need Ensemble Averages for Disease State	High Bandwidth/ Power & Data Processing Req.
Field Potentials	Less Sensitive to Interface Stability, Reuse Existing Technology	Medium Fidelity, Direct Relation to Disease State	Less Bandwidth/ Power & Data Processing Req.
Surface EEG	Irritation High Interference	Lower Fidelity, Less Spatial, Temporal, & Spectral Resolution	External Power Source Can Be Used

Figure 1.4: *Comparison of electrophysiological recording modalities. Adopted from (Rouse et al., 2011)*

LFPs can provide insight into brain processes under normal and pathological conditions (Gatev et al., 2006; Uhlhaas and Singer, 2006) and may provide a surrogate marker of oscillatory activity at the single-unit level (Creutzfeldt et al., 1966; Pettersen et al., 2012). Indeed, the magnitude of the

LFP reflects the number of oscillatory neurons and the degree of their synchronization (Kühn et al., 2005; Weinberger et al., 2006; Lindén et al., 2011; Buzsáki et al., 2012). Additionally, the SUA and LFP have been linked on a spatial (Telkes et al., 2016) and non-linear level (Meidahl et al., 2019). It is well-reported that the excessive neural synchrony can be pathological in PD (Levy et al., 2000; Brown, 2003; Brittain and Brown, 2014) and biomarkers derived from the resulting oscillations respond to medication (Foffani et al., 2003; Priori et al., 2004; Marceglia et al., 2006; Kane et al., 2009; Lopez-Azcarate et al., 2010; Özkurt et al., 2011) and DBS (Kühn et al., 2008; Eusebio et al., 2011; McConnell et al., 2012) therapies.

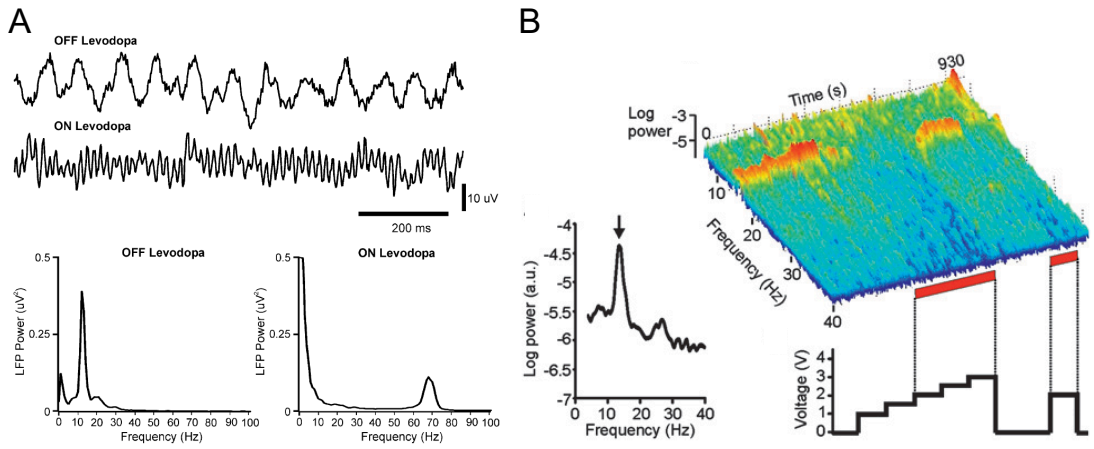

Figure 1.5: *Suppression in the beta band with (A) medication and (B) stimulation therapies. A is adopted from (Brown and Williams, 2005) and B is adopted from (Eusebio et al., 2011)*

Due to the oscillatory nature of the basal ganglia (Brown, 2003; Brittain and Brown, 2014), LFP is commonly studied in specific frequency bands. In PD, exaggerated beta band (13-30 Hz) activity in the STN is considered as the hallmark (Oswal et al., 2013; Brittain and Brown, 2014) and suppression in the power of this band upon treatment (Figure 1.5) have been shown to correlate

with improvement in the akinetic cardinal symptoms (bradykinesia and rigidity) of the disease (Brown et al., 2001; Priori et al., 2004; Kühn et al., 2006, 2008; Weinberger et al., 2006; Wingeier et al., 2006; Ray et al., 2008; Eusebio et al., 2011). Thus, beta oscillations are considered anti-kinetic, as beta power also decreases during movement preparation and execution in the STN and pallidum (Cassidy et al., 2002; Levy et al., 2002; Priori et al., 2002; Kühn et al., 2004; Williams et al., 2005). These features prompted the development of tools to improve the targeting of STN and select the optimal stimulation contacts for DBS (Chen et al., 2006; Miyagi et al., 2009; Holdefer et al., 2010; Yoshida et al., 2010; Zaidel et al., 2010; Telkes et al., 2016; Kolb et al., 2017).

Investigation of higher frequencies in the LFP spectrum have revealed the existence of pro-kinetic high frequency oscillations (HFO, 200-400 Hz) in STN of PD patients, that modulate with dopaminergic medication intake or movement (Lopez-Azcarate et al., 2010; Özkurt

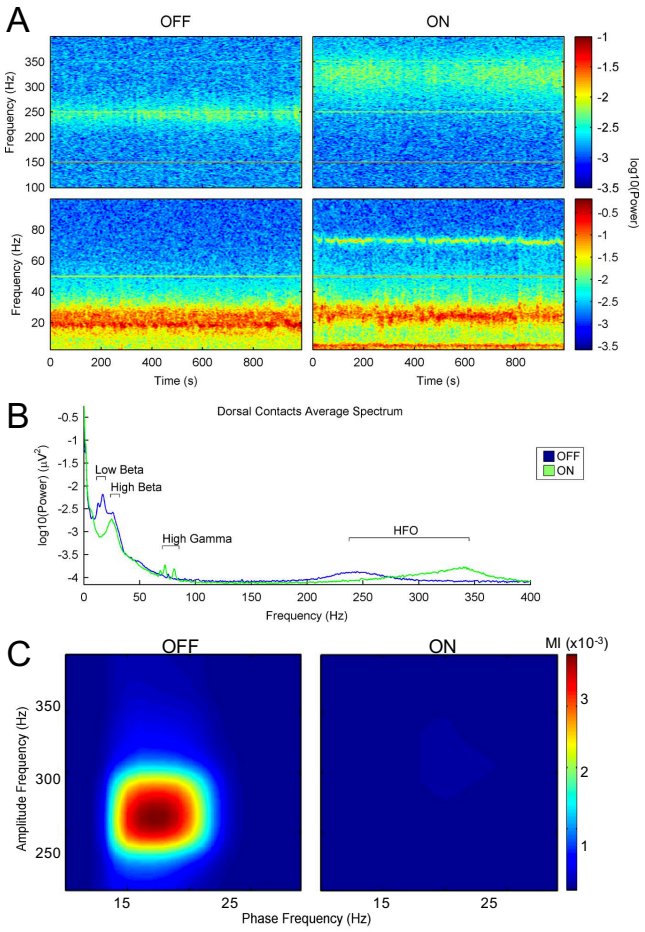

Figure 1.6: *HFO, gamma and alpha-theta bands enhance after dopaminergic therapy. (A, B), unlike suppressed beta and these changes are reflected to the CFC analysis (C).*
Adopted from (Lopez-Azcarate et al., 2010)

et al., 2011; van Wijk et al., 2016). Specifically, 200-300 Hz slow HFOs are observed in the unmedicated state and the peak shifts to 300-400 Hz in the medicated state (Figure 1.6A, B). It has been hypothesized that basal ganglia require these fast HFOs (>300 Hz) for functional brain processes, similar to a “microprocessor clock”, and that the harmonics of high frequency stimulation could drive this activity to induce therapeutic effect (Foffani et al., 2003). However, due to the large stimulus artifact and recording amplifier saturation, HFO band during DBS have not been studied yet, to validate this claim. Additional to the spectral bandpower, a non-linear measure of LFPs termed “cross-frequency coupling” (CFC) between the phase of beta and amplitude of HFOs (Figure 1.6C) have been recently associated with the symptoms of PD as well (Lopez-Azcarate et al., 2010; Özkurt et al., 2011; van Wijk et al., 2016), indicating that analyzing the spectral power of oscillatory bands only may not be sufficient to capture the complex pathophysiology of PD.

Theta-alpha (4-12 Hz) oscillations were reported previously in the STN, with an increase in power after medication intake (Figure 1.6A, B) (Priori et al., 2004; Lopez-Azcarate et al., 2010) and DBS therapies (Priori et al., 2006; Giannicola et al., 2013). The extent of increase was correlated with the clinical improvement, which is contradicting the hypothesis that these oscillations are anti-kinetic (Brown, 2003). It was also suggested that excessive synchronization in the STN at low frequencies in the levodopa-induced ON state might indicate the presence of dyskinesias (Foffani et al., 2005; Alonso-Frech et al., 2006; Rodriguez-Oroz et al., 2011). Similarly, finely-tuned gamma oscillations (70-90

Hz) in the cortex and the STN (Figure 1.6A, B) of medicated subjects were also associated with dyskinesias (Swann et al., 2016). Moreover, the sharp gamma activity in the STN and in the motor cortex has been labeled as “prokinetic” due to its enhancement with voluntary movement (Cassidy et al., 2002; Cheyne et al., 2008; Thompson et al., 2014). Although not necessarily pathological, the theta-alpha and sharp gamma bands might be contributing to the levodopa-induced dyskinesia (LID) generation when they are exaggerated (Alonso-Frech et al., 2006; Swann et al., 2016).

LFPs can be recorded from the microelectrode and DBS lead, and their long-term stability is promising, unlike microelectrode SUA recordings with less robust interface stability (Figure 1.4). Beta band LFPs recorded from 30 days up to 10 years after implant were similar to those recorded acutely, and had a comparable response to DBS (Rosa et al., 2010, 2011; Abosch et al., 2012; Giannicola et al., 2012). Thus, there exist a high potential in the utility of LFPs for the development of chronic closed-loop DBS systems (Hoang et al., 2017; Bouthour et al., 2019). An implantable, bi-directional interface was already developed that enables concurrent sensing of LFPs and stimulation (Rouse et al., 2011) to explore the feasibility of a closed-loop DBS system for PD (Stanslaski et al., 2009) and epilepsy (Stanslaski et al., 2012). The closed-loop approach here involves triggering the stimulation to the changes in the bandpower of an LFP band (e.g., beta). However, with the possible non-linear mechanisms involved in the complex pathological circuitry inducing PD (Lopez-Azcarate et al., 2010; Özkurt et al., 2011), a controller based on a single LFP

bandpower may not be sufficient for a robust adaptive stimulation therapy. Hence, the success of closed-loop DBS depends critically on the identification of reliable symptom-specific biomarkers, which -ideally- reflect the mechanisms of the underlying pathophysiology (Bouthour et al., 2019).

1.5.3 Evoked Compound Activity

Evoked compound activity (ECA) is the response generated by the synchronous activation of a population of nerve fibers around the recording electrode, reaching up to mV levels in amplitude (Miller et al., 1998; Briaire and Frijns, 2005). Cochlear implant research and computational models have suggested that the ECA magnitude increases largely with the number and size of the activated single-fiber action potentials, and partially with the synchrony between the fibers, whereas the duration of the ECA is determined by both the duration and the synchrony of the single-fiber action potentials (Rubinstein, 2004; Briaire and Frijns, 2005). It can be assumed that the amplitude is approximately proportional to the number of activated nerves, and the resulting waveform obtained is weighted towards the closest fibers (Miller et al., 2008). Furthermore, the ECA magnitude is shown to be largest when the recording contact was the closest to the stimulating contact, although this also causes a large stimulus artifact that might mask the ECA and make the analysis more challenging (Miller et al., 2008). It is, therefore, expected that the ECA generated during DBS could provide a population view of the number and type of activated neural elements, and thus, ECA patterns might be used as an indicator of

sufficient activation of the appropriate types of neural elements necessary for therapeutic benefit.

ECAs have been successfully utilized previously as a feedback control signal for programming stimulation parameters in cochlear implants (Brown and Abbas, 1990; Miller et al., 2008). ECA recordings have also been used for the treatment of epilepsy with DBS (Stypulkowski et al., 2011). It was reported that the characteristics of the ECAs were dependent on the location of the stimulating electrode as well as the DBS parameters such as amplitude and frequency (Stypulkowski et al., 2011). Increasing the stimulation amplitude initially generated increases in ECA magnitude before eventually reversing (Miller et al., 1998; Matsuoka et al., 2001; Westen et al., 2011), whereas increasing the stimulation frequency reduced ECA amplitude, starting at frequencies as low as 250 Hz, possibly due to the neural refractoriness or adaptation (Miller et al., 2008). In the STN of PD patients, ECA amplitude and delay during electrical stimulation was shown to correlate with clinical improvement and has been proposed as an intraoperative method to localize the STN (Figure 1.7A), the optimal stimulation contact (Sinclair et al., 2018) and therapeutic DBS current levels (Figure 1.7B) (Gmel et al., 2015). However, the other features of the ECA

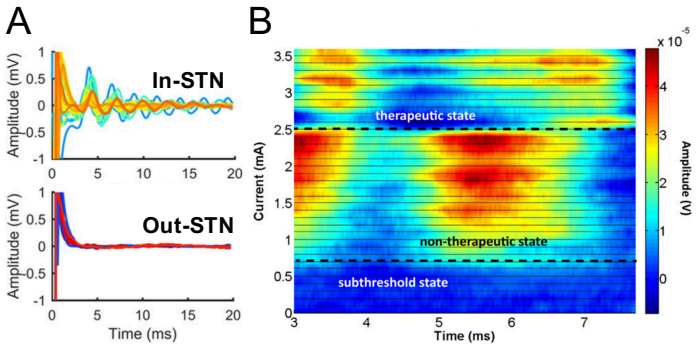

Figure 1.7: *Evoked activity is observed in STN but not in thalamus (A), and its timing and morphology changes with the stimulation reaches to the therapeutic levels for PD symptoms (B). A is adopted from (Sinclair et al., 2018) and B is adopted from (Gmel et al., 2015)*

waveforms such as the resonance damping time have not been investigated and may provide further details regarding the mechanisms of the DBS therapy.

ECA can have other additional clinical applications such as testing the integrity of the implant (Rubinstein, 2004), identifying redundant or interacting electrodes (Boëx et al., 2003), measuring cell survival (R.D., 1990), assessing the effectiveness of different stimulation paradigms (Miller et al., 2008) and monitoring the changes in neural response over time (Miller et al., 2008). Therefore, biomarkers derived from ECA characteristics have promising functional utility in clinical care such as adaptive DBS (Hoang and Turner, 2019).

1.6 Specific Aims and Outline

The encompassing purpose of this dissertation is to study the modulations of LFPs recorded from STN in PD subjects with medication and stimulation therapy. Such work not only contributes to the pathophysiological knowledge of PD and brain in general, but also helps develop novel therapies such as closed-loop DBS by means of biomarker identification. Although the exact mechanism of DBS is still unknown, its therapeutic effect on the cardinal symptoms of PD by stimulating the STN is well studied. For an optimal outcome, accurate localization of the DBS electrode in STN to maximize the symptom alleviation and minimize the side effects by preventing the current spread to surrounding structures is a crucial step.

Aim-1: Development of a Soft Real-Time System for the Localization of STN with LFP Guidance: Therefore, after the introductory Chapter 1, an

online electrophysiological targeting tool for refining the chronic DBS lead placement is proposed in Chapter 2, prior to investigating the LFP modulations with treatment. By utilizing bio-signal processing to reveal spatio-spectral features of LFPs en route to STN, the optimal trajectory and the dorsal border of the STN for DBS lead implantation was automatically detected and provided to the clinician. A pilot feasibility study comparing the proposed system to the clinical practice in a randomized, double-blinded manner was also conducted.

Aim-2: Subband Power Modulations and Cross Frequency Coupling of STN LFPs in Medication OFF and ON States: Next, with a well-targeted STN, the modulatory effects of dopaminergic medication on the LFP oscillations are investigated in Chapter 3. Day-long recordings were performed for each patient postoperatively using externalized leads while patients were in the medication OFF and ON states to allow continuous monitoring of the changes in neural oscillations.

Aim-3: Modulation of High Frequency Oscillations and Evoked Activity in the STN with Therapeutic and Non-therapeutic DBS: In Chapter 4, a similar investigation of the LFP activity is reported with the acute therapeutic and non-therapeutic DBS applied to the STN intraoperatively. Since DBS exerts its effect in a more immediate way, the prolonged recordings were not necessary, as in the pharmacological study presented in the previous chapter.

Finally, Chapter 5 summarizes the overall outcomes and their scientific contribution in a broader sense by relating the work presented here to the literature and assessing its significance.

2 Development of a Soft Real-Time System for the Localization of STN with LFP Guidance

2.1 Overview

The efficacy of deep brain stimulation (DBS) therapy in Parkinson's disease (PD) patients is highly dependent on the precise localization of the target structures such as subthalamic nucleus (STN). Most commonly, microelectrode single unit activity (SUA) recordings are performed to refine the target. This process is heavily experience based and can be technically challenging. Local field potentials (LFPs), representing the activity of a population of neurons, can be obtained from the same microelectrodes used for SUA recordings and allow flexible online processing with less computational complexity due to lower sampling rate requirements. Although LFPs have been shown to contain biomarkers capable of predicting patients' symptoms and differentiating various structures, their use in the localization of the STN in the clinical practice is not prevalent.

Here we present, for the first time, a randomized and double-blinded pilot study with intraoperative online LFP processing in which we compare the clinical benefit from SUA- versus LFP-based implantation. Ten PD patients referred for bilateral STN-DBS were randomly implanted using either SUA or LFP guided targeting in each hemisphere. Although both SUA and LFP were recorded for

each STN, the electrophysiologist was blinded to one at a time. Three months postoperatively, the patients were evaluated by a neurologist blinded to the intraoperative recordings to assess the performance of each modality. While SUA-based decisions relied on the visual and auditory inspection of the raw traces, LFP-based decisions were given through an online signal processing and machine learning pipeline.

We found a dramatic agreement between LFP- and SUA-based localization (16/20 STNs) providing adequate clinical improvement (51.8% decrease in 3-month contralateral motor assessment scores), with LFP-guided implantation resulting in greater average improvement in the discordant cases (74.9%, n=3 STNs). The selected tracks were characterized by higher activity in beta (11-32 Hz) and high-frequency (200-400 Hz) bands ($p<0.01$) of LFPs and stronger non-linear coupling between these bands ($p<0.05$).

Our pilot study shows equal or better clinical benefit with LFP-based targeting. Given the robustness of the electrode interface and lower computational cost, more centers can utilize LFP as a strategic feedback modality intraoperatively, in conjunction to the SUA-guided targeting.

2.2 Introduction

Deep brain stimulation (DBS) is an effective treatment option for patients suffering from various neurological disorders such as Parkinson's disease (PD) (Benabid et al., 2008; Groiss et al., 2009; Schiefer et al., 2011; Hariz, 2012, 2014; Odekerken et al., 2013; Gunduz et al., 2017; Lee et al., 2018). Although

the exact mechanism of DBS remains to be explored, it is well-established that stimulation of the subthalamic nucleus (STN) alleviates the cardinal symptoms of PD (Limousin et al., 1998; Krack et al., 2003; Herzog et al., 2004; Benabid et al., 2009). However, stimulation can also result in side effects arising from unintended activation of structures surrounding the STN (Krack et al., 2001; Okun et al., 2003; Deuschl et al., 2006; Guehl et al., 2006; Wojtecki et al., 2007; Benabid et al., 2009; Groiss et al., 2009; Richardson et al., 2009; Zhang et al., 2016). Moreover, a multi-center study has reported that the sub-optimal positioning of DBS electrodes accounts for 46% of cases with inadequate clinical improvement postoperatively (Okun et al., 2005). Thus, the clinical efficacy of DBS therapy depends critically on accurate localization of the STN (Zonenshayn et al., 2000; Sterio et al., 2002; Amirnovin et al., 2006; Gross et al., 2006; Campbell et al., 2019).

Precise placement of the DBS lead can be challenging due to the small size and the anatomical variability in the human STN (Patel et al., 2008; Richardson et al., 2009). While MRI-guided asleep DBS is being performed by some centers (Aziz and Hariz, 2017; Brodsky et al., 2017; Chen et al., 2018; Ho et al., 2018; Wang et al., 2019; Liu et al., 2020), intraoperative electrophysiology remains to be an important technique for localizing the STN, despite the variations in the surgical procedure between medical centers (Zonenshayn et al., 2000; Sterio et al., 2002; Amirnovin et al., 2006; Gross et al., 2006; Abosch et al., 2013; Campbell et al., 2019). A worldwide survey involving 143 DBS centers reported that 83% of them use single unit activity (SUA) recordings for DBS lead

implantation (Abosch et al., 2013). Typically, up to five microelectrodes are advanced towards the target structure to obtain a 3-dimensional perspective (Gross et al., 2006; Benabid et al., 2009; Abosch et al., 2013). SUA is used to identify cells with firing characteristics consistent with STN neurons and response characteristics confirming the motor sub-territory of the STN based on a variety of visual and auditory cues (Hutchison et al., 1998; Magnin et al., 2001; Rodriguez-Oroz et al., 2001; Abosch et al., 2002; Benazzouz et al., 2002). This procedure is subjective, heavily experience-based and depends critically on the neurosurgeon's or electrophysiologist's ability to recognize the STN (Benazzouz et al., 2002; Benabid et al., 2009; Marceglia et al., 2010; Abosch et al., 2013). Aside from difficulties in interpreting the data and small number of neurons sampled by 1-5 microelectrodes, challenges in interface stability (e.g., necessity of turning lights or other devices off in the operating room) and high bandwidth/sampling frequency requirements may complicate the collection and real-time analysis of SUA (Novak et al., 2011; Rouse et al., 2011; Thompson et al., 2014).

Local field potentials (LFPs), which represent the aggregated synaptic potentials of a population of neurons (Priori et al., 2004; Gross et al., 2006; Buzsáki et al., 2012), can be obtained from the shaft of the same microelectrode used for SUA recordings. Although LFPs have been shown to contain biomarkers capable of predicting Parkinsonian symptoms (Foffani et al., 2003; Ray et al., 2008; Lopez-Azcarate et al., 2010; Özkurt et al., 2011; Little and Brown, 2012; Oswal et al., 2013; Priori et al., 2013; Brittain and Brown, 2014;

Ozturk et al., 2019) and differentiating basal ganglia structures (Chen et al., 2006; Telkes et al., 2016; Kolb et al., 2017) only a handful of centers around the world rely on LFPs for the localization of the STN (Abosch et al., 2013).

Here, we present, for the first time, a randomized, double-blinded study comparing the targeting performance of SUA- vs LFP-based implantation. While SUA was interpreted by visual and auditory inspection of the raw traces as done in clinical practice, we employed real-time intraoperative processing of LFPs to facilitate the selection of the implantation track.

2.3 Patients and Methods

2.3.1 Patients

Ten patients (four females, six males) with PD undergoing bilateral STN-DBS implantation at Baylor St. Luke's Medical Center were included in the study. Their ages ranged between 40 to 64 (mean ± standard deviation = 55±8.8) with disease duration ranging from 4 to 16 years (mean ± standard deviation = 9±3.9). Nine patients were implanted with Medtronic lead model 3389, and one was with model 3387 (Medtronic, Ireland). The study protocol was approved by the Institutional Review Boards of Baylor College of Medicine and University of Houston. All patients provided written informed consent.

2.3.2 Study Design

This study investigates the functional utility of LFP versus SUA in targeting the STN with an online processing pipeline (Figure 2.1A) and

compares both modalities in terms of clinical outcomes postoperatively. The implantation modality for each hemisphere (SUA vs. LFP) was randomly identified prior to the surgery. If one hemisphere was implanted using LFP, the other one was implanted using SUA. Three track MER was performed with only the guiding waveform provided to the electrophysiologist for decision making, while the other signal was recorded in the background (blinded recordings) for off-line comparison. After DBS lead placement in the selected track, an intraoperative computed tomography (CT) fused with preoperative magnetic resonance imaging (MRI) was used to verify lead location. Finally, a neurologist blinded to the recordings tested the patients for clinical benefit and side effects intraoperatively and 3-months postoperatively (blinded testing). To prevent possible interference induced by inter-rater variability on the paired statistics performed in this study, the rating neurologists (authors JS and AT, both MDS-UPDRS certified) performed the clinical assessment for each patient consistently (the same rater performed both OFF and ON assessments of a patient, for both the left and right hemispheres). The systematic testing done at 3-months postoperatively was used to assess the clinical improvement by stimulation (medication OFF/DBS ON). The clinical scores were computed as the sum of Movement Disorders Society Unified Parkinson's Disease Rating Scale (MDS-UPDRS) Part-III items 3.3-3.8, 3.15-3.17 of the side contralateral to the implant.

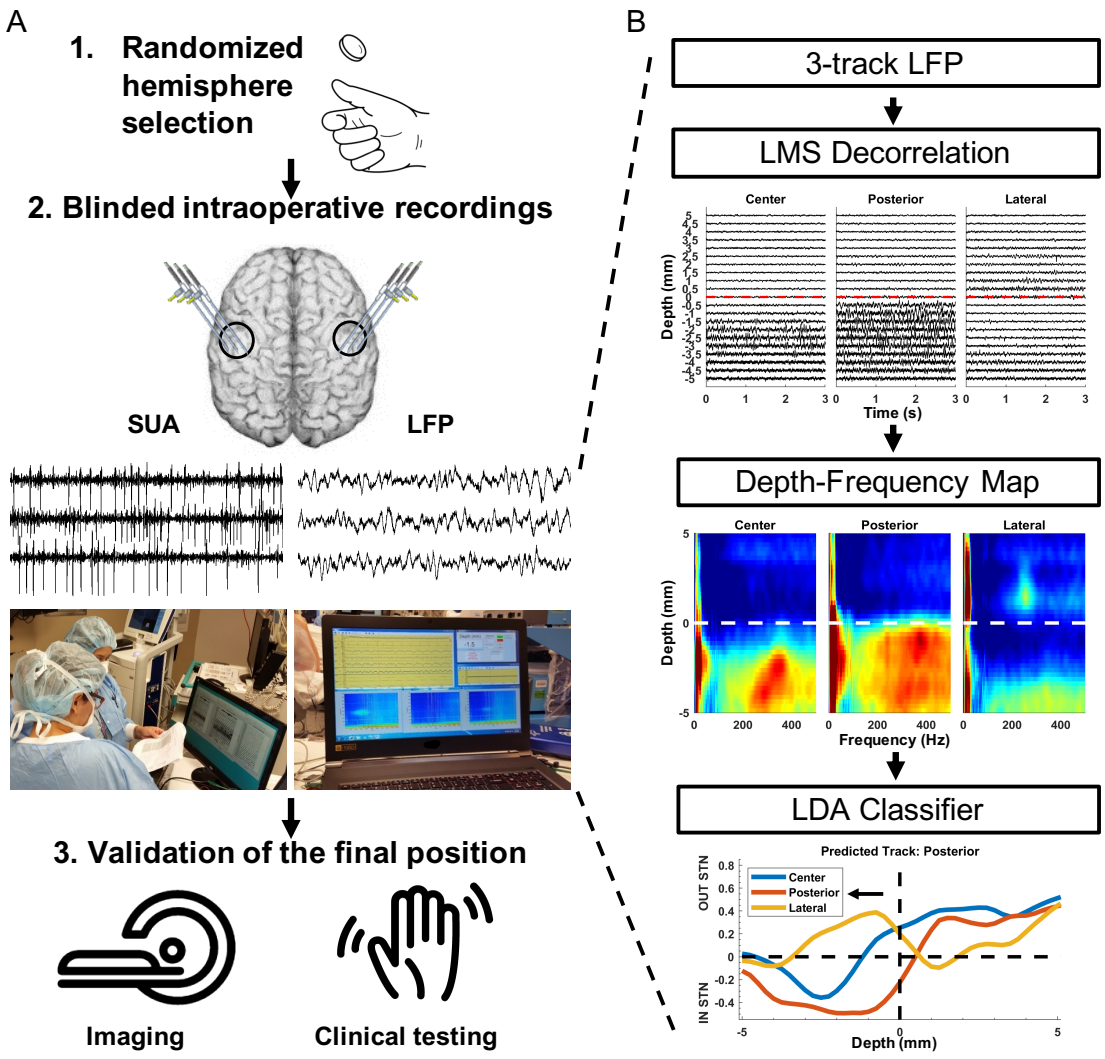

Figure 2.1: *Randomized double-blinded paradigm (A) and the processing pipeline for LFPs (B).*

The description of each panel in Figure 2.1 is: **(A)** The decision modality for each hemisphere was determined in the beginning of the operation randomly. Intraoperative recordings included both SUA and LFP activity. However, only the decision modality, either SUA or LFP, was made available to the electrophysiologist. After the implantation site was selected, the final position was confirmed with intraoperative imaging and clinical testing for motor improvement and side effects, which was performed by a neurologist blinded to

the electrophysiological recordings. **(B)** Signal processing and machine learning pipeline for LFP-based decision making. The raw traces are de-correlated using least mean squares (LMS) algorithm with the steepest descent update. Then, the LFP traces were analyzed in the spectral domain using modified Welch periodogram with a 1s Hamming window and 50% overlap. Individual spectra across depths were combined to generate a 2D depth-frequency map (DFM) representing the depth-varying power spectrum of the LFPs. The track selection was performed automatically using a linear discriminant analysis (LDA) classifier developed by Telkes et al. (Telkes et al., 2016), using the power in beta and HFO bands as input features. License note: The “coin flipping”, “cat scan” and shaking “hand” icons in Figure 2.1A are downloaded from nounproject.com under CC-BY license with credits to Oleksandr Panasovskyi, Sergey Demushkin and Gregor Cresnar respectively.

2.3.3 Intraoperative Recordings

Patients were requested to stop medication at least 12 hours prior to surgery and all recordings were obtained in the awake state using local anesthesia. On the morning of the surgery, all patients obtained a head CT after application of the stereotactic head frame. The stereotactic coordinates and trajectories to the STN were identified by fusing preoperative MRI and CT scans on a neuro-navigational platform (StealthStation, Medtronic, Ireland). In each hemisphere, awake recordings were performed using a set of three parallel microelectrodes separated by 2 mm (center-to-center) using the 5-cannula

BenGun with “+” configuration. The preoperative planning using direct targeting methods determined the “center” track. Among “anterior, posterior, lateral and medial” tracks, two other tracks were selected by the neurosurgeon on a patient specific basis by taking into account the subject’s anatomy. The microelectrodes (NeuroProbe, AlphaOmega, Israel) were initially placed at least 15mm above the stereotactic target and advanced deeper with 0.5-1mm steps using NeuroOmega drive (AlphaOmega, Israel), in order to refine the radiographic target. At each depth, by using the cannula as reference, at least 20s of SUA from the high-impedance tungsten tip (0.6-0.8 MOhm) and LFP from the low impedance stainless-steel ring (<10KOhm, 3mm above the tip) on the shaft were obtained simultaneously. The entire data was recorded with Grapevine Neural Amplifier (Ripple Neuro, UT) at 30KHz and 16-bit A/D resolution, and LFPs were down-sampled to 2KHz before further processing.

2.3.4 Signal Processing

The signals were recorded and visualized in real-time with an in-house built Simulink model and processed with custom MATLAB scripts using version R2014a (Mathworks, MA) and gHiSys high-speed online processing library (gTec, Austria). The entire online processing was performed on a 17” laptop with quad-core (2.4GHz) processor and 12GB memory. The SUA data were high-pass filtered at 300Hz with a 2^{nd} order infinite-impulse response filter and presented to the electrophysiologist in visual and auditory format, similar to the commercially available devices. After the mapping was completed, the SUA

traces were plotted depth by depth form all three tracks for reviewing and final decision. The entry to and exit from the STN was determined by an experienced neurophysiologist by listening to and visually observing the firing patterns of neurons. The entry to the STN was identified with a prominent increase in the background activity and discharge rates (Figure 2.2A), as reported previously (Hutchison et al., 1998; Novak et al., 2007). Among three, the track with the longest span of cell firing and background activity was selected for the chronic DBS electrode implantation (Abosch et al., 2002; Benazzouz et al., 2002; Gross et al., 2006). In those hemispheres where the implantation was performed based on LFPs, the same procedures were used to process SUA data offline, following the implantation of the DBS electrode.

The LFPs were processed intraoperatively with the real-time implementation of the signal processing pipeline (Figure 2.1B) provided by Telkes et al. (Telkes et al., 2016). Specifically, LFP raw traces were visualized initially and it was noted that tracks were difficult to distinguish, due to common activity coming from the reference contact (cannula) masking spatially localized patterns. In order to eliminate the common activity without affecting the localized neural activity, the LFP from tracks were de-correlated using LMS algorithm with the steepest descent update. Explicitly, each track was predicted by using a linear weighted combination of other two channels and the residual was used for the further processing. With this adaptive approach, the common activity was eliminated across tracks and only spatially specific information was preserved (Telkes et al., 2016). LFP traces were then analyzed in the spectral domain

using a modified Welch periodogram. A fast Fourier transform was computed at each depth with a 1s Hamming window and 50% overlap and presented to the electrophysiologist in near real-time in the form of online spectrograms (Supplementary video). After the mapping was completed, a median spectrum was calculated from the spectra to eliminate localized artifacts at each depth. Then, spectra across depths were combined to generate a 2D depth-frequency map (DFM) representing the depth-varying power spectrum of the LFPs of each track (Telkes et al., 2016, 2018). The maps were then normalized with the average baseline of three tracks and transformed into log scale (Figure 2.1B). The tracks were not normalized by their own baseline but by the mean of all three tracks in order to compare the signal power between them. The baseline used for normalization was selected as the highest depths which are assumed to be in the white matter. The STN was identified by distinct LFP activity in beta (11-32Hz) and HFO (200-400Hz, high-frequency oscillations) ranges. The track containing the largest beta and HFO bandpower for the longest span was selected as the implantation site for the DBS electrode (Zaidel et al., 2010; Wang et al., 2014; Telkes et al., 2016; van Wijk et al., 2017). This selection was performed automatically using a linear discriminant analysis (LDA) classifier developed by Telkes et al. (Telkes et al., 2016). Specifically, after obtaining the normalized depth-frequency maps, the beta and HFO sub-band powers were extracted for each track and depth from these maps. Then, the sub-band power features were normalized between zero and one with a Min-Max normalization method for the minimization of inter-subject variability in LFP power, and a

binary LDA classifier was applied for classification. This classifier was trained by contrasting the LFP sub-band features coming from selected and non-selected tracks using the data from the 24 PD patients analyzed in (Telkes et al., 2016). During online classification, the neural data in each track and at each depth were fed to the classifier. Therefore, each electrode trajectory received a vote at each depth from the classifier. The decision distance of the LDA classifier was plotted to give visual feedback regarding the votes and related confidence of the classifier (Figure 2.1B). The track that received the longest span of decision distances voting for in-STN was selected for the final DBS electrode implantation (Figure 2.1B). Once again, in those hemispheres where the implantation was performed based on SUA, the same signal processing pipeline was executed offline to process LFPs, following the implantation of the DBS electrode.

Additional offline analysis was performed postoperatively to investigate the cross-frequency coupling (CFC) between beta and HFO bands. The comodulograms representing CFC were computed using the phase-locking principle (Penny et al., 2008) with amplitude frequency axis from 150 to 450 Hz with 10 Hz steps and 50 Hz filter bandwidth, and phase frequency axis from 6 to 40 Hz with 1 Hz steps and 3 Hz filter bandwidth.

2.3.5 Statistics

Normality of all distributions was tested using Anderson-Darling test and it was found that most of them are non-normal ($p < 0.05$). Statistical tests were

performed in a paired fashion using non-parametric Wilcoxon signed rank test to compare the clinical scores in the OFF- and ON- DBS states, the beta and HFO bandpowers and the coupling strength between them. The sample size and significance levels are provided throughout the text, when referred.

2.4 Results

A total of 60 microelectrode tracks from 20 STNs were included in this study. Figure 2.2 illustrates offline comparison of representative LFP and SUA data from two STNs, where both modalities suggested the same track in one (Pt5, left hemisphere) and different tracks in another (Pt10, right hemisphere). The SUA-predicted tracks were determined by the longest span of background and spiking activity (Figure 2.2A, B) whereas the longest span of IN-STN vote of the classifier were considered in LFP-based selection (Figure 2.2C-F). The decision distance (y-axis of Figure 2.2G and 2H) represented the confidence of the classifier which used the power in beta and HFO bands of LFP as input features. Note that, although the randomized decision modality was SUA for the right hemisphere of patient 10 (Figure 2.2, right panel) suggesting implantation in the medial track, intraoperative CT favored the center track as the target, which was used as the final implantation location. The offline analysis of LFPs agreed with the radiographic decision as well.

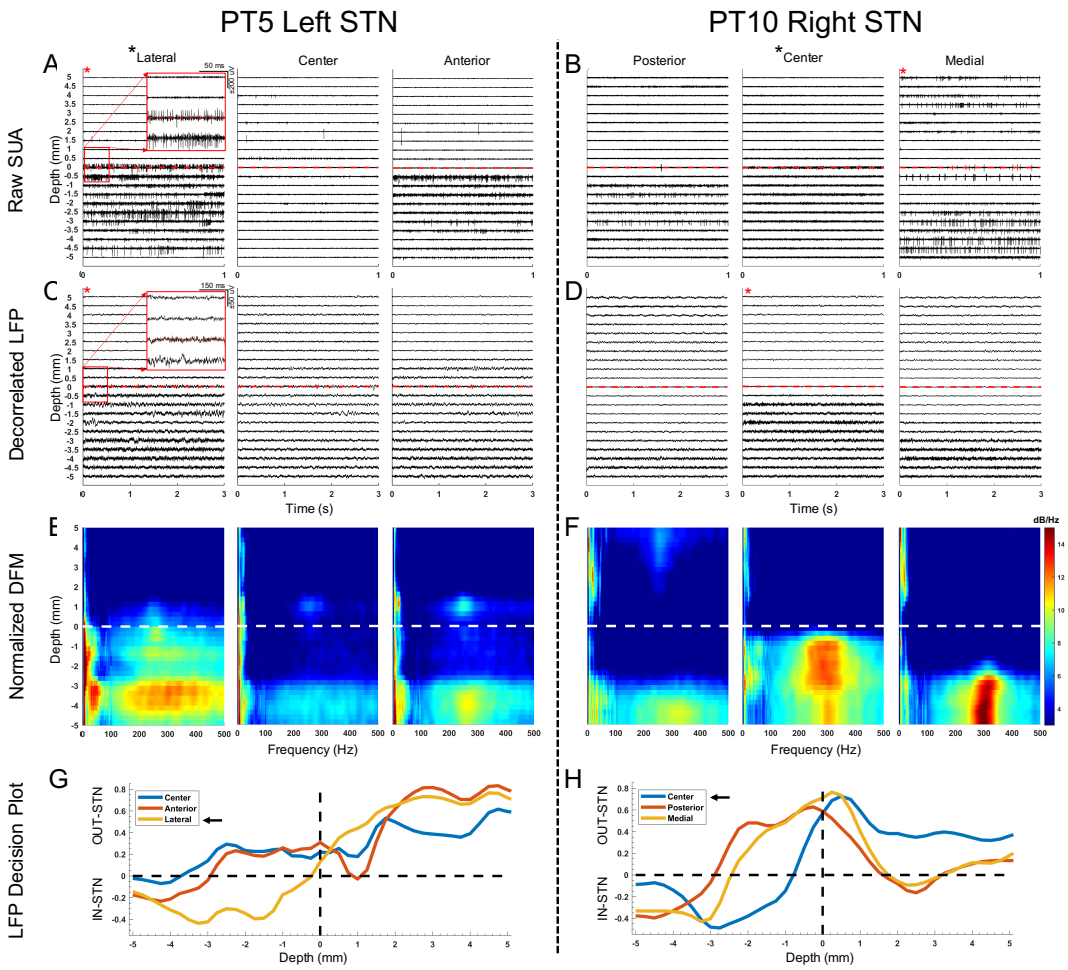

Figure 2.2: *Representative SUA- and LFP- raw traces and depth-frequency maps (DFM) from two STNs where the suggested track by SUA and LFP overlapped (PT5) and did not overlap (PT10).*

The description of each panel in Figure 2.2 is: **(A, B)** SUA raw traces presented from 5 mm above down to 5 mm below the dorsal border of the STN, with 0.5 mm steps. The dorsal border is marked by an increased spiking and background activity. Red stars denote suggested track by the corresponding modality and black star next to the track name denotes the implanted track. **(C, D)** The decorrelated LFP traces are provided in a similar fashion to SUA traces. Although it can be observed that the oscillatory activity increases after crossing the dorsal border, the nature of the change can be visualized better in the

spectral domain where **(E, F)** DFMs of the corresponding LFPs are presented. The entry to STN is characterized with increased activity in both beta (8-32Hz) and HFO (200-400Hz) ranges. **(G, H)** Decision plots of the classifier voting whether each track is in- or out-STN at each traversed depth. The track with the longest in-STN vote is selected as the implanted track, as indicated with the black arrows. The SUA activity was stronger in the lateral track (A) and the corresponding LFPs agreed (G) in the left panel. On the right panel, SUA (B), which was the decision modality, suggested the medial track. However, after intraoperative imaging validation the lead was placed in the center track, which agreed with the LFP-based decision (H).

Distribution of decisions for all hemispheres given by each modality as well as their randomization is provided in Figure 2.3A. In 16/20 hemispheres, the SUA and LFP recordings were concordant in their prediction of implantation track. In those four discordant hemispheres, the LFP was the decision modality in only one of them and the final implantation validated by intraoperative CT and clinical testing agreed with LFP-suggested track. In remaining three STNs where SUA was the decision modality, the lead had to be repositioned based on intraoperative CT validation and/or stimulation testing. For two STNs (Pt6, left; Pt10 right), the track suggested by the SUA, did not agree with the track residing within the target confirmed radiographically (according to intraoperative CT scans merged with preoperative MRI). Therefore, the DBS electrode was placed into the most likely track suggested by the radiography. Interestingly, for these two STNs, the track suggested by the imaging agreed with LFPs. In one

STN (Pt1, left), the lead was moved to posterior track due to stimulation side-effects during intraoperative testing and imaging considerations, without the use of microelectrode recordings. This STN was excluded from further analysis. The repositioned hemispheres are marked with a star on Figure 2.3A. Overall, the track favored by SUA was implanted in total of 16 chronic lead placements whereas LFP-favored track was used in 19. In addition to intraoperative radiographic validation, all 20 implantations were visualized postoperatively by merging the preoperative MRI and postoperative CT images using LeadDBS (Horn and Kühn, 2015). It was observed that at least one contact of the DBS lead was within the STN (Figure 2.3B).

The mean lateralized MDS-UPDRS part III improvement for 19 STNs was 51.8% at 3-month postoperative programming (mean ± standard deviation OFF score= 16.3±5.4, ON score=6.5±4.6, Figure 3C). When the track decisions were compared across modalities in terms of outcome measures, the 16 STNs where both modalities agreed had average clinical improvement of 55.5%. Of the tracks with LFP-SUA mismatch, the mean improvement in three LFP-concordant implantations was 74.9% (Figure 3D).

The description of each panel in Figure 2.3 is: **(A**) The BenGun representation of suggested and implanted tracks for individual STNs. For each hemisphere, the randomized implantation modality is written at the bottom. There were three cases where the decision modality was SUA, but the lead had to be repositioned (denoted by asterisk): left hemisphere of patient 1 moved to posterior track due to intraoperative stimulation side effects, without use of

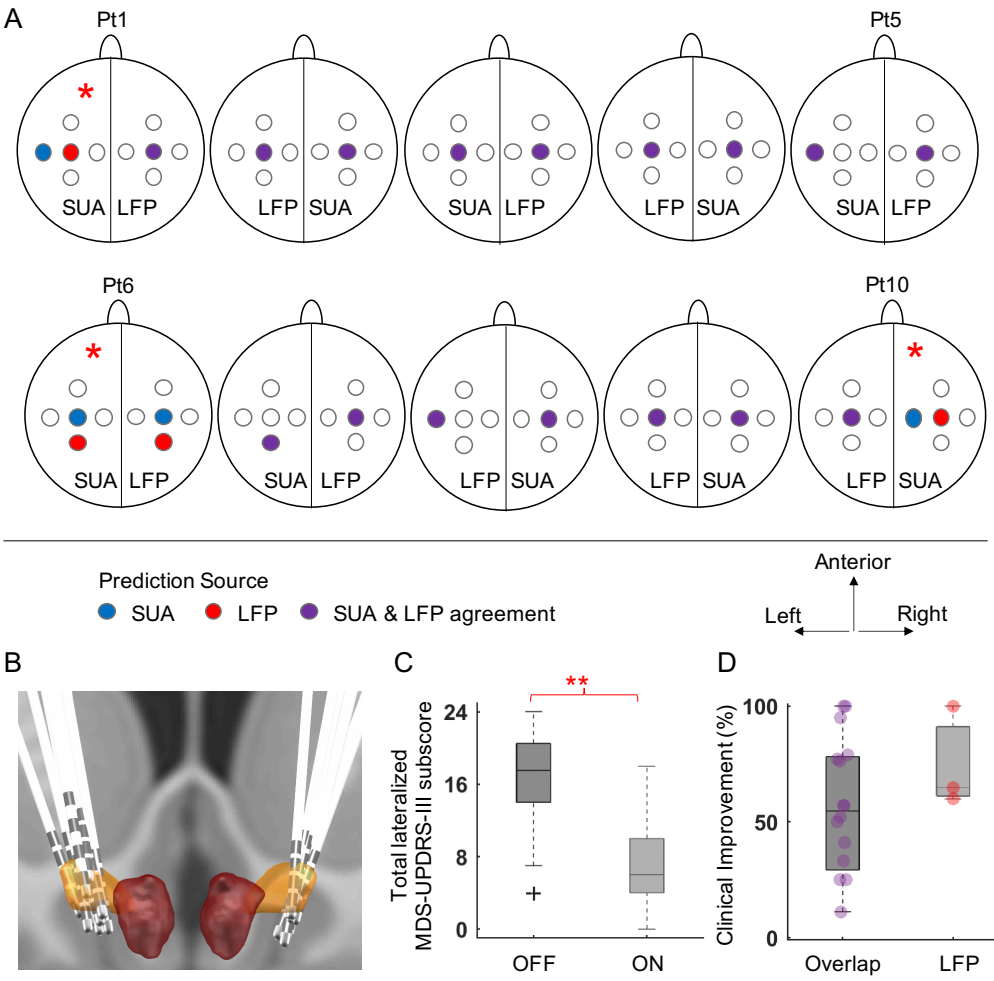

Figure 2.3: *The distribution of selected tracks by SUA and LFP, and the corresponding improvement.*

electrophysiology (excluded from further analysis); left hemisphere of patient 6 and right hemisphere of patient 10 repositioned due to discrepancy with the intraoperative imaging. In the latter two cases, the LFP suggested track agreed with the final decision. **(B)** The illustration of implanted DBS leads generated by merging preoperative MRI and intraoperative CT using Lead DBS toolbox (Horn and Kühn, 2015). In all hemispheres, at least one contact was observed to be in STN. **(C)** The distribution of total contralateral motor UPDRS scores in the DBS OFF and DBS ON states for 19 hemispheres. There was a significant

clinical motor improvement (51.8%) after DBS treatment ($p<0.01$, n=19). **(D)** The tracks suggested by SUA and LFP overlapped for 16 STNs, with average improvement of 55.5%. When there was a disagreement and the implant location agreed with LFP (n=3), the average improvement was 74.9%. Individual data points are presented with circles to emphasize the unequal sample size between groups.

The average DFMs and CFC comodulograms of selected vs other tracks from 19 STNs are presented in Figure 2.4. The left hemisphere of patient 1 was excluded since the electrode was repositioned due to side effects observed during intraoperative stimulation testing without neural recordings. The STN was characterized by exaggerated activity in the beta and HFO ranges in the selected track while the average map of the non-selected tracks contained weaker beta and HFO activity, as presented in Figure 2.4A. The power of these two bands were significantly higher in the selected track, both in dorsal and ventral regions (Figure 2.4B, $p<0.01$, n=19). Although three patients had localized HFO activity above the STN border (see representative DFMs in Figure 2E & F), there was no significant difference in HFO bandpower between selected and other tracks at this depth range. The dorsal half of STN demonstrated CFC between the phase of beta and the amplitude of slow HFO (200-280Hz) oscillations whereas the ventral half was coupled with fast HFO (280-400Hz) band as illustrated in Figure 2.4C. Amongst all selected tracks, the beta-HFO coupling strength was significantly higher in both dorsal and ventral territories, when compared to other tracks (Figure 2.4D, $p<0.05$, n=19).

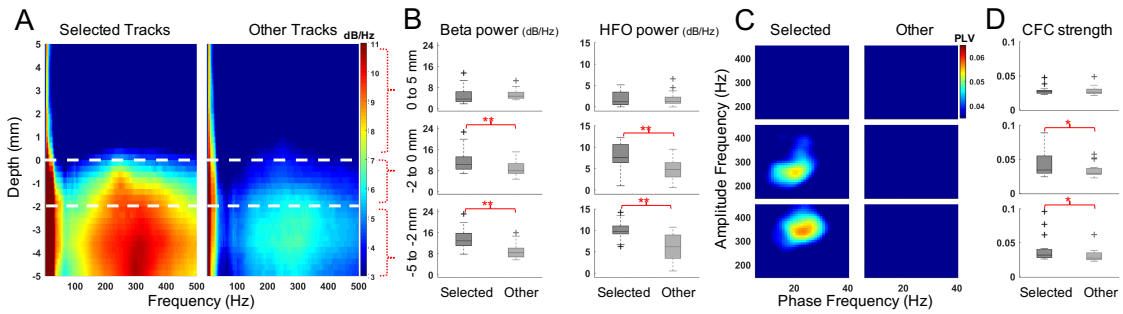

Figure 2.4: *LFP patterns of selected and non-selected (other) tracks above and in the STN.*

The description of each panel in Figure 2.4 is: **(A)** DFM averages of LFPs recorded from selected and other tracks 5mm above and below the dorsal border of 19 STNs. One hemisphere which was repositioned due to side effects without recordings was excluded from the electrophysiological averages. The white dashed lines represent the dorsal border and, the dorsal and ventral regions of STN. Upon entry to the STN, there was a marked increase in the beta and HFO activity. The dorsal half was dominated with slow HFOs (200-280 Hz) whereas the ventral half had HFOs in the 280-400 Hz range. **(B)** The beta and HFO bandpowers are contrasted between selected and other tracks in three spatial regions: above (5 to 0 mm), dorsal (0 to -2 mm) and ventral (-2 to -5 mm) STN. There was significant difference in both beta and HFO bandpower in dorsal and ventral regions ($p<0.01$, $n=19$). **(C)** The CFC patterns contrasted from the same depth regions revealed beta-slow HFO coupling in the dorsal territory, whereas there was beta-fast HFO coupling in the ventral territory of the selected track. **(D)** The mean beta-HFO coupling strength was significantly higher in both dorsal and ventral territories ($p<0.05$, $n=19$).

2.5 Discussion

In this blinded study, we compared the functional utility of LFPs for the implantation of DBS electrode against the widely used method, SUA (Benabid et al., 2009; Przybyszewski et al., 2016; Valsky et al., 2017). We observed an overall agreement in track prediction between both modalities (16/20 hemispheres) with adequate clinical benefit (55.5%) from chronic DBS, comparable to previous reports (Limousin et al., 1998; Krack et al., 2003; Walter and Vitek, 2004). In the three discordant cases, our findings suggest that the mean improvement in motor symptoms with LFP guided implantation may be greater.

The large overlap between optimal tracks predicted by both SUA and LFP is not a surprise as firing activity and field potentials have shown to be linked (Kühn et al., 2005; Buzsáki et al., 2012; Telkes et al., 2016; Meidahl et al., 2019), and supports the use of LFP-guided lead placement. A possible explanation for the mismatched hemispheres could be the stability issues in the electrode tip - tissue interface (Amirnovin et al., 2006; Hill et al., 2011; Harris et al., 2016). In one STN presented in Figure 2.2B, although the background activity in center track SUA increases after the border (0 mm), a potential tip failure (i.e., bending or damage to the fine tip of microelectrode that could reduce the high impedance, which is essential to capture SUA) could have prevented the isolation of individual neurons. Since the LFP traces (Figure 2.2D) and DFM (Figure 2.2F) of the same STN show strong activity correlated with intraoperative CT, a technical or hardware issue specific to the tip of the

microelectrode is a distinct possibility. Even without any damage, the SUA tip may not necessarily isolate single neurons at every site (Benazzouz et al., 2002; Weinberger et al., 2006; Sharott et al., 2014) by being too far to the cells or by damaging them (Buzsáki, 2004; Harris et al., 2016). In such instances, the electrophysiologist faces the uncertainty of missing the target or missing the neurons. By contrast, the stainless-steel ring on the shaft where LFPs are recorded has more structural integrity, larger surface and smaller impedance (Lenz et al., 1988; Gross et al., 2006), and captures the oscillatory activity from a population of neurons (Priori et al., 2004; Gross et al., 2006; Buzsáki et al., 2012), thereby limiting the chances of missing the electrophysiological activity (Buzsáki et al., 2012; Priori et al., 2013; Thompson et al., 2014). Supporting the favorability of LFP recordings, we found that among three cases where SUA was the deciding modality but the implantation track had to be modified, two of the final locations agreed with the LFP-based track selection (Figure 2.3A).

Intraoperative electrophysiological recordings for the accurate localization of STN have been a vital step for DBS electrode implantation (Zonenshayn et al., 2000; Sterio et al., 2002; Amirnovin et al., 2006; Gross et al., 2006; Abosch et al., 2013; Campbell et al., 2019). SUA has been the most commonly used electrophysiological signal for targeting (Gross et al., 2006; Abosch et al., 2013; Campbell et al., 2019), which strongly relies on subjective interpretation of single unit firings (Benazzouz et al., 2002; Benabid et al., 2009; Marceglia et al., 2010; Abosch et al., 2013). Recently, there have been reports to ameliorate this disadvantage by identifying and clustering firing types (Kaku

et al., 2019, 2020) or by detecting entry and exit of the STN automatically (Wong et al., 2009; Zaidel et al., 2009; Pinzon-Morales et al., 2011; Valsky et al., 2017; Thompson et al., 2018a). However, the volatile interface stability and increased computational power requirement arising from higher sampling rates might still favor LFPs (Rouse et al., 2011; Buzsáki et al., 2012; Priori et al., 2013; Thompson et al., 2014). Growing literature supports the utility of LFPs in intraoperative mapping (Chen et al., 2006; Przybyszewski et al., 2016; Telkes et al., 2016; Kolb et al., 2017; Lu et al., 2019). Our results also support the use of LFPs intraoperatively for DBS lead implantation. The processing pipeline and real-time visualization tool (supplementary video) presented here can facilitate this process.

The exploration of disease biomarkers for the development of novel technologies such as closed loop DBS have been of great interest lately (Little and Brown, 2012; Priori et al., 2013; Meidahl et al., 2017; Hell et al., 2019). In this regard, LFPs can provide variety of non-binary patterns including power of distinct oscillatory bands and their nonlinear interactions. There is an abundance of studies reporting the response of LFP-derived biomarkers to medication (Foffani et al., 2003; Priori et al., 2004; Marceglia et al., 2006; Kane et al., 2009; Lopez-Azcarate et al., 2010; Özkurt et al., 2011; Ozturk et al., 2019) and DBS (Kühn et al., 2008; Eusebio et al., 2011; McConnell et al., 2012) therapies, as well the correlation between these biomarkers and cardinal symptoms of PD (Kühn et al., 2006; Weinberger et al., 2006; Ray et al., 2008; Lopez-Azcarate et al., 2010; Oswal et al., 2013; Brittain and Brown, 2014;

Ozturk et al., 2019). We and others have previously shown that these patterns can provide utility in contact selection (Ince et al., 2010; Connolly et al., 2015) or targeting the optimal location for DBS implantation (Chen et al., 2006; Thompson et al., 2014; Telkes et al., 2016; Kolb et al., 2017; Lu et al., 2019). Specifically, oscillations in the beta and HFO range and their cross-frequency interactions have been used to pinpoint the “sweet spot” for DBS (Wang et al., 2014; Connolly et al., 2015; Telkes et al., 2016; Horn et al., 2017; van Wijk et al., 2017; Hell et al., 2019). When comparing the selected track with others, we have observed that the bandpowers of beta and HFO oscillations were significantly higher in both dorsal and ventral parts of the STN. Postoperative analyses revealed that the coupling pattern between phase of beta and amplitude of HFO differed in dorsal and ventral territories, similar to previous reports distinguishing both regions with electrophysiology (Rodriguez-Oroz et al., 2001; Theodosopoulos et al., 2003; Zaidel et al., 2009; Telkes et al., 2018). This difference is expected as the dorsolateral STN has been associated with motor functions and exhibited distinct oscillatory/bursting single unit firings whereas ventromedial STN is associated with limbic functions and tonic firings (Abosch et al., 2002; Gross et al., 2006; Zaidel et al., 2010; Thompson et al., 2018a; Campbell et al., 2019; Kaku et al., 2020). Interestingly, we also noted HFOs above STN in three patients (see Figure 2.2E). This activity could be originating from other structures such as thalamus or zona incerta (ZI) (Thompson et al., 2014; Yang et al., 2014; Lu et al., 2019; Meidahl et al., 2019). Previous work has shown that dorsolateral STN and ZI stimulation provides the

greatest improvement in PD motor symptoms (Gourisankar et al., 2018), which correlates with our observation. However, lack of activity in the bulk of our recordings begs for further investigation regarding the out-of-STN oscillatory activity in more patients.

In this report, we assessed the functional utility of LFP-based lead implantation against the gold standard SUA method using intraoperative online signal processing and compared these modalities in terms of clinical outcomes. Our results suggest that the LFP oscillations can be a more stable, less processing-intensive method that can be integrated in the intraoperative workflow together with SUA-based mapping, without affecting the surgical procedure. In addition to the functional role of LFPs in intraoperative target mapping, the fact that LFPs can also be recorded from the chronic DBS lead after the surgery is another potential advantage that might guide therapeutic programming to a higher efficacy and efficiency. Here, we provided results of a pilot study with ten patients. Future clinical trials with more subjects will be needed to establish if LFPs can become the standard of care for intraoperative mapping.

3 Subband Power Modulations and Cross Frequency Coupling of STN-LFPs in Medication OFF and ON States

This chapter has been published and its content is used with permission from the publisher (Ozturk et al., 2019).

3.1 Overview

Cross-frequency coupling has been reported in the subthalamic nucleus of patients with Parkinson's disease, but its significance and functional role are still not well understood. This study investigates pharmacological modulations of subthalamic oscillations and their non-linear cross-frequency interactions across three consecutive cycles over unique 24-hour-long recordings.

We recorded local field potentials three weeks post-operatively from externalized leads in nine patients and correlated the neural patterns with improvements in motor signs over three medication intake cycles. We used two modalities to assess symptoms in the unmedicated OFF and the levodopa-induced motor ON state: a subsection of the Unified Parkinson's Disease Rating Scale and a keyboard tapping score measuring bradykinesia.

In the OFF state, the amplitude of high-frequency oscillations in 200-300Hz range was coupled with the phase of low-beta (13-22Hz) in all patients. After transition to the ON state, three distinct coupling patterns were observed among subjects. Amongst these, patients showing ON coupling between high-beta (22-30Hz) and high-frequency oscillations in the 300-400Hz range had

significantly greater improvement in bradykinesia, according to the keyboard scores.

Observing diminished coupling in the ON state, previous studies have hypothesized that the sole existence of coupling in the subthalamic nucleus has an “impeding” effect on normal processes, and thus it was considered it to be pathological. In contrast, our observation of ON state coupling at distinct frequencies associated with the improvements in motor features suggest that the underlying mechanism of coupling might have impeding or enhancing effects depending on the coupled frequencies.

3.2 Introduction

The identification of neuro-biomarkers in Parkinson’s disease (PD) that can describe motor manifestations is important for both clinical neuroscience and the neuromodulation field. Such biomarkers can help objectively assess the patient’s clinical state and facilitate the development of individualized therapies. In particular, local field potential (LFP) recordings from the subthalamic nucleus (STN) have revealed the existence of distinct frequency bands that have been correlated to the motor impairment in PD (Brown et al., 2001; Levy et al., 2002; Foffani et al., 2003; Priori et al., 2004; Kane et al., 2009; Lopez-Azcarate et al., 2010). Furthermore, modulation of these oscillations in response to dopaminergic medication (Brown et al., 2001; Priori et al., 2004; Kühn et al., 2006; Weinberger et al., 2006; Ray et al., 2008) along with motor improvement suggests that they have potential to serve as neurophysiological biomarkers.

Consequently, we and others have previously discussed the importance of LFP oscillations and their functional role in understanding and treating movement disorders (Brown and Williams, 2005; Ince et al., 2010; Little et al., 2013; Priori et al., 2013; Thompson et al., 2014).

Among all the frequency ranges, the beta (13-30 Hz) band has attracted the most attention, and the presence of exaggerated beta band activity is widely accepted as the leading indicator of akinetic Parkinsonian features (Ray et al., 2008; Oswal et al., 2013; Brittain and Brown, 2014). STN oscillations in higher frequency bands have also been ascribed relevance to PD clinical manifestations (Foffani et al., 2003; Kane et al., 2009). Initially, high-frequency oscillations (HFOs) above 300Hz were reported in the resting medicated (ON) state (Foffani et al., 2003) and were proposed as a marker for the pro-kinetic state (Foffani et al., 2003; Oswal et al., 2013). However, more recent work has reported HFOs at a lower frequency range (200-300Hz) in the unmedicated (OFF) state of Parkinsonian patients as well (Lopez-Azcarate et al., 2010; Özkurt et al., 2011; van Wijk et al., 2016), and that the lower-range HFO shifts to frequencies higher than 300Hz following dopaminergic treatment, confirming the earlier findings of Foffani *et al.*(Foffani et al., 2003). Together these observations suggest that the presence of HFO is not a marker of the motor state, but rather the change in the center frequency may be more important.

Accordingly, the non-linear interactions between low and high frequency bands have gained increasing interest. Recent studies have demonstrated that the amplitude of HFOs and the phase of beta oscillations from the STN of PD

patients are coupled (Lopez-Azcarate et al., 2010; Özkurt et al., 2011; Yang et al., 2014; van Wijk et al., 2016; Shreve et al., 2017). In unmedicated patients, the cross-frequency coupling (CFC) has consistently been shown to occur between 20Hz in the beta and 250Hz in the HFO range; whereas in medicated patients, the coupling strength diminishes dramatically, and its peak shifts either in the beta (Lopez-Azcarate et al., 2010) or HFO (Özkurt et al., 2011; van Wijk et al., 2016) ranges. Although a correlation between coupling in the OFF state and severity of akinetic symptoms was reported by Lopez-Azcarate *et al.*(Lopez-Azcarate et al., 2010), the exact nature and significance of coupling—especially in the ON state—has yet to be fully addressed.

Here, we sought to explore the pharmacological modulation of LFP subbands as well as the coupling between them, in nine patients with PD through a prolonged monitoring period of 24 hours. We show that different patterns of CFC exist in the STN in OFF and ON states, and importantly, that distinct cross-frequency relationships in the ON state can distinguish between patients with better levodopa-induced motor improvement.

3.3 Patients and Methods

3.3.1 Patients and Medication

Nine patients with idiopathic PD who underwent unilateral DBS electrode implantations in the STN at Fairview Hospital of the University of Minnesota participated in the study. The patients were unilaterally implanted to treat the more severely affected side first. Data analysis was performed at the University

of Houston. The study was approved by the Institutional Review Board of the University of Minnesota and the University of Houston, and all patients provided informed consent for participation.

The demographics and prescribed medication levels of the patients are provided in Table 1. In an effort to minimize variability, immediate-release levodopa was administered to each patient for the ON state testing, with the levodopa-equivalent dose calculated from their routine out-patient medication schedule (Ince et al., 2010).

Table 3.1: *Subject demographic information.*

Pt	Gender	Age	Side	Mean Keyboard Scores (OFF/ON)	Mean Bradykinesia Subscore (OFF/ON)	Mean Total UPDRS Subscores (OFF/ON)	L-dopa Dose (mg)	Dyskinesia
1	M	70	Left	124.7 / 227.3	9 / 3.7	18 / 5.7	200	None
2	M	43	Left	39.2 / 126.8	13 / 0.3	26.3 / 0.3	500	None
3	M	61	Right	87.3 / 219.3	11.7 / 1	17.3 / 3.7	250	Mild
4	M	68	Left	94.3 / 151.5	7.3 / 1.5	12 / 3.3	400	Mild
5	F	62	Right	99.3 / 147.7	12.7 / 2.3	26 / 3.7	200	None
6	**M**	**58**	**Right**	**113.5 / 110.2**	**11.3 / 6**	**17.3 / 9.7**	**150**	**None**
7	F	69	Right	107.8 / 177.5	12 / 0.7	18.5 / 1.5	150	None
8	M	39	Left	70.2 / 112.8	13.3 / 2	24.7 / 4.7	200	Mild
9	**M**	**54**	**Right**	**92 / 103.8**	**9.5 / 2.5**	**15.3 / 5**	**300**	**None**

UPDRS: Unified Parkinson's Disease Rating Scale
OFF: Motor state without medication
ON: Motor state with dopaminergic treatment

In Table 3.1, the keyboard scores are reported as average taps per 30 seconds. The UPDRS subscore has a maximum value of 32. The bradykinesia subscore has a maximum value of 16. All behavioral scores provided are the

average of assessments from three trials. Levodopa dose is the equivalent pre-surgery dose of all dopaminergic medications taken by each patient and was calculated using the formula given in Ince et al. 11. Note that Pt6 and Pt9 (marked bold) were given additional 50mg levodopa after 20 and 40 minutes respectively in their first trials due to no clinical response to the initial dose (the values in the table are the total amount given in the second and the third trials).

3.3.2 Surgery and Post-operative Recordings

The study timeline is provided in Figure 3.1. A quadripolar DBS lead (Model #3389, Medtronic, MN) was placed in the target region of the STN per standard clinical procedure as described previously (Abosch et al., 2002).

Three weeks after the implantation, the electrode leads were externalized as described earlier (Ince et al., 2010). Prior to the surgical placement of the implantable pulse generator (IPG), the LFPs were recorded from the externalized lead in the epilepsy monitoring unit (EMU) with a wearable amplifier (XLTEK-EMU40, Natus, CA) in monopolar configuration for ~24 hours continuously. The signals were digitized at 1024Hz sampling frequency and 16-bit ADC resolution with an anti-aliasing filter at 400Hz. The data were annotated appropriately either in real time or offline by reviewing synchronized video and bipolar electromyogram (EMG) recordings obtained from upper and lower limbs.

Recordings began in the morning (at least 12 hours after the last dose of any PD medication) with a 30-minute baseline recording in the motor OFF state, followed by administration of the calculated dose of levodopa (annotated as

"Med IN"). Subjects were instructed to report when they felt that their medications had kicked in, in terms of motor function (marked as "Verbal ON"). When symptoms returned and the effects from the prior dose had completely worn off, the cycle was repeated two more times. As depicted in Figure 3.1, this cycle is referred to as a "trial". Hence, the entire 24-hour recording for a patient included three trials. The first two trials were on the first day and the third one was in the next morning before IPG implantation.

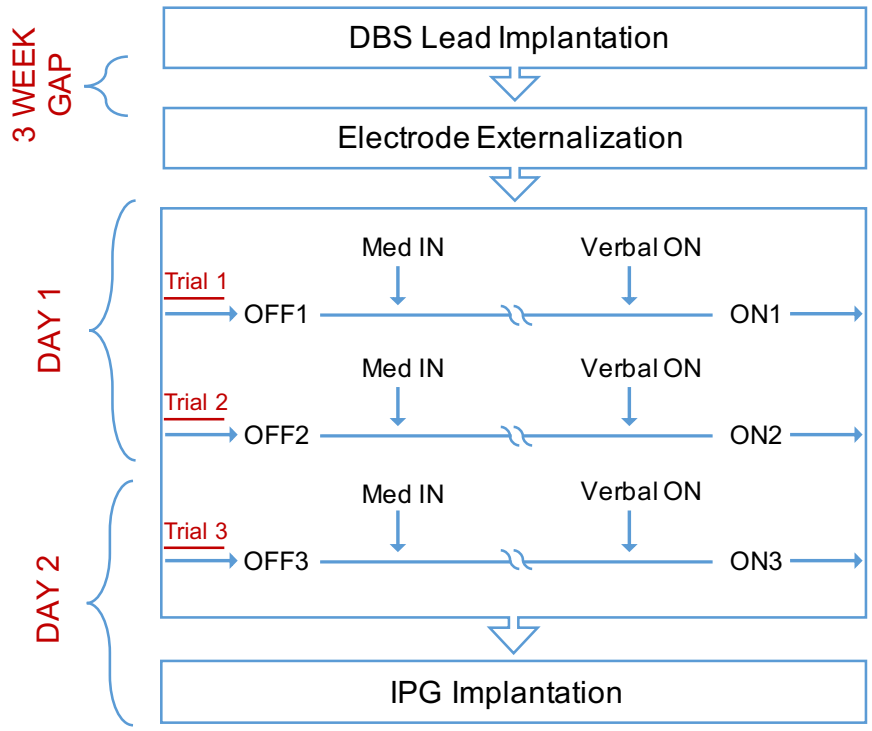

Figure 3.1: *Study design diagram outlining the timing of the medication intake and recording periods.*

3.3.3 Clinical and Behavioral Assessment

All patients were assessed within 30 minutes before the medication intake and within 30 minutes after their verbal confirmation of transition to the ON state. A subsection from the motor section of Unified PD Rating Scale

(UPDRS) was used for the unilateral evaluation of the patients: hand and foot tremor (UPDRS item 20); upper and lower extremity rigidity (UPDRS item 22); and finger tapping, hand open/close, hand pronation/supination and leg agility (UPDRS items 23-26). The clinical assessment was performed for all trials and states separately.

Together with the UPDRS testing, a computer-based keyboard task was performed as an objective behavioral measurement, alternative to the bradykinesia score (Tavares et al., 2005). The task was to press left and right arrow keys on a computer keyboard sequentially as fast as possible for 30 seconds, using the index and middle fingers. The task was performed twice with a 1- to 2-minute break in between and the total number of key presses for each run was saved on the computer for further analysis. For the correlation statistics between keyboard task and neural measures, the improvement in keyboard tapping was represented as the log-scale ratio of ON and OFF state performance to reduce the skewness of the distribution.

In the following analyses, only keyboard and bradykinesia subscore results are reported in detail, due to their comparability. More details on the correlations involving the UPDRS subscores can be found in Table 3.3.

3.3.4 Signal Processing

Signals were processed in MATLAB version R2014a (Mathworks, MA). The LFP data for each trial was exported, starting 30 minutes before the medication intake and extending up to 120 minutes after the verbal confirmation

of the ON state. Zero phase finite-impulse response filters were employed for pre-processing. The raw data was high-pass filtered at 1.5Hz to remove DC offset and the baseline wander, and notch filtered at 60Hz and its harmonics to eliminate the power line noise. After preprocessing, monopolar LFP channels were converted to bipolar derivation by subtracting adjacent channels.

In order to visualize spectro-temporal dynamics of the pharmacologically modulated LFPs over long duration, artifact-rejected time-frequency (TF) maps were generated using short time Fourier transform (Thompson et al., 2018b). The TF maps were visualized for each bipolar pair of each trial to investigate patient specific transitions from OFF to ON state. The power spectral density (PSD) of each state was estimated from manually selected 10-minute-long segments with minimal movement and artifact by scrutinizing the video and EMG recordings. The peak frequencies and the relative band powers of theta-alpha (4-12Hz), beta (13-30), gamma (70-90Hz), slow HFO (sHFO, 200- 300Hz) and fast HFO (fHFO, 300-400Hz) ranges were obtained from these estimates. Additionally, the beta band was further divided into low and high beta based on the peaks observed (13-22Hz and 22-30Hz) (Lopez-Azcarate et al., 2010; Oswal et al., 2016; van Wijk et al., 2016) to prevent having multiple peaks per band (Figure 3.2). Prior to obtaining band powers in each trial, PSDs were normalized with the average power between 120-160Hz computed from the OFF state, due to consistent peak-freeness of this region. Similar normalization techniques were previously employed (Foffani et al., 2003; Hirschmann et al., 2016) to eliminate the variations due to subject dependent parameters (e.g.,

electrode impedance) and thus, have comparable power levels among subjects for averaging and statistical analyses. As different frequency bands (e.g., beta, gamma, HFO) peaked in different contact pairs, the average of normalized spectra from three bipolar derivations was used for band power calculations in order to ensure that no peak is excluded from the analysis (van Wijk et al., 2016). The log-scale powers for individual bands and sHFO/fHFO power ratio (Özkurt et al., 2011; Hirschmann et al., 2016) were then extracted from average spectra for the correlation analyses with behavioral data.

Figure 3.2 illustrates how the cut-off between low and high beta was determined. Three subjects with one peak in the beta range ('1-peak' group) had an average peak frequency in the low beta band (18.5Hz). Those subjects with two peaks in the beta range had one peak in the low (mean peak frequency: 16.7Hz) and another in the high beta band (mean peak frequency: 25Hz). The high peak was significantly different from the other two distributions (p=0.02, Mann-Whitney U test). Therefore, the beta band was further divided into low-beta (13-22Hz) and high-beta (22-30Hz).

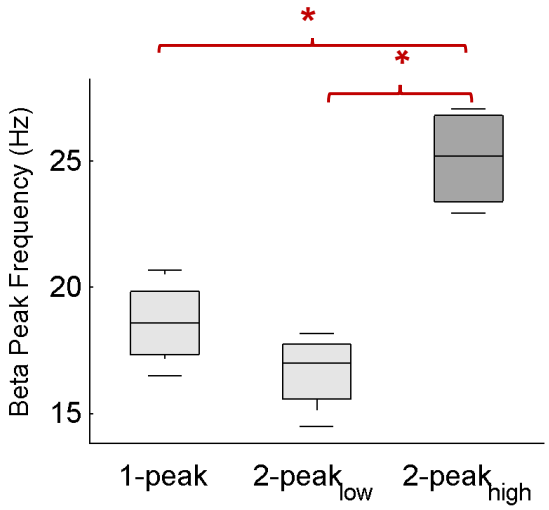

Figure 3.2: *Peak frequency distribution for beta band.*

CFC was estimated using a method based on the phase-locking principle (Cohen, 2008; Penny et al., 2008). The 10-minute long segments selected for PSD estimation were used for calculation of CFC as well. The comodulograms

representing the CFC have amplitude frequency axis from 190 to 410 with 10Hz steps and 50Hz filter bandwidth and phase frequency axis from 4 to 36 with 1Hz steps and 3Hz filter bandwidth. These parameters were selected after observing the average spectra. Since the peak coupling did not always appear in the same contact pair of the DBS electrode in the OFF and ON states (Figure 3.3), the comodulograms were averaged over all contact pairs to obtain a single map per trial per state (van Wijk et al., 2016). For inter-patient comparability, the comodulograms from each trial were normalized by the mean value of the OFF-state map of the same trial. In each comodulogram, the coupling values in 13-22 Hz and 200-300 Hz, 4-12 Hz and 300-400 Hz and 22-30 Hz and 300-400 Hz were averaged to obtain mean low-beta – sHFO, theta-alpha – fHFO and high-beta – fHFO coupling strength respectively. In order to group trials with similar coupling patterns, a k-means clustering (Duda et al., 2000) with squared Euclidean distance measure was used.

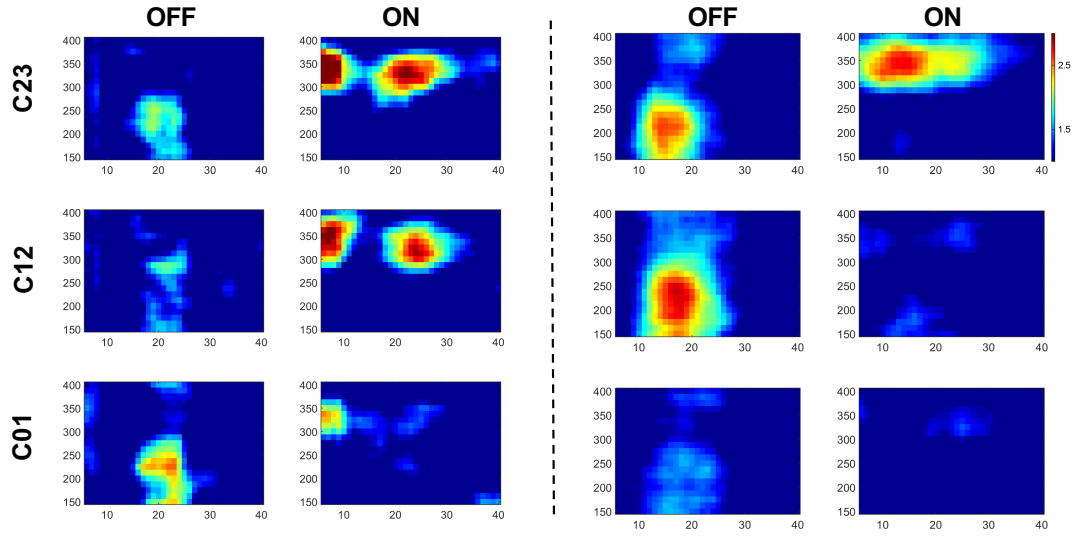

Figure 3.3: *Coupling strength per contact pairs show distinct variations between pharmacological states.*

Figure 3.3 displays representative OFF and ON coupling maps for Pt2 (left) and Pt10 (right). Due to spatial variability in appearance of neural markers, we averaged spectra and coupling maps over contact pairs for each trial and state, instead of picking one contact pair. Color scale is consistent across maps.

3.3.5 Statistical Analysis

SAS Version 9.4 (SAS Institute, NC) and MATLAB version R2014a (Mathworks, MA) were used for statistical analyses. A mixed linear model (PROC MIXED procedure in SAS) was used to examine linear associations between neural and behavioral measures on a trial by trial basis, and for analysis of mean differences across trials in the OFF and ON state. A mixed linear model was selected because of its ability to account for non-independence across observations made on the same individual and to accommodate imbalance in repeated measures data (Wolfinger and Chang, 1995; Algina and Swaminathan, 2011). This approach is different from the traditional mixed models in the way that it does not involve the use of expected mean squares but attempts to model the residual covariance matrix. For repeated measures analyses, the mixed model approach used in PROC MIXED is more flexible and more widely applicable than either the univariate or multivariate approach since it provides a larger class of covariance structures and a better mechanism for handling missing trials (Wolfinger and Chang, 1995; Algina and Swaminathan, 2011). Therefore, by using PROC MIXED, one can use all available data in the analysis instead of ignoring subjects with missing data, hence having more

statistical power. Although the effects of state, trial, and trial by state interaction were examined through the univariate and multivariate approaches to the repeated measures as well, those effects were not reported due to redundancy, even though they are consistent with the mixed model findings in terms of significance.

The variables entered the model were the neural and behavioral measures referred in the manuscript, namely, bandpowers (e.g., low-beta, high-beta, gamma, sHFO, fHFO) and the behavioral performance measurements (e.g., UPDRS scores, keyboard taps). The only effects in the models are state, trial, and trial by state for the analyses of the repeated measures. There was no adjustment for multiple comparisons since the effects of state, trial, and the interaction are typically each tested at .05 as these represent the design factors in the repeated measures experiment. Additionally, there was no adjustment for the number of dependent variables since each neural measure is viewed as its own experiment for type-I error control.

In the mixed models used to estimate the correlation, only the measure that is being correlated with the outcome is in the model. The mixed model is used as an approach to estimate the “total” correlation which consists of within person and between person parts. The between person component is the correlation between the means; the within person component removes the association between the means and focuses on the deviations around the person level means. To estimate correlations, the mixed linear model was used to fit a simple regression model for standardized variables. In this model, the

Table 3.2: *Output of mixed model statistics analysis regarding the state and trial effects on neural and behavioral measures.*

Outcome	State				Trial				State by Trial Interaction			
	Num Df	***Den Df***	***F***	***p***	***Num Df***	***Den Df***	***F***	***p***	***Num Df***	***Den Df***	***F***	***p***
bradykinesia	1	8	73.99	<.0001	2	15	0.50	0.6177	2	14	0.32	0.7284
bradykinesia+ rigidity	1	8	56.45	<.0001	2	15	1.28	0.3061	2	14	0.68	0.5247
keyboard	1	8	13.90	0.0058	2	14	1.47	0.2625	2	13	0.19	0.8284
tremor	1	8	10.09	0.0131	2	15	0.10	0.9043	2	14	0.05	0.9483
UPDRS	1	8	52.75	<.0001	2	15	0.38	0.6907	2	14	0.97	0.4014
fHFO power	1	8	8.49	0.0195	2	15	1.75	0.2068	2	14	1.46	0.2656
gamma power	1	8	6.75	0.0317	2	15	2.09	0.1583	2	14	2.31	0.1357
high-beta power	1	8	1.28	0.2907	2	15	0.57	0.5788	2	14	0.63	0.5446
high-beta – fHFO CFC	1	8	5.42	0.0483	2	15	0.10	0.9052	2	14	0.01	0.9892
low-beta power	1	8	8.55	0.0192	2	15	1.52	0.2499	2	14	0.25	0.7789
low-beta – sHFO CFC	1	8	29.01	0.0007	2	15	0.92	0.4212	2	14	0.05	0.9482
sHFO power	1	8	1.33	0.2828	2	15	1.85	0.1921	2	14	2.10	0.1591
theta-alpha power	1	8	11.38	0.0097	2	15	2.83	0.0905	2	14	0.61	0.5563

slope for the predictor is the correlation because we have one regression coefficient. The t-statistic associated with the regression coefficient is the ratio of the estimate to its standard error and the p-value associated with the t-statistic is the reported p-value. The correlations reported take into account both within

and between patient interactions and give appropriate standard errors due to the repeated measures aspect of the data – i.e., the fact that each person contributes multiple observations to the association between the predictor and the outcome. The peak frequencies and the mean bandpower changes were contrasted between states using non-parametric Wilcoxon signed-rank test for paired samples.

3.4 Results

Nine unilateral recordings with three medication trials per patient were included in this study, constituting 27 OFF and 27 ON states in total. The neural data from one trial of one patient was corrupted and thus it was completely excluded from further analysis. Another trial had missing neural data in the ON state only. There were significant ($p<0.05$) differences detected between OFF and ON states for all behavioral and all neural measures except high-beta and sHFO. However, trial and state-by-trial effects were not significant ($p>0.05$), as the response of a patient was consistent across trials (Table 3.2). Thus, findings will not be contrasted across trials. Data from all trials are included in all analysis as repeated measurements, unless otherwise stated.

The mean time gap between the medication intake and verbal ON confirmation was 58±12 minutes. As representative examples, the spectral dynamics of LFPs over the transition from OFF to ON state with related clinical and behavioral data for two patients are provided in Figure 3.4. While both patients improved in terms of their motor signs, these patients demonstrated

opposite behavior in the beta band whereas their HFO and coupling characteristics were similar.

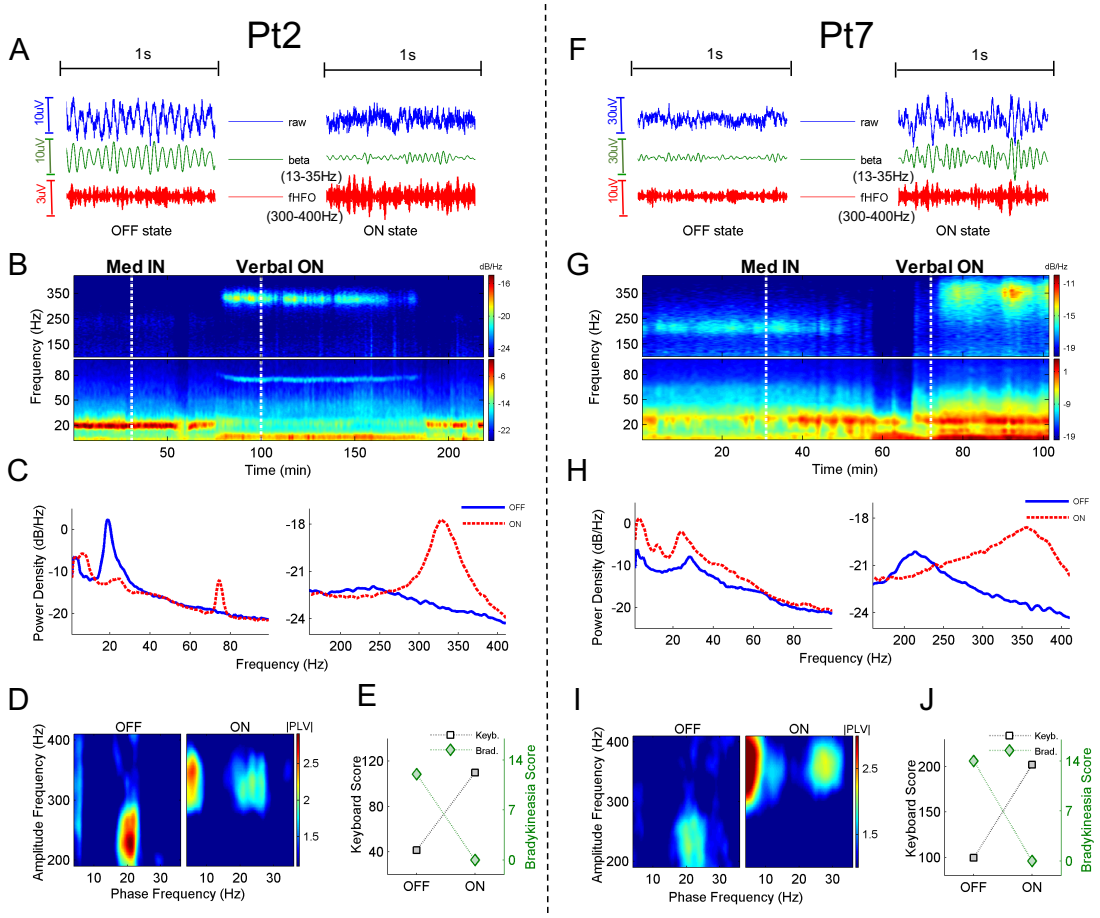

Figure 3.4: *Summary of neural and behavioral data from representative trials from Pt2 and Pt7.*

The description of each panel in Figure 3.4 is: **(A, F)** Representative raw LFP data as well as beta and fHFO filtered signals in the OFF and ON states. Although there is an increase in fHFO activity in both patients after transition to the ON state, LFP recordings from Pt2 demonstrate a clear suppression in beta band whereas Pt7 has an overall beta band enhancement. **(B, G)** Time evolving LFP spectra from the same patients **(C, H)** Normalized OFF-ON spectra estimated using 10-minute long segments. In addition to the previous

observations, a narrow band gamma enhancement between 70-90Hz is seen concomitant to fHFO in PT2. **(D, I)** Cross-frequency coupling maps from 10-minute segments in the OFF and ON states. Although the strength varies, the pattern of coupling is similar between the two patients. Transition to the ON state causes a change in the coupled frequencies in both beta and HFO ranges. **(E, J)** UPDRS bradykinesia subscore and keyboard score changes upon transition to ON state. Both patients had marked improvement in their keyboard and contralateral bradykinesia scores, indicating an improvement in motor symptoms. Pt7 was noted as an outlier due to the unusual beta enhancement in the ON state LFP recordings, despite obvious motor improvement.

3.4.1 Behavioral Response

Bradykinesia and keyboard scores were significantly different between the states (mean OFF=11.2, mean ON=2.5, $p<0.001$; mean OFF=91.6, mean ON=152.3, $p=0.002$ respectively). However, as shown in Table 1 and Figure 3.5, the response in bradykinesia and keyboard scores did not match in every case. Although the UPDRS bradykinesia subscore revealed an improvement for Pt6 and Pt9, they showed minimal to no improvement according to their keyboard task performance. Therefore, these patients might not have experienced a true ON state according to the computer-based measurements. Later, we show that these patients can be isolated/predicted based on their CFC patterns.

The description of each panel in Figure 3.5 is: **(A)** Keyboard task score: average of the number of alternating keystrokes in two 30-second executions. Mean OFF=91.6, mean ON=152.3, p=0.002, 85±83% increase, Wilcoxon signed rank test. **(B)** Bradykinesia UPDRS: subitems 23-26. Mean OFF=11.2, mean ON=2.5, p<0.001, 78±22% decrease, Wilcoxon signed rank test **(C)** The keyboard and bradykinesia score difference between states (ON score - OFF score) for individual patients and trials. The red line marks the no change level. Bradykinesia scores improved in all patients after transitioning to the ON state, whereas keyboard scores worsened in some trials for Pt6 and Pt9. Note that one trial (Pt4) was excluded due to corruption in the recordings and another trial (Pt3) was missing keyboard assessment in the ON state due to time limitations. The markers indicating bradykinesia score have overlapped in patients 1, 2 and 8, due to having the exact same value for multiple trials.

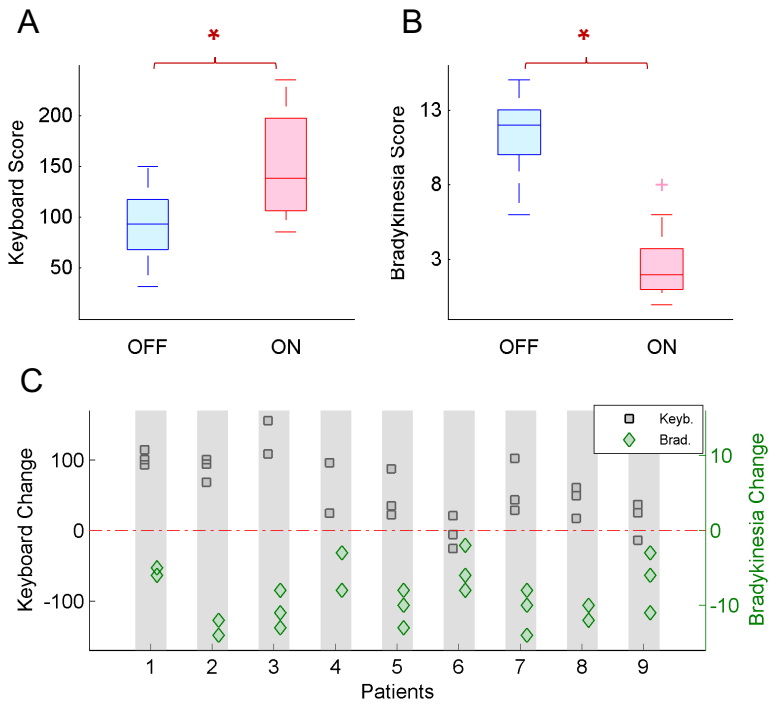

Figure 3.5: *Contrast of clinical and behavioral data in OFF and ON states.*

3.4.2 Modulations of LFP Subbands

The grand averages of time-varying spectral changes for a 60-minute period centered around the medication intake and verbal ON response are presented in Figure 3.6A. The grand average spectra in each state is also provided in Figure 3.6B. Spectral analysis of LFPs in the OFF and ON states revealed distinct peaks in theta-alpha, beta, gamma and HFO bands. The OFF state was characterized by an exaggerated activity in the low-beta and sHFO bands. After the transition to the ON state, low-beta band activity was suppressed and the HFO peak shifted from sHFO to fHFO range (Figure 3.6D) together with a sharply localized peak in the gamma range in six of the patients (e.g., Figure 3.4C). The theta-alpha band was also enhanced in seven patients. The mean change in the bandpowers from OFF to ON state is summarized in Figure 3.6C.

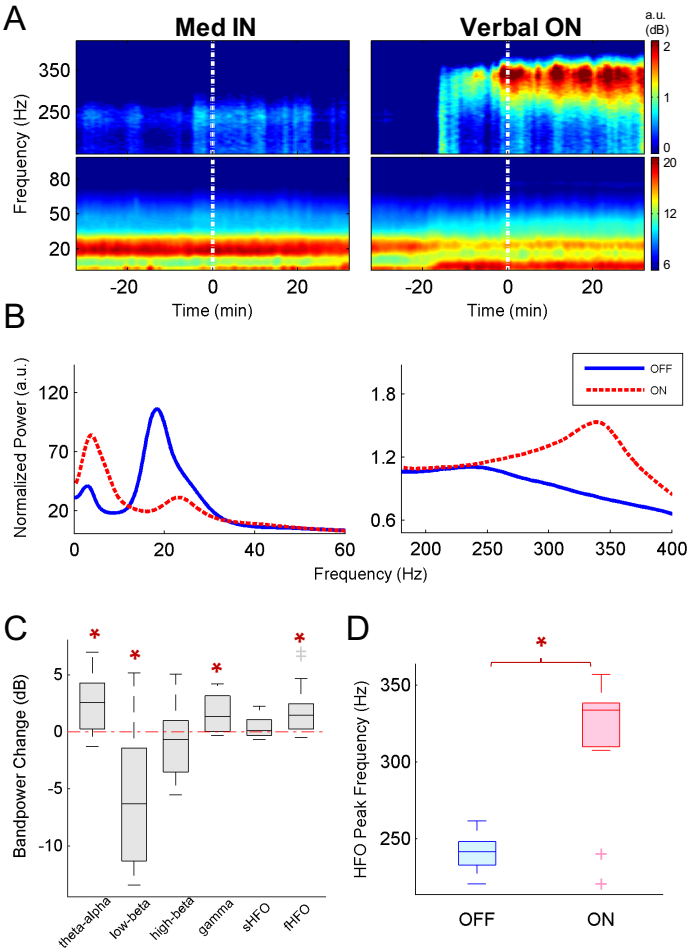

Figure 3.6: *Subband power and HFO peak frequency changes after the administration of dopaminergic medication*

The description of each panel in Figure 3.6 is: **(A)** Grand average of 1-hour-long normalized time-frequency maps aligned with levodopa administration and verbal confirmation of ON state onsets. **(B)** Grand average of normalized spectra, representing spectral content of the OFF and ON state LFPs. **(C)** Change in the bandpowers averaged over trials with OFF to ON state change. The red line represents no change level. Except high-beta and sHFO, all bands have significantly changed after the transition to the ON state (mean change for theta-alpha: 2.6 dB, low-beta: -6.5 dB , gamma: 1.5 dB, fHFO: 1.8 dB, '*' denotes significant change, $p<0.01$, Wilcoxon signed rank test). As shown in HFO range spectra in Figure 3.6B, despite having a distinct peak in the OFF state, the band power of the sHFO region was not significantly different between the states, likely due to masking from the wideband fHFO in the ON state. Thus, normalized power of HFO may not be a suitable metric for investigating its role. Alternatively, the ratio between sHFO and fHFO (i.e., sHFO/fHFO bandpower ratio for OFF and ON states) can be utilized to obtain a relative measure for each motor state as proposed previously (Özkurt et al., 2011; Hirschmann et al., 2016). **(D)** HFO peak frequencies from spectra – peaks at 241±12.6 Hz in the motor OFF state and at 306±49.4 Hz in the ON motor state ($p<0.02$, Wilcoxon signed rank test). The two outliers are Pt6 and 9, whose motor symptoms did not improve according to the keyboard task score (Figure 3.7).

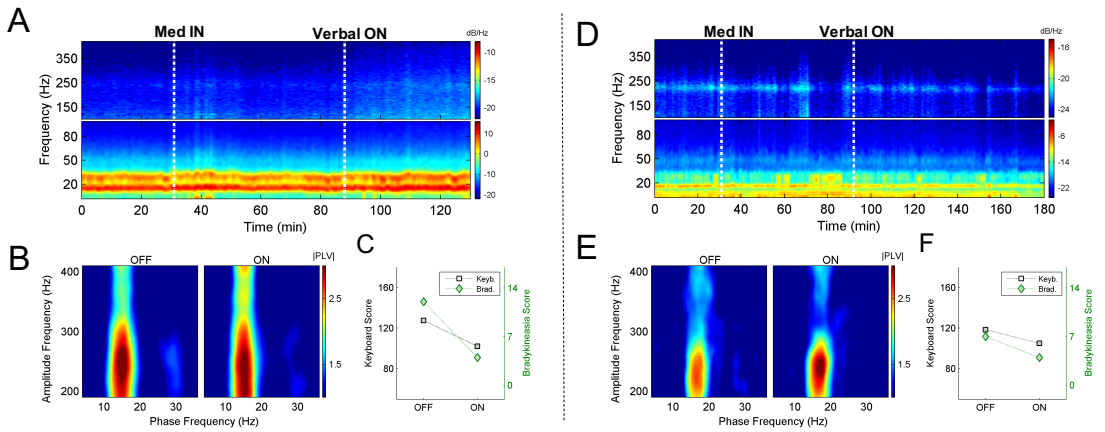

Figure 3.7: *Representative trials for patients without improvement based on keyboard assessment, from Pt6 (left column) and Pt9(right column)*

The description of each panel in Figure 3.7 is: **(A, D)** Time evolving LFP spectra including 30 minutes before the medication intake and at least 30 minutes after the verbal confirmation of ON state. **(B, E)** Cross-frequency coupling maps in the OFF and ON states. The ON state pattern is in the same cluster as the OFF state, indicating a lack of change in the locked frequencies. **(C, F)** UPDRS bradykinesia subscore and keyboard score changes upon transition to ON state. Both patients appear to have marked improvement in contralateral bradykinesia scores, but not according to keyboard task.

3.4.3 Cross-frequency Coupling

The grand average coupling maps in the OFF and ON states are provided in Figure 3.8A. The comodulograms related to the OFF state consistently peaked within the low-beta – sHFO range (18.8±2.2 Hz and 243.3±15.8 Hz, Figure 3.8B) in all subjects indicating that the phase of the low beta band modulated the amplitude of sHFO. In the ON state, the coupling

between low-beta – sHFO vanished and moved to the fHFO range. In particular, the amplitude of fHFOs (354.3±9.8 Hz) were modulated by the phase of theta-alpha (6.5±2.43 Hz) and high-beta (26.2±1.3 Hz) oscillations.

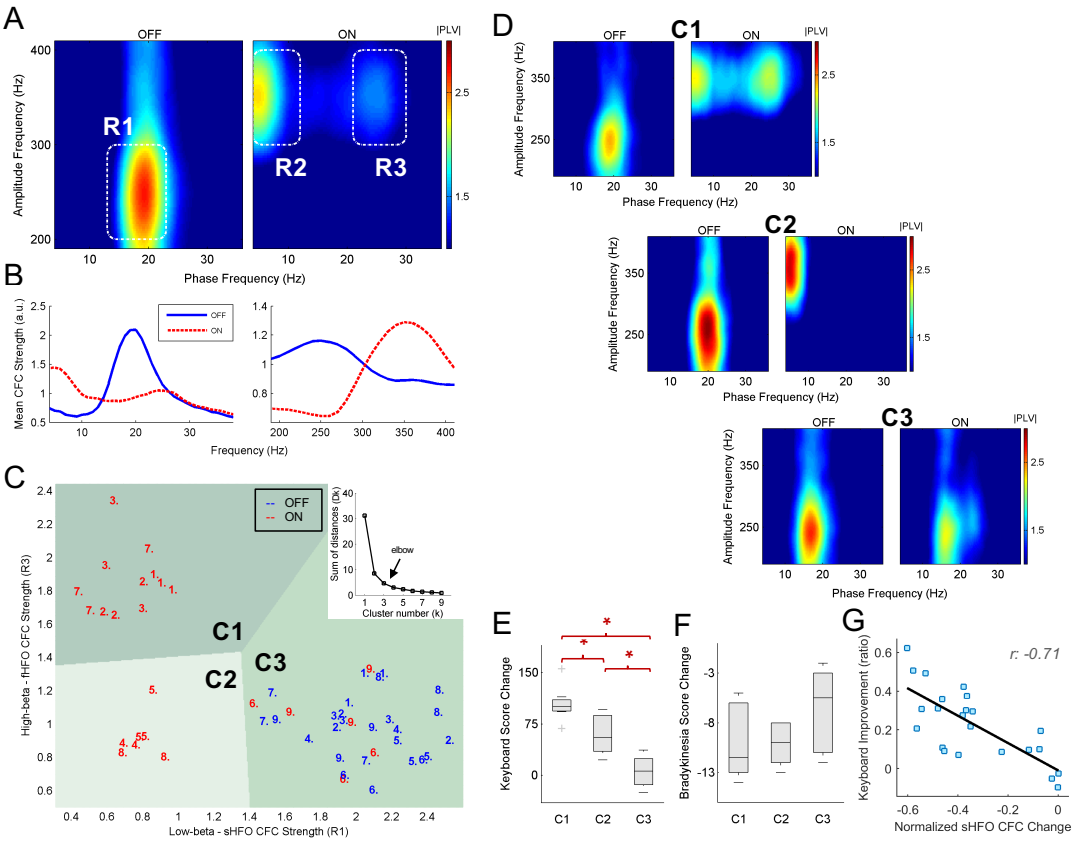

Figure 3.8: *Analysis of the beta-HFO coupling indicates distinct CFC patterns in the medicated state.*

In order to investigate the variability of these coupling patterns among all subjects across trials, the CFC between beta and HFO ranges in the OFF and ON states are visualized as a scatter plot in Figure 3.8C. After employing a k-means clustering method and selecting the k value by elbow method (Figure 3.8C, indent), interestingly, the data formed three clusters: C1, C2 and C3. The average CFC patterns of clustered patients are provided in Figure 3.8D. Two of these clusters (C1 and C2) included ON state trials only. The third cluster (C3)

included all trials from the OFF state and six trials from ON state. It was noted that each patient follows one of the ON coupling patterns consistently. More importantly, the patients in cluster C1 with high-beta – fHFO coupling had significantly greater improvement in their keyboard scores than the rest of the patients whereas the patients whose ON state coupling was in cluster C3 (Pt6 and Pt9) showed little to no improvement in keyboard tapping ($p<0.01$, Figure 3.8E). Bradykinesia scores failed to show any significant difference between these neural data driven clusters (Figure 3.8F).

The description of each panel in Figure 3.8 is: **(A)** The grand average of CFC response in the OFF and ON states. Three regions depicted as R1, R2 and R3 are averaged to obtain low-beta – sHFO, theta-alpha – fHFO and high-beta – fHFO coupling strength values respectively. **(B)** The average CFC strength across beta and HFO frequency ranges. The plot on the right and left are obtained by averaging the OFF and ON maps over x and y axes respectively. The peaks in the average comodulograms shown here are similar to the LFP spectra shown in Figure 3.6B, especially in the <40 Hz range, indicating a possible relationship between bandpower and coupling strength. **(C)** CFC strength obtained from R1 and R3 regions are presented in a scatter plot according to the clinical state of the patient. Each point represents a trial corresponding to the patient index. K-means clustering formed three clusters: C1, C2, C3. OFF state was uniquely represented in C3 whereas ON state was distributed across all three clusters. The optimal k value is chosen by inspecting the summation of intra-cluster distance (Dk) for different k values. In particular,

we gradually increased k from 1 to 9 and observed the curvature of Dk with respect to different k values. The optimal cluster number generally corresponds to the index (elbow of the curve) when adding more clusters doesn't contribute much to the reduction of Dk. This observation resulted in k=3. **(D)** Average coupling maps of patients in each cluster. **(E, F)** Group comparison of behavioral data from keyboard and bradykinesia scores respectively (* indicates significance $p<0.01$, mixed model). Keyboard scores reveal that patients in C1 had the greatest improvement (mean 104.2 strokes) followed by C2 (mean 58.6 strokes), and the patients whose ON state coupling was in C3 showed minimal to no improvement (mean 5.8 strokes). Bradykinesia scores failed to show significant differences between groups. **(G)** Correlation between the ratio of ON and OFF keyboard scores vs normalized low-beta – sHFO CFC strength change ($r=-0.71$, $p< 0.001$). Each square represents a trial, but the correlation value is obtained with mixed model statistics.

3.4.4 Correlations Between Clinical Parameters and Neural Data

In order to explore the predictive power of LFP features, the correlation between motor improvement and the neural data was estimated (Table 3.3). It was observed that the improvement in keyboard score always correlated with neural patterns better than the bradykinesia subscore. Specifically, low-beta – sHFO coupling change was associated with the highest correlation with the improvements (Figure 3.8G, $r=-0.71$, $p<0.001$) where low-beta power had correlation value of 0.5 ($p=0.03$).

Table 3.3: *Pairwise correlations between improvement in behavioral scores and changes in neural markers.*

	Keyboard Tapping	Bradykinesia	Bradykinesia + Rigidity	Tremor	Total UPDRS Subscore
theta-alpha power	r=0.47, p=0.04	r=0.35, p=0.07	r=0.35, p=0.04	r=0.22, p=0.08	r=0.34, p=0.02
low-beta power	r=-0.5, p=0.03	r=-0.2, p=0.37	r=-0.4, p=0.06	r=-0.06, p=0.75	r=-0.25, p=0.2
gamma power	r=0.59, p=0.02	r=0.29, p=0.26	r=0.37, p=0.12	r=0.33, p=0.17	r=0.17, p=0.35
sHFO power	r=-0.01, p=0.96	r=-0.06, p=0.77	r=-0.12, p=0.28	r=-0.11, p=0.5	r=-0.21, p=0.24
fHFO power	r=0.29, p=0.35	r=0.17, p=0.58	r=0.31, p=0.23	r=0.33, p=0.14	r=0.1, p=0.65
sHFO/fHFO power ratio	**r=-0.54, p=0.01**	r=-0.37, p=0.1	r=-0.37, p=0.06	r=-0.15, p=0.37	r=-0.31, p=0.08
low-beta –sHFO coupling	**r=-0.71, p<0.001**	r=-0.45, p=0.03	r=-0.41, p=0.02	r=-0.22, p=0.11	r=-0.33, p=0.03
high-beta –fHFO coupling	r=0.41, p=0.08	r=0.21, p=0.4	r=0.08, p=0.75	r=0.1, p=0.61	r=0.07, p=0.75
120-160Hz power-OFF state	r=0.08, p=0.8	r=0.22, p=0.45	r=0.26, p=0.41	r=0.48, p=0.11	r=0.38, p=0.21
Mean of comodulogram-OFF state	r=-0.05, p=0.73	r=0.17, p=0.27	r=0.12, p=0.35	r=-0.1, p=0.3	r=0.04, p=0.71

UPDRS: Unified Parkinson's Disease Rating Scale

In Table 3.3, the predictive power of neural measures is tested against various behavioral measures. The correlations with a p value of 0.01 and less are highlighted with bold text. The improvement in keyboard score always correlated better than bradykinesia subscore for all neural markers. Last two

rows are the 120-160Hz power from OFF state spectrum used for normalization of the OFF and ON state spectra and the mean of the OFF state comodulogram used for the normalization of OFF and ON state maps. They are not correlated with the improvement in any of the behavioral measures.

3.5 Discussion

In this study, we recorded STN-LFPs from externalized DBS electrodes over three consecutive medication-intake cycles across nine subjects, and assessed motor performance by UPDRS and a custom keyboard task performed in the OFF and ON states. Our results show that CFC between beta and HFO rhythms does not only exist in the OFF state but also in the medication-induced motor ON state. Importantly, we observed distinct patterns of coupling in the ON state –for the first time– and present preliminary evidence regarding their clinical relevance. Although beta and HFO bandpower changes discriminated the OFF and ON states most of the time, the CFC patterns explained the degree of levodopa-induced motor improvement at an individual level, with an added dimension of detail.

3.5.1 Dynamics of Beta and HFO Rhythms

The suppression of beta band activity in STN of PD patients has been observed in previous studies, and has been shown to correlate with motor improvement following administration of anti-Parkinson's medications (Brown et al., 2001; Priori et al., 2004; Kühn et al., 2006; Weinberger et al., 2006; Ray et

al., 2008) and with DBS (Wingeier et al., 2006; Kühn et al., 2008; Eusebio et al., 2011). Hence, exaggerated beta synchronization has been described as a dependable biomarker for PD, that can be used for adaptive or closed-loop DBS (Little et al., 2013; Priori et al., 2013), and for the selection of optimal DBS contacts (Ince et al., 2010). We observed beta band suppression in the ON state in all improved patients except one (Pt7 in Figure 3.4, right column) who demonstrated increased power in the low and high beta bands but still showed improvements in both bradykinesia scores and keyboard task. One can argue that the elevation observed here is not specific to the beta band. In that case, however, there would be an increase in the rest of the spectrum as well, absent distinct peaks in the low (13Hz) and high (27Hz) beta ranges (Figure 3.4H). Moreover, time-varying spectrum (Figure 3.4G) shows that the increase in the beta band power is not momentary or artefactual but, on the contrary, sustained throughout the ON state. The fact that this patient manifested the neural and behavioral markers of the ON state observed in improved patients, except beta suppression, perhaps indicates a multi-modal pathophysiology for PD, such that generalization of a single feature might not provide a reliable estimation of symptom severity.

HFOs have also been previously observed in the STN (Foffani et al., 2003; Kane et al., 2009; Lopez-Azcarate et al., 2010; Özkurt et al., 2011; van Wijk et al., 2016) despite having different peak frequencies and spectral morphologies. In this study, we observed sHFO in the OFF state between 200-300Hz and a shift to fHFO (300-400Hz) upon motor state change, similar to

recent reports (Lopez-Azcarate et al., 2010; Özkurt et al., 2011; van Wijk et al., 2016). We also investigated the ratio between sHFO and fHFO (i.e., sHFO/fHFO bandpower ratio for OFF and ON states) to obtain a relative measure for each motor state (Özkurt et al., 2011; Hirschmann et al., 2016) and found this ratio to be significantly correlated with the degree of improvement (Table 3.3).

3.5.2 Cross-frequency Interactions as in OFF-ON States

CFC has been implicated in the pathophysiology of PD in the STN (Lopez-Azcarate et al., 2010; Özkurt et al., 2011; Yang et al., 2014; van Wijk et al., 2016; Shreve et al., 2017) and it is hypothesized that exaggerated coupling in the STN in the OFF state prevents neurons from initiating firing patterns as expected during movement (Lopez-Azcarate et al., 2010; van Wijk et al., 2016). However, these investigations found reduced or no coupling between beta band and HFOs in the ON state. While we observed coupling between the amplitude of sHFO and the phase of the low-beta in the OFF state in all patients, we also found distinct strong coupling in the ON state in all subjects except two, who lacked clinical improvement as discussed before, possibly related to suboptimal levodopa dosing. We found new coupling patterns in theta-alpha – fHFO and high-beta – fHFO ranges when patients transitioned to the ON state. Importantly, those patients with high-beta – fHFO coupling in the ON state had significantly better improvement in their performance, according to the keyboard task (Figure 3.8E).

Nonlinear interactions in the form of phase-amplitude coupling have previously been associated with various neural processes of motor (Miller et al., 2012; Yanagisawa et al., 2012) and cognitive origin (Canolty et al., 2006; Lakatos et al., 2008). Since larger neuron populations tend to oscillate at lower and smaller populations at higher frequencies (Buzsáki, 2006), CFC can act as the mechanism of coordination between them (Canolty and Knight, 2010; Aru et al., 2015). Consequently in PD electrophysiology, widespread beta band is coupled with more localized HFO (Lopez-Azcarate et al., 2010; van Wijk et al., 2017; Telkes et al., 2018) in the STN. Our results suggest that the true correlate of the motor state is not simply the existence of coupling, but the frequency pair that is coupled. Similar to the distinction between low-beta/high-beta and sHFO/fHFO bandpower changes, coupling at low-beta – sHFO could represent the pathological akinetic form of coupling, whereas high-beta – fHFO coupling might be prokinetic and physiological or could be unrelated to the motor impairment. Further work is necessary to more definitively elucidate the clinical and pathophysiologic implications of CFC in PD between OFF and ON states. Additionally, a possible explanation for theta-alpha - fHFO coupling can be dyskinesia, as discussed in the next section along with exaggerated theta-alpha and gamma bands.

3.5.3 CFC and Levodopa-Induced Dyskinesias

Theta-alpha oscillations were reported previously in the STN with medication (Priori et al., 2004; Lopez-Azcarate et al., 2010) and DBS (Priori et

al., 2006). It was suggested that excessive synchronization in the STN at low frequencies in the levodopa-induced ON state might indicate dyskinesia (Alonso-Frech et al., 2006). Similarly, sharp-peaked gamma oscillations in the cortex and the STN of medicated subjects were also associated with dyskinesias (Swann et al., 2016). We observed an overall increase in power of the theta-alpha band -which was coupled to fHFO- and sharp gamma oscillations in 6/9 patients in the ON state but could not relate it to the severity of symptoms measured. Although we observed mild-moderate dyskinesias in three patients (Table 1), we could not detect an exclusive pattern either in their theta-alpha band or in any other LFP measures investigated. It is fair to note that our records of dyskinesias were based on the notes of attending clinician/nurse and observation of continuous video recordings by an experienced neurologist. We did not perform any specific measurements for this purpose.

3.5.4 Reliability of CFC Estimation

Coupling in the motor cortex between beta phase and broadband gamma (50-200Hz) amplitude was reported previously by de Hemptinne *et al.* (de Hemptinne et al., 2013, 2015). Yet, recent studies have suggested that this coupling could have originated from the harmonics of non-sinusoidal sharp-edged beta band activity (Lozano-Soldevilla et al., 2016; Cole et al., 2017). The HFO activity we observed, however, does not appear as a broadband signal. Both sHFO and fHFO were band-limited and had clear peaks as well as the

CFC estimates, similar to the beta band. These observations suggest that our CFC patterns are products of band-limited frequency components with clear peaks in the beta and HFO ranges. Conversely, we discuss why CFC patterns we observed are not solely an outcome of bandpower changes next.

Theoretically, phase-amplitude coupling estimation is dependent on the accurate detection of the phase of beta band and the amplitude of HFO. Thus, having a sufficient signal-to-noise ratio (SNR) where beta phase and HFO amplitude can reliably be estimated is important (Penny et al., 2008; Aru et al., 2015). Going back to our results, visual observation suggests that the frequency pair in beta and HFO ranges where coupling peaks were similar to the peaks observed in the LFP spectra, especially in the beta range (see Figure 3.6B and Figure 4.4B). Furthermore, we observed a correlation between low-beta power and low-beta – sHFO coupling strength (mean over trials, Spearman r=0.45, p=0.03) but we failed to find a significant correlation between high-beta power and high-beta – fHFO CFC strength. Similarly, we did not find sHFO or fHFO strength to be correlated with CFC strength. These observations overlap with reports by van Wijk et al. (van Wijk et al., 2016) but contradicts with Ozkurt et al. (Özkurt et al., 2011), since latter study claims that one cannot infer coupled frequencies from the power spectra. It is important to note that Ozkurt et al. (Özkurt et al., 2011) selected the contact with maximum HFO power for CFC analysis. In conclusion, the bandpower might have an effect due to SNR improvement but CFC is not solely dependent on it. The literature also attributed

distinct meaning to coupling (Lopez-Azcarate et al., 2010; Özkurt et al., 2011; Yang et al., 2014; van Wijk et al., 2016; Shreve et al., 2017).

Although we agree that bandpower and coupling strength can be parallel since it helps with SNR, we also provided a clear example of bandpower and coupling strength mismatch in Pt7 (Fig2, right column). Despite the increased beta power, the coupling pattern still changes in a similar way to the other subjects with behavioral improvement. Moreover, if the CFC strength solely depended on the beta bandpower, the correlation between beta power and behavioral scores would be at least as high as the correlation of CFC strength change. Yet, our findings suggest that the correlation between keyboard improvement and low-beta bandpower change was significant ($r=-0.5$, $p=0.03$), but low-beta – sHFO CFC change had a higher correlation ($r=-0.71$, $p<0.001$).

It is possible that previous studies failed to capture fHFO coupling in the ON state because of the parameters selected for CFC analysis. A narrow-band filter might have missed fHFO interactions which have a wider bandwidth and resulted in false negatives (Berman et al., 2012; Aru et al., 2015). We selected the filter cutoffs based on the bandwidths of beta and HFO observed from spectra. Another potential explanation for our novel findings compared to other groups is the time gap between the initial surgery and the post-operative LFP recordings. Recordings obtained a short duration after the implantation are more likely to be influenced by the micro-lesion effect (Granziera et al., 2008), which can temporarily disrupt the bandpower dynamics (Rosa et al., 2010). Our recordings were performed three weeks after the lead implantation whereas

other studies included recordings from 1 to 6 days after the initial operation (Kühn et al., 2006; Lopez-Azcarate et al., 2010; Özkurt et al., 2011), a time period during which the microlesion effect can more likely be a confounding factor.

In conclusion, among all neural measures we explored, the change in coupling at low-beta – sHFO between OFF and ON states had the highest correlations with objectively quantified motor improvement in the keyboard task (Table 3.3, r=-0.71), which mitigates the potential bias of unblinded UPDRS assessments that was performed. Together with the differences in the ON state coupling according to the degree of motor improvement, our observations suggest that CFC patterns provide a broader insight into pathophysiologic mechanisms in PD, and have potential utility as a biomarker for the clinical state of patients for various applications such as closed-loop DBS. Combined with the beta band dynamics as a control signal, as has been previously proposed (Little et al., 2013; Priori et al., 2013), CFC patterns may help monitor motor fluctuations with higher accuracy. With the advancement of chronic recording systems, future studies with larger patient populations will be needed to validate the ON state coupling patterns presented here.

4 Modulation of High Frequency Oscillations and Evoked Activity in the STN with Therapeutic and Non-therapeutic DBS

4.1 Overview

Despite the remarkable utility in treating movement disorders, lack of understanding in the underlying mechanisms of deep brain stimulation (DBS) limits its effectiveness. Here we investigate the modulations in local field potentials (LFP) induced by electrical stimulation of the subthalamic nucleus (STN) in ten Parkinson's disease patients undergoing DBS surgery.

We present that in the STN, therapeutic high-frequency stimulation (130-180 Hz) induces high-frequency oscillations (200-400 Hz, HFO), similar to the effect of dopaminergic medication. Accompanied with HFOs, we also observed evoked compound activity (ECA) after each stimulus. While this activity was observed in both therapeutic and non-therapeutic (20-40Hz) stimulation, it was significantly more resonant with the former (lasting 18 ms versus 10 ms after the cessation of stimulation, $p<0.05$). The bandpower of induced HFOs with therapeutic stimulation and the ECA amplitude correlated as well ($r=0.83$, $p<0.01$).

We speculate that high frequency STN-DBS tunes the neural oscillations to their healthy state, similar to pharmacological treatment. The induced HFOs can, therefore, be utilized as a marker of successful recalibration of the dysfunctional circuit generating PD symptoms.

4.2 Introduction

Chronic high-frequency (>100 Hz) deep brain stimulation (DBS) is an established medical treatment for movement disorders such as Parkinson's disease (PD) and being explored for the treatment of many other neurological and psychiatric disorders (McIntyre and Hahn, 2010; Miocinovic et al., 2013). Yet, despite decades of clinical use, its underlying therapeutic mechanism is still unclear (McIntyre and Hahn, 2010; Miocinovic et al., 2013).

The electrophysiological studies seeking a basis for the mechanisms of DBS have focused on the investigation of neuronal spiking and oscillatory activity from the basal ganglia. Early hypotheses suggested that high frequency DBS mimics lesioning by inhibiting the neuronal firings from the stimulated structure (Benazzouz et al., 2000; Dostrovsky et al., 2000; Filali et al., 2004; Welter et al., 2004; Meissner et al., 2005). Shortly after, new evidence was found in favor of increased firing output with electrical stimulation through recordings from the downstream nuclei (Anderson et al., 2003; Hashimoto et al., 2003; Montgomery, 2006; Vitek et al., 2012). This paradoxical observation was explained by models demonstrating that the stimulation directly activated axons and suppressed cell bodies through activation of the inhibitory synaptic terminals (McIntyre et al., 2004a). Experimental and modeling studies verified this phenomenon and found that the axonal response time was synchronized to stimulus frequency, which regularized the neuronal activity (Hashimoto et al., 2003) and ameliorated the Parkinsonian symptoms (Zhuang et al., 2018). Additionally, the high-frequency stimulation was shown to suppress the pathological excessive beta (13-30 Hz)

oscillations in the basal ganglia (Brown et al., 2004; Kühn et al., 2008; Xu et al., 2008; Eusebio et al., 2011; McConnell et al., 2012). Ergo, it was proposed that DBS therapy overrides the pathological burst-type firings with a stimulus induced regular (tonic) pattern. This effect is not only in the stimulated structure but also travels downstream to the basal ganglia-thalamo-cortical circuit (Hashimoto et al., 2003; Xu et al., 2008) and creates an “informational lesion” preventing the relay of pathological firings and oscillatory activity (Grill et al., 2004). However, recent studies suggest that DBS, by regularizing basal ganglia activity, enhances the information processing and restores responsiveness of the thalamocortical cells to the incoming sensorimotor information (Rubin and Terman, 2004; Guo et al., 2008; Johnson et al., 2008), suggesting that rather than causing “lesioning”, DBS might exert its therapeutic effect through promotion of neural activity similar to the “healthy” state (Saenger et al., 2017).

Local field potentials (LFP) of basal ganglia have long attracted interest due to their utility as a feedback modality for closed-loop DBS. Particularly in the subthalamic nucleus (STN), one of the frequently targeted structures in PD patients (Gross et al., 2006; Benabid et al., 2009), excessive beta band oscillations are considered as the hallmark (Oswal et al., 2013; Brittain and Brown, 2014) and have shown to diminish with DBS (Brown et al., 2004; Xu et al., 2008) and dopaminergic medication therapies (Brown et al., 2004). Other biomarkers derived from LFPs include finely tuned gamma (70-90 Hz) and broadband high-frequency oscillations (200-400 Hz, HFO) and cross-frequency coupling (CFC) between beta and HFO bands (Özkurt et al., 2011; Swann et

al., 2016; Hoang and Turner, 2019; Ozturk et al., 2019). Although the pharmaceutical modulations of the LFP oscillations (e.g., suppression of beta and enhancement in the HFO bands) and coupling between them have been well-documented (Foffani et al., 2003; Lopez-Azcarate et al., 2010; Özkurt et al., 2011; van Wijk et al., 2016; Ozturk et al., 2019), the large stimulus artifact observed during DBS have hindered further investigation of these biomarkers for closed-loop applications (Zhou et al., 2018). Consequently, the contribution of LFPs to uncovering the mechanisms of DBS have been limited.

Here, we recorded LFPs intraoperatively from 12 hemispheres and studied the modulations above and in STN during multiple low- and high-frequency stimulation paradigms. LFPs were obtained from the stainless-steel ring contact during microelectrode recordings. We observed HFOs similar to the ones in the medically treated patients with high-frequency therapeutic DBS. In conjunction, we noted evoked activity after each stimulus pulse. This activity was only resonant with high-frequency stimulation. The HFO power and the amplitude of the evoked activity correlated.

4.3 Patients and Methods

4.3.1 Patients

Eight patients (four females, six males) with PD undergoing bilateral STN-DBS implantation at Baylor St. Luke's Medical Center were included in the study. Their ages ranged between 40 to 64 (mean ± standard deviation = 55±8.8) with disease duration ranging from 4 to 16 years (mean ± standard

deviation = 9±3.9). Recordings from four patients were obtained bilaterally with out- and in-STN stimulation testing and four patients were recorded unilaterally on the more affected hemisphere with additional multiple frequency testing. The study protocol was approved by the Institutional Review Boards of Baylor College of Medicine and University of Houston.

4.3.2 Surgery and Recordings

Patients were requested to stop medication at least 12 hours prior to the surgery and all recordings were obtained in the awake state using local anesthesia. The stereotactic coordinates and trajectories to the STN were identified by fusing preoperative magnetic resonance imaging (MRI) and computerized tomography (CT) scans on a neuro-navigational platform (StealthStation, Medtronic, Ireland). In each hemisphere, awake recordings were performed to validate the targeting, using a set of two parallel microelectrodes separated by 2 mm (center-to-center) using the 5-cannula BenGun with “+” configuration. Additional to the center track, one of the anterior, posterior, lateral or medial tracks was selected by the neurosurgeon on a patient specific basis by taking into account the subject’s anatomy. The microelectrodes (NeuroProbe, AlphaOmega, Israel) were initially placed at 15mm above the target (ventral border of the STN) and advanced towards the target in 0.5-1mm steps using NeuroOmega drive (AlphaOmega, Israel). The dorsal and ventral borders of STN were determined by an experienced neurologist via visual and auditory inspection of the single unit firings from the high-impedance tungsten

tip (0.4-0.8 MOhm), per standard clinical protocol. The dorsal STN border was identified with a prominent increase in the background activity and spiking. The LFPs from the stainless-steel ring (3mm above the tip, 3-4KOhm impedance) on the shaft were recorded by using the cannula as reference at 10mm and 2mm below the dorsal border, where stimulation experiments were performed (Figure 4.1). The recordings were obtained with the gHiamp bio-amplifier (gTec, Austria) at 38.4 KHz sampling frequency, 24bit A/D resolution and ±250 mV input range. The stimulation was delivered monopolarly using the Grapevine neural processor (Ripple, UT) at 30KHz resolution. The data was stored in a computer hard drive for offline processing.

4.3.3 Signal Processing

The data acquisition, stimulation and processing were performed using custom developed scripts in Matlab R2014a (Mathworks, MA). The raw LFP traces were visualized to ensure the recordings were within the input range of the amplifier (±250 mV). The traces were forward and backward filtered with a 2^{nd} order Butterworth high-pass filter with 2Hz cut-off frequency. The spectral analyses were conducted using Thompson multi-taper estimate with 4 slepian windows for each 1s of data (with 50% overlap). The spectra were normalized using the mean activity between 500-600 Hz to account for amplitude differences between patients. The beta and HFO bandpowers were calculated by mean power between 13-30Hz and 200-400Hz respectively.

Evoked activity waveforms were processed by subtraction of a fitted exponential first, to remove the decaying response from the amplifier settling. The waveform was then smoothed with a Savitzky-Golay filter. The processing did not affect the morphology or the duration of the evoked activity.

Inter-pulse evoked activity was reconstructed from the segmented traces, in order to investigate if HFO activity is an artifact caused by the evoked waveform. The peaks of stimulus pulses were detected, and the 22s of data during each stimulation was aligned with respect to the peak. A moving template was extracted using the Principal Component Analysis method over each 1s of data with 50% overlap. The largest eigenvector corresponded to the stimulus artifact and accompanying inter-pulse evoked activity. Each waveform in the aligned data was reconstructed in this way and the residual was calculated by subtraction of the reconstructed data from the original raw trace.

4.3.4 Statistical Analysis

Statistical analyses were performed in Matlab as well, using paired non-parametric tests (signed-rank tests and Spearman correlation) given the non-normal distribution of most variables studied. The significance of the decay of evoked activity was tested with one-tailed t-test.

4.4 Results

The LFPs recorded from eight awake PD patients (four bilateral and four unilateral) depth by depth from two microelectrodes separated by 2mm, as

depicted in Figure 4.1A. The recordings started 15mm above the intended target (ventral border of STN) and at 10mm above, the “out-STN” stimulus was performed. The “in-STN” experiments were performed 2mm below the dorsal border of STN, characterized by the increased background activity and neuronal spiking recorded from the fine microelectrode tip. One electrode was the recording electrode whereas the other was used to deliver monopolar, biphasic, cathodic stimulation with 2mA, 60us pulse width at various frequencies for 22 seconds. The recorded waveform was verified to be within the amplitude range of the amplifier (Figure 4.1B).

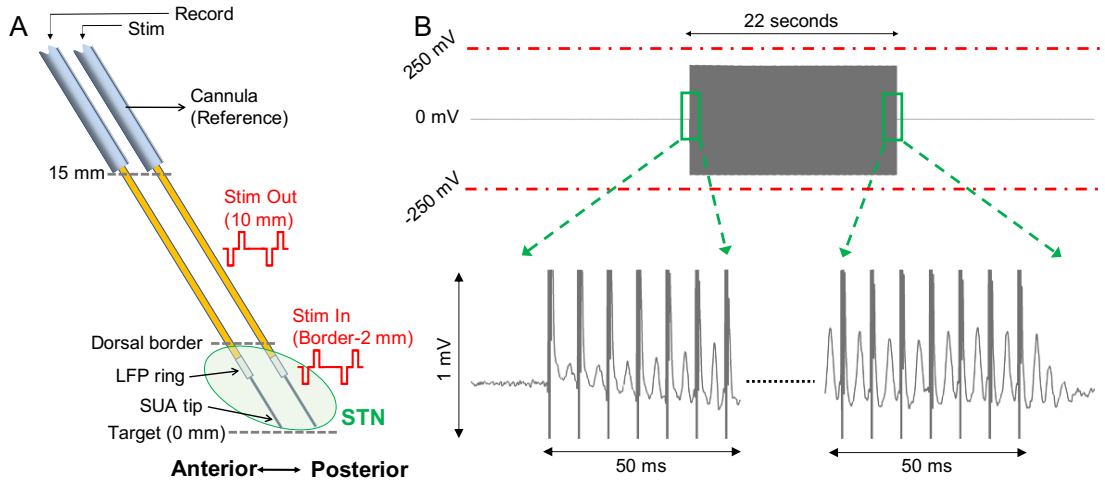

Figure 4.1: *Experimental paradigm and sample stimulation segments with and without saturation.*

4.4.1 Therapeutic DBS Modulates HFO and Evokes Resonant Compound Activity in the STN

Figure 4.2A illustrates the changes in LFP spectrum before, during and after high-frequency stimulation, out- and in-STN for a representative subject. Top panels are the time-frequency maps (TFM) showing the temporal changes

whereas the bottom panels represent the average spectral content of baseline and stimulation periods of the corresponding TFMs. There was a consistent enhancement around 300 Hz induced by high-frequency therapeutic stimulation in-STN, whereas no modulation was present out-STN (Figure 4.2C). The modulated HFO disappeared after the cessation of the stimulation. The lack of modulation out-STN suggests that the enhanced activity is not a stimulation artifact. Figure 4.2B illustrates the average spectral response to therapeutic in-STN stimulation from all patients. The HFO and beta bandpowers were compared between baseline and stimulation periods using non-parametric Wilcoxon signed-rank test for paired samples, given the distributions were not normal (Anderson-Darling test, $p<0.05$). There was a significant suppression in the beta band accompanied by a significant enhancement in the HFO range ($p<0.001$). The beta and HFO bandpowers or their change were not significantly correlated ($r=0.1$, $p>0.05$).

DBS in the therapeutic frequencies also evoked resonant compound activity in-STN between pulses (Figure 4.1B) as well as at the end of stimulation (Figure 4.2D). Similarly, lack of observation of evoked activity out-STN suggests that this response is specific to STN and not a stimulation artifact (Figure 4.2D). The amplitude of the evoked activity, calculated by the difference between the first positive and the first negative peaks, was significantly higher in-STN (Figure 4.2E). Interestingly, the enhanced HFO bandpower was significantly correlated with evoked activity amplitude (Figure 4.2F, $r=0.83$, $p<0.01$). Although beta

band was also suppressed with stimulation, no significant correlation was found with evoked activity strength.

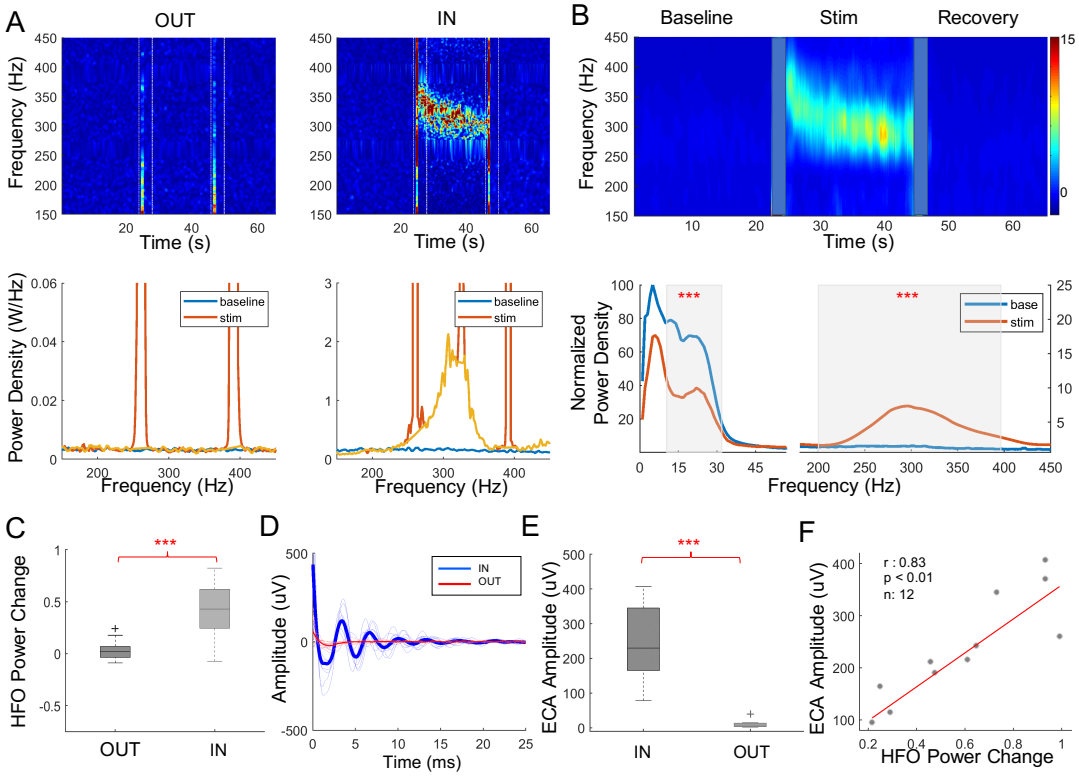

Figure 4.2: *HFO and resonant evoked compound activity are observed during various high-frequency DBS only in the STN.*

4.4.2 Low-frequency DBS Only Evokes Non-resonant Compound Activity

The modulation observed in the HFO range with therapeutic high frequency stimulation was not present with non-therapeutic 20 Hz stimulation. Figure 4.3A illustrates representative time-frequency maps from before, during and after high and low frequency stimulation respectively in a representative patient. Unlike therapeutic stimulation, there was no significant change in

neither beta nor HFO band during stimulation when compared to baseline (Figure 4.3B).

Despite the lack of modulation in the LFP spectrum, interestingly, the evoked compound activity was still present with low frequency stimulation (Figure 4.3C). While there was a slight decrease in amplitude (Figure 4.3D), the activity was no longer resonant, compared to 130 Hz stimulation, as illustrated in Figure 4.3E. To quantify the resonance, the envelope of the ECA was detected using Hilbert transform (Figure 4.3F) and first 20 ms of the envelope was compared to the mean envelope between 20-25ms after stimulation (one tailed t-test, $p<0.05$). Compared to 130 Hz, the evoked waveform dampened significantly faster after 20 Hz stimulation (18 ms vs 10 ms, Figure 4.3F). Unlike high-frequency stimulation, HFO bandpower change was not correlated with the evoked activity amplitude with the low frequency stimulation (Figure 4.3G).

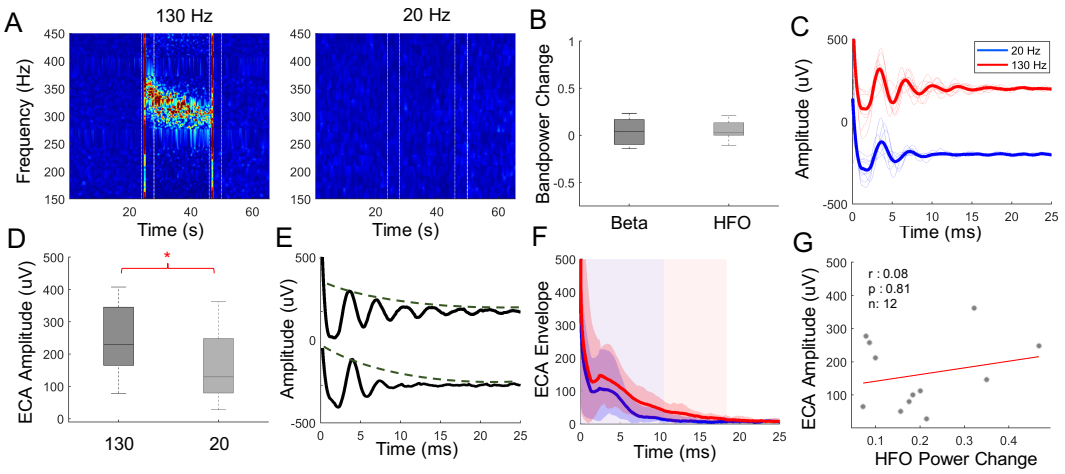

Figure 4.3: *Low-frequency DBS does not induce HFO but evokes non-resonant compound activity.*

4.4.3 HFO Power is Independent from the Evoked Resonant Compound Activity

The correlation observed between induced HFO bandpower and evoked resonant compound activity during high-frequency stimulation was relatively high (Figure 4.2F, $r=0.83$, $p<0.01$). To test whether these two phenomena are dependent, a moving average template removal filter was applied to the raw data, in order to isolate the evoked peaks during stimulation. Figure 4.4A illustrates the representative raw data aligned and segmented around the detected stimulation pulses whereas Figure 4.4B is the reconstructed templates of the stimulation artifact and the evoked activity during stimulation. The residual data (raw-reconstructed) was considered as denoised (Figure 4.4C). As illustrated in Figure 4.4D, the denoising process removed the stimulation artifact and achieved amplitude ranges comparable to the baseline segment before the stimulation, except the short transient periods in the beginning and the end. Figure 4.4E, F further demonstrate that not only the large stimulus artifact but also the inter-pulse evoked activity was also removed. As illustrated in a corresponding TFM (in Figure 4.4G, H) and spectra (in Figure 4.4I), although this process suppressed the very large stimulus-caused artifacts in the spectrum, it did not change the spectral content of the data in the beta and HFO ranges (or any other frequency range of interest).

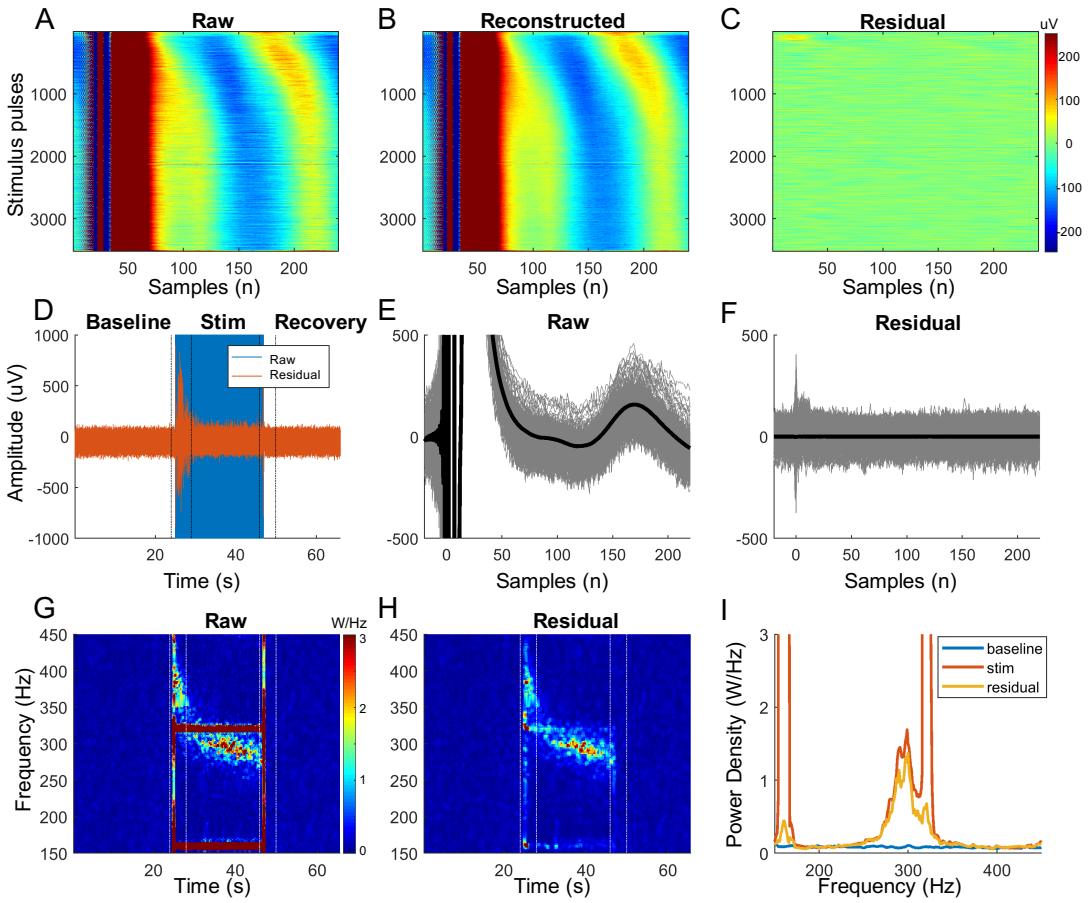

Figure 4.4: *HFO induced by therapeutic DBS is present even after removal of evoked waveform between stimulation pulses.*

4.4.4 High-frequency DBS Causes Temporal Adaptation in ECA

The analysis of segmented and aligned data around stimulus pulses have revealed that the inter-pulse evoked activity adapts to a steady state with high-frequency stimulation. While the time between pulse and the first peak of the evoked activity stayed the same throughout the low frequency stimulation, it took 3-10s for the evoked activity to reach the steady state (Figure 4.5A). The adaptation between different high frequency stimulations were different but we could not find a consistent pattern across four patients where the multi-

frequency experiment was performed, indicating that the response could be patient specific. The representative evoked waveforms at the end of stimulation revealed that 20 and 40 Hz had similar non-resonant ECA whereas 130, 160 and 180 Hz stimulation induced resonance in ECA (Figure 4.5B). The degree of HFO enhancement was also visually similar during high-frequency stimulation in the representative subject (Figure 4.5C). We further investigated population response. Figure 4.5D illustrates that there was no significant difference between 20 and 40 Hz stimulation in ECA amplitude. The same analysis

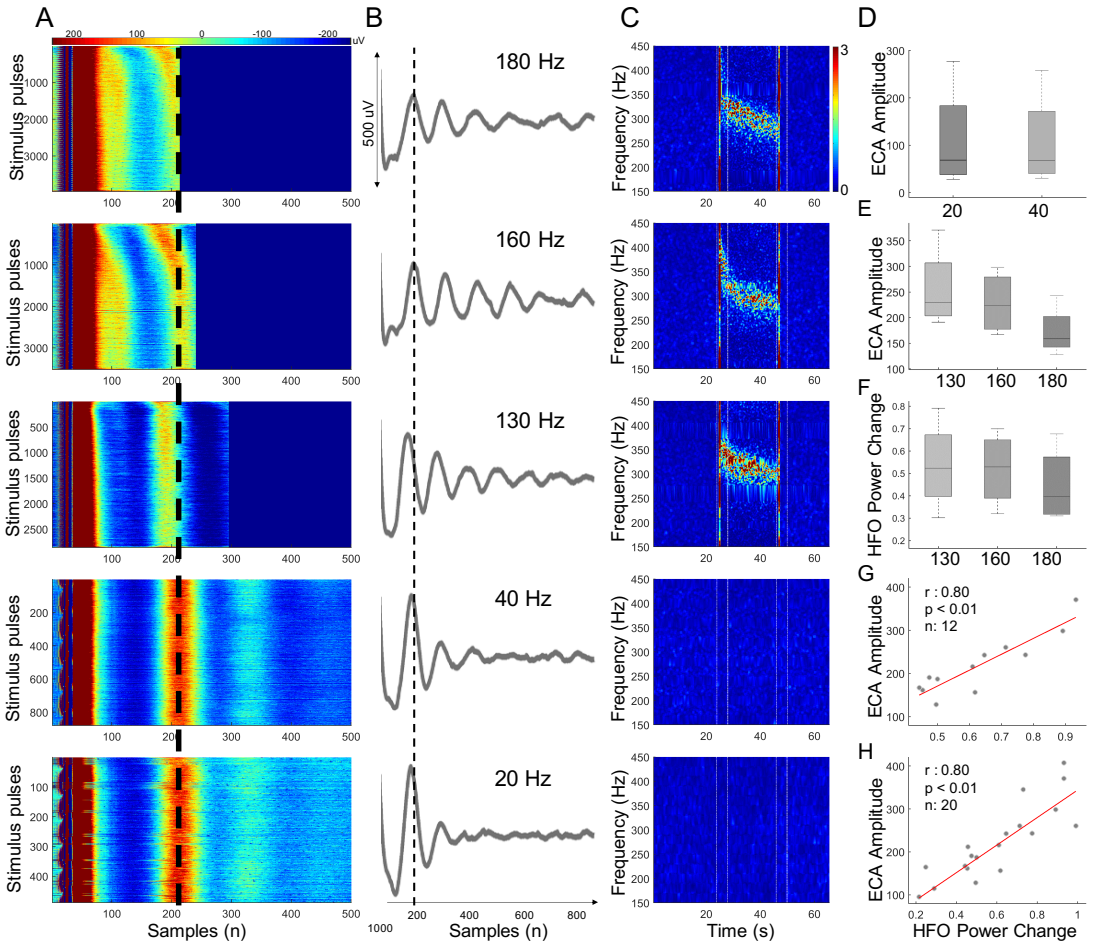

Figure 4.5: *Only high-frequency stimulations modulate adaptation in the evoked response over time, which correlates with the stimulation-induced HFO activity.*

revealed a trend that ECA amplitude after 130 Hz was larger than 160 Hz and that was larger than 180 Hz (Figure 4.5E). However, the difference was not significant, perhaps due to the low sample size. A similar trend was observed in HFO enhancement but again, the difference was not significant. Finally, we correlated the HFO enhancement with ECA amplitude for patients with multi-frequency therapeutic stimulation (Figure 4.5G, n=4 hemispheres with 130, 160 and 180 Hz per each hemisphere, 12 stimulations) and with all patients (Figure 4.5H, n=12 hemispheres, 20 stimulations combined). There was a consistent correlation of 0.80 ($p<0.01$) between ECA amplitude and HFO power change in both cases.

4.5 Discussion

To investigate the mechanisms of therapeutic high-frequency chronic DBS therapy, we have studied the modulations of STN-LFP oscillations recorded from PD patients intraoperatively during stimulation. We have observed an increased activity in the HFO range as well as an independent evoked resonant compound activity with high-frequency stimulation. When DBS was delivered at non-therapeutic low-frequency, the HFO did not modulate and the evoked compound activity was not resonant. We also observed that the evoked activity adapts to a steady state with high-frequency DBS only but due to the low sample size, could not assess the significance of the outcomes. Regardless, our findings suggest that DBS may exert its therapeutic effect by bringing neuronal populations to a “healthy” oscillatory state.

4.5.1 Modulation of the Healthy HFO Activity with Therapeutic DBS

There is an abundance of reports regarding the modulation of ~300Hz HFO in the STN of PD patients undergoing dopaminergic therapy (Foffani et al., 2003; Lopez-Azcarate et al., 2010; Özkurt et al., 2011; van Wijk et al., 2016; Ozturk et al., 2019). This activity appears concurrently with the therapeutic effect of the medication, representing the “ON state” (Foffani et al., 2003; Lopez-Azcarate et al., 2010; Ozturk et al., 2019). This rhythm was suggested to be a “coordinated clock” that paces the neural excitability (Foffani et al., 2003). Although there are no reports of LFP activity in the healthy human STN, similar HFO activity has been observed in the healthy non-human primates and disappeared after 1-methyl-4-phenyl-1,2,3,6-tetrahydropyridine (MPTP) treatment inducing PD (Escobar et al., 2017). In 12 STNs recorded, we observed a consistent enhancement in the HFO range as well (Figure 4.2A, B), indicating that the high-frequency therapeutic DBS may have similar mechanisms to pharmaceutical therapy (Stefani et al., 2011), which is to drive the basal ganglia circuit into a physiological oscillatory equilibrium (Foffani et al., 2003; Saenger et al., 2017).

Previous work has shown the regularizing effects of therapeutic STN-DBS on firing rates of STN (Garcia et al., 2005b; Zhuang et al., 2018) and other basal ganglia structures (Hashimoto et al., 2003; Reese et al., 2011; McConnell et al., 2012; Cleary et al., 2013). Recently, a unique case report presenting the firing patterns and LFP activity from the STNs of a PD patient after dopaminergic treatment reported that there were no pathological burst-type firings associated

with PD (Ozturk et al., 2020a). This is in accordance with the healthy non-human primate studies reporting an increase in bursting neuronal activity and instantaneous firing rates after MPTP treatment (Bergman et al., 1994; Soares et al., 2004). In this patient, unlike recordings from PD patients in the unmedicated state (Kaku et al., 2020), tonic (regular) spiking was observed together with ~300Hz HFOs instead of bursts-type firings, further strengthening that DBS may function by promoting neural activity similar to the stable physiological state in the basal ganglia (Garcia et al., 2005b).

4.5.2 Resonant versus Non-resonant ECA and Their Relation to HFO

Evoked potentials have been reported in the various structures of the nervous system, such as hippocampus (Stypulkowski et al., 2011), spinal cord (Kent et al., 2015; Parker et al., 2020) as well as the STN of PD patients (Gmel et al., 2015; Sinclair et al., 2018, 2019). In PD-STN, it was shown that the evoked activity during therapeutic DBS can be used to identify clinically beneficial amplitudes (Gmel et al., 2015). Using a custom stimulation scheme, Sinclair et al. (Sinclair et al., 2018) recently has demonstrated that evoked resonant activity can also be used to locate the most beneficial stimulation site. We also observed evoked resonance during high-frequency DBS (Figure 4.2D). Additionally, we studied stimulation at different frequencies and found that the evoked response exists with every stimulus pulse (Figure 4.5A). Both the high- and the low-frequency stimulation produced similarly strong evoked activity (Figure 4.3D). However, the response was significantly more resonant with

high-frequency stimulation and lasted longer after cessation of DBS (18 versus 10 ms, Figure 4.3F).

Due to its presence after every stimulus pulse in the STN, we speculate that the evoked activity could be the immediate involuntary response of the neurons within the volume of tissue activated (VTA). From a control theory perspective, if a single pulse is an impulse input to the network, then the evoked response is an output of the neurons in the VTA. The reason for the longer lasting effect of high-frequency stimulation can be explained with a pendulum analogy. Each stimulus pulse is the force hitting the pendulum in one direction. With low-frequency stimulation, there is a longer period between each hit and that time is enough for the pendulum to reach equilibrium. Therefore, we observe a steady response over 22s of stimulation (Figure 4.5A). However, with frequent hits not allowing the pendulum to come to a stop, high-frequency stimulation starts to activate a larger pool of neurons than the initial VTA. The adaptation on the inter-pulse evoked response (Figure 4.5A) shows that the network reaches a steady state after an initial ramp-up period (3-10s). In that sense, therapeutic DBS entrains the pendulum to its steady state oscillation (HFO) and the resonance in the evoked activity could also be a sign of that entrainment. In favor of this claim, we found a significant correlation between HFO enhancement and evoked response amplitude (Figure 4.2F). The difference in adaptation with various high-frequency stimulations could be related to the phase they hit the pendulum as well as the patient specific physiological oscillatory state. Thus, although multiple high-frequency DBS

might work for a patient, we may pinpoint the most efficient one by checking the adaption of the evoked activity and modulation of the HFO band.

It is possible that even 20Hz stimulation with high amplitude might cause a longer lasting evoked response, similar to a large push to the pendulum causing a longer lasting swing. However, an animal study reported that even at high amplitudes, 20Hz stimulation did not pace the subthalamic neurons, as it did during >100Hz stimulation (Garcia et al., 2005b). The same group also reported that the pulses must be close enough to one another to override the deleterious STN activity (Garcia et al., 2005a). Our take is that the evoked response, regardless of stimulation frequency, is local and specific to structures (Sinclair et al., 2018) and can be used for identification of the optimal target whereas HFO is the network activity generated by the circuit and can be used for the detection of the "motor ON" or the "healthy state".

4.5.3 Modulated HFO Is not an Artifact and Is Independent of ECA

The relatively high stimulation voltage (V range) and subsequent artifact in the recording systems have historically prevented the exploration of LFPs (uV range), especially in the HFO band due to overlapping artifact harmonics. Therefore, in addition to recording with an amplifier with large input amplitude range, we performed the stimulation experiments in- and out-STN to verify that our observations of HFO and evoked activity are not due to stimulus or hardware artifacts (Figure 4.1A). We also ensured that the recorded waveforms were within the range of our amplifier (Figure 4.1B). While HFO was induced only with

high-frequency therapeutic DBS in-STN, evoked activity was resonating with therapeutic stimulation and non-resonant with low-frequency DBS. Similar to HFO, there was no evoked response during out-STN stimulation experiments, indicating that both HFO and evoked activity are specific to the structure and they are not mere artifacts.

The dependence of HFO and evoked resonant activity was tested by the comparison of spectral analyses of raw and denoised data. By employing a temporal template extraction filter, we reconstructed the DBS artifact at each pulse and the associated evoked response between pulses, devoid of LFP activity. This reconstruction was then subtracted from the raw signal to obtain the denoised (residual) data. When the spectral content of the raw and residual data was compared (Figure 4.4G-I), we observed no decrease in the HFO activity while the DBS artifacts and the evoked waveform were substantially eliminated. Furthermore, we observed an evoked activity at a similar amplitude with 20-40 Hz stimulation as well (Figure 4.5B) but the HFO enhancement did not occur (Figure 4.5C). Observation of HFO activity even after removal of the evoked response and observation of evoked activity without HFO suggests that HFO modulation is independent of the evoked response.

4.5.4 Going Beyond the Beta Band

Suppression of exaggerated beta band oscillations in the STN of PD patients after DBS (Kühn et al., 2008; Eusebio et al., 2011; McConnell et al., 2012) and dopaminergic therapy (Foffani et al., 2003; Priori et al., 2004; Kane

et al., 2009; Lopez-Azcarate et al., 2010; Ozturk et al., 2019) is a well-established phenomenon. We also observed a significant decrease in beta power with high-frequency stimulation as well but there was no correlation with evoked activity amplitude and indirectly, with symptom improvement (Sinclair et al., 2019). A compelling argument for the lack of such a relationship could be that the beta band is associated with many healthy functions in the brain, such as its suppression with movement or even planning or imagination of it (Kühn et al., 2004; Litvak et al., 2012), its modulations with wakefulness (Urrestarazu et al., 2009; Thompson et al., 2018b) and decision-making (Leventhal et al., 2012). Therefore, despite established reports of its modulations in PD, the multifaceted involvement of beta band in physiological processes might make it a poor biomarker by itself for the diseased state, especially in the freely behaving patients with a chronic DBS implant. It is likely that, as Foffani et al. (Foffani et al., 2003) proposed, there might be a high frequency “clock” that is not directly involved in motor functions, but rather regulating the neural synchrony in order to guarantee the specific modulation of individual actions that are controlled by lower frequencies. Therefore, we speculate that beta band must be -at least- combined with other state specific biomarkers for robust and reliable operation of long-term adaptive stimulation schemes such as closed-loop chronic DBS.

4.5.5 Limitations

The predicting power of the HFO and evoked activity on the patient’s symptoms would be a great addition to our study. However, due to the

experimental paradigm (22s stimulation), it was not possible to test patients intraoperatively during this short period. Fortunately, Sinclair et al. (Sinclair et al., 2019) were able to perform this testing due to their extended stimulation period and have shown that the amplitude of evoked resonant activity is a predictor of symptom improvement. Thus, we utilized the evoked activity amplitude as an indirect measure of clinical benefit.

Additionally, the studies involving medicated PD subjects have reported slower HFOs around 250Hz before the medication intake (Lopez-Azcarate et al., 2010; Özkurt et al., 2011; van Wijk et al., 2016; Ozturk et al., 2019). Yet, we did not observe this activity in most of our patients in the baseline. This could be due to the micro-lesion effect caused by the fresh disruption of the tissue by the microelectrodes, which has been reported to alter neural dynamics (Granziera et al., 2008; Rosa et al., 2010). The aforementioned studies recorded LFPs several days or even weeks postoperatively, where the tissue-electrode interface might have come to an equilibrium already.

Finally, despite consistency of our observation and satisfactory statistical significance of our results, our sample size is -at best- exploratory. Especially the analyses regarding multi-frequency stimulation lacked in statistical power despite visible trends. Therefore, more studies with additional subjects are warranted, in order to discover the parameter specific effects of DBS further.

5 Significance and Concluding Remarks

PD is the second most common neurological disorder and the surgical treatment for it allows recording neural activity from the various depths of the brain. Investigation of such activity can reveal the secrets of the physiological and pathological neural circuits. Moreover, modulations to these various electrophysiological readings during treatment can also help us decipher the corrective mechanisms induced by the treatment as well and consequently, this knowledge can be used to devise novel diagnostic or therapeutic tools, as presented in this dissertation.

5.1 Clinical Relevance and Future Implications

First, we demonstrated an online processing pipeline for the purpose of assisting with clinical decision making in refining the STN targeting for the implantation of DBS lead. This is a crucial step that must be taken prior to the analysis of modulations in LFP, as non-optimal targeting could result in false-negative outcomes. On the clinical side, accurate localization of the target contributes to the efficacy of DBS by reducing the stimulation voltage and associated side effects. To that end, we developed an automated approach by processing LFPs from multiple tracks to localize the dorsal border of STN and predict the optimal implantation track in a randomized, double-blinded pilot study for the first time. Ten patients referred for bilateral DBS were implanted randomly with SUA in one hemisphere and with LFP on the other. While SUA

side was implanted by visual and auditory observation of the spiking patterns depth by depth, as done in commercial clinical systems, different sub-bands of microelectrode LFPs in beta and high-frequency ranges were utilized to identify the optimal track for chronic DBS electrode placement in the other hemisphere. We demonstrated that the LFP-based implantations achieved equal or better improvement with the robust readings of oscillations, compared to the fragile electrode tip used for the SUA recordings. Since LFP acquisition does not require any additional hardware or clinical procedures, we believe that it can be integrated into the existing mapping systems in the operating room with our automated processing pipeline presented here. Although we demonstrated the targeting of STN, similar systems can be built for other DBS targets in the future if the classifier is trained with LFP signatures from those nuclei.

Once the DBS lead is implanted in the right location, we studied the modulations of LFPs with dopaminergic medication therapy. Neural oscillations have long been investigated under medication and movement in order to characterize the role of specific bands in PD pathophysiology. However, due to long wash-in and wash-out times associated with pharmacological therapy, these changes must be studied through long-duration recordings. We have recorded LFPs for 24-hours from nine patients referred for unilateral DBS after their leads were externalized for the battery connection. During this time, patients were given medication three times and thus, the pharmacological response of LFPs were studied over three repetitive trials. We not only verified the previously reported changes in the bandpowers of beta, gamma and HFO

bands, but also recorded strong non-linear CFC patterns in the medicated state for the first time. This is an important observation for the neuroscientific community, since CFC in the STN was thought to be pathological. We believe that, similar to CFC in the other parts of the brain, this coupling can be physiological or pathological depending on the frequencies involved. Although CFC is a computationally costly analysis, future developments in the algorithms for its estimation could help integrate it into closed-loop DBS systems.

Finally, we investigated the effects of therapeutic and non-therapeutic DBS on LFPs oscillations, in order to help decipher the mechanisms of DBS and to find suitable biomarkers for the closed-loop stimulation paradigm. Due to the near-immediate effect of STN-DBS, we performed the LFP recordings from eight patients intraoperatively under 22 second stimulus periods. For the first time, we observed induced HFO activity only with therapeutic stimulation, similar to the healthy non-human primates and medicated PD patients. This observation implicates that the healthy basal ganglia might have a fast-oscillatory state, as in a microprocessor base clock, and only DBS parameters restoring this activity can have a therapeutic effect. Additionally, we observed a resonant ECA with the therapeutic high-frequency stimulation in the STN whereas ECA was still present but not resonant with the non-therapeutic low-frequency stimulation. The rapidly adapting response of ECA, alternatively, can also be utilized for selection of optimal parameters for an effective and energy efficient DBS therapy. In this study, we only discerned the effects of high- and low-frequency stimulation conclusively. However, future research that further

investigates the electrophysiological modulations induced by other parameters of DBS will be needed for the development of truly independent closed-loop systems.

5.2 Conclusion

PD pathophysiology is well-studied with the serendipitous discoveries of PD inducing MPTP substance and high-frequency DBS therapy. Despite numerous animal studies and years of clinical use, the underlying mechanisms of DBS have not been deciphered yet and this lack of understanding limits its effectiveness. We postulated that through the study of modulations of LFPs, which is a promising electrophysiological measure readily recordable from the current clinical electrodes, we not only uncover insights regarding the pathophysiology of the PD but also identify signature oscillatory patterns indicating the healthy and the diseased state. After demonstrating the feasibility of LFP-based clinical targeting system, we presented interesting and consistent modulations in neural oscillations, especially in the HFO range with pharmacological and electroceutical therapies. Our observations support the idea that basal ganglia might have oscillatory patterns specific to the healthy or diseased state. More practically, these patterns are promising biomarkers that can be used for diagnostic purposes such as target localization, and treatment purposes such as selection of optimal stimulation parameters and adaptive closed-loop DBS.

References

Abosch, A., Hutchison, W. D., Saint-Cyr, J. A., Dostrovsky, J. O., and Lozano, A. M. (2002). Movement-related neurons of the subthalamic nucleus in patients with Parkinson disease. *J Neurosurg* 97, 1167–1172. doi:10.3171/jns.2002.97.5.1167.

Abosch, A., Lanctin, D., Onaran, I., Eberly, L., Spaniol, M., and Ince, N. F. (2012). Long-term recordings of local field potentials from implanted deep brain stimulation electrodes. *Neurosurgery* 71, 804–814. doi:10.1227/NEU.0b013e3182676b91.

Abosch, A., Timmermann, L., Bartley, S., Rietkerk, H. G., Whiting, D., Connolly, P. J., Lanctin, D., and Hariz, M. I. (2013). An International Survey of Deep Brain Stimulation Procedural Steps. *Stereotact Funct Neurosurg* 91, 1–11. doi:10.1159/000343207.

Algina, J., and Swaminathan, H. (2011). “Centering in two-level nested designs.,” in *Handbook for advanced multilevel analysis.* European Association for Methodology series. (New York, NY, US: Routledge/Taylor & Francis Group), 285–312.

Alonso-Frech, F., Zamarbide, I., Alegre, M., Rodríguez-Oroz, M. C., Guridi, J., Manrique, M., Valencia, M., Artieda, J., and Obeso, J. A. (2006). Slow oscillatory activity and levodopa-induced dyskinesias in Parkinson’s disease. *Brain* 129, 1748–1757. doi:10.1093/brain/awl103.

Amirnovin, R., Williams, Z. M., Cosgrove, G. R., and Eskandar, E. N. (2006). Experience with microelectrode guided subthalamic nucleus deep brain

stimulation. *Neurosurgery* 58, 96–102. doi:10.1227/01.NEU.0000192690.45680.C2.

Anderson, M. E., Postupna, N., and Ruffo, M. (2003). Effects of High-Frequency Stimulation in the Internal Globus Pallidus on the Activity of Thalamic Neurons in the Awake Monkey. *J Neurophysiol* 89, 1150–1160. doi:10.1152/jn.00475.2002.

Aru, J., Aru, J., Priesemann, V., Wibral, M., Lana, L., Pipa, G., Singer, W., and Vicente, R. (2015). Untangling cross-frequency coupling in neuroscience. *Curr Opin Neurobiol* 31, 51–61. doi:10.1016/j.conb.2014.08.002.

Aziz, T. Z., and Hariz, M. (2017). To sleep or not to sleep during deep brain stimulation surgery for Parkinson disease? *Neurology* 89, 1938–1939. doi:10.1212/WNL.0000000000004635.

Ballanger, B., Van Eimeren, T., Moro, E., Lozano, A. M., Hamani, C., Boulinguez, P., Pellecchia, G., Houle, S., Poon, Y. Y., Lang, A. E., and Strafella, A. P. (2009). Stimulation of the subthalamic nucleus and impulsivity: Release your horses. *Ann Neurol* 66, 817–824. doi:10.1002/ana.21795.

Benabid, A. L. (2003). Deep brain stimulation for Parkinson's disease. *Curr Opin Neurobiol* 13, 696–706. doi:10.1016/j.conb.2003.11.001.

Benabid, A. L., Benazzouz, A., Hoffmann, D., Limousin, P., Krack, P., and Pollak, P. (2008). Long-Term Electrical Inhibition of Deep Brain Targets in Movement Disorders. *Mov Disord* 13, 119–125. doi:10.1002/mds.870131321.

Benabid, A. L., Chabardes, S., Mitrofanis, J., and Pollak, P. (2009). Deep brain stimulation of the subthalamic nucleus for the treatment of Parkinson's disease. *Lancet Neurol*, 67–81.

Benabid, A. L., Pollak, P., Gross, C., Hoffmann, D., Benazzouz, A., Gao, D. M., Laurent, A., Gentil, M., and Perret, J. (1994). Acute and Long-Term Effects of Subthalamic Nucleus Stimulation in Parkinson's Disease. *Stereotact Funct Neurosurg* 62, 76–84. doi:10.1159/000098600.

Benabid, A. L., Pollak, P., Louveau, A., Henry, S., and de Rougemont, J. (1987). Combined (Thalamotomy and Stimulation) Stereotactic Surgery of the VIM Thalamic Nucleus for Bilateral Parkinson Disease. *Stereotact Funct Neurosurg* 50, 344–346. doi:10.1159/000100803.

Benarroch, E. E. (2008). Subthalamic nucleus and its connections: Anatomic substrate for the network effects of deep brain stimulation. *Neurology* 70, 1991–1995. doi:10.1212/01.wnl.0000313022.39329.65.

Benazzouz, A., Breit, S., Koudsie, A., Pollak, P., Krack, P., and Benabid, A. L. (2002). Intraoperative microrecordings of the subthalamic nucleus in Parkinson's disease. *Mov Disord* 17, 145–149. doi:10.1002/mds.10156.

Benazzouz, A., Gao, D. ., Ni, Z. ., Piallat, B., Bouali-Benazzouz, R., and Benabid, A. . (2000). Effect of high-frequency stimulation of the subthalamic nucleus on the neuronal activities of the substantia nigra pars reticulata and ventrolateral nucleus of the thalamus in the rat. *Neuroscience* 99, 289–295. doi:10.1016/S0306-4522(00)00199-8.

Bergman, H., Feingold, A., Nini, A., Raz, A., Slovin, H., Abeles, M., and

Vaadia, E. (1998). Physiological aspects of information processing in the basal ganglia of normal and parkinsonian primates. *Trends Neurosci* 21, 32–38. doi:10.1016/S0166-2236(97)01151-X.

Bergman, H., Wichmann, T., Karmon, B., and DeLong, M. R. (1994). The primate subthalamic nucleus. II. Neuronal activity in the MPTP model of parkinsonism. *J Neurophysiol* 72, 507–20. doi:10.1152/jn.1994.72.2.507.

Berman, J. I., McDaniel, J., Liu, S., Cornew, L., Gaetz, W., Roberts, T. P. L., and Edgar, J. C. (2012). Variable Bandwidth Filtering for Improved Sensitivity of Cross-Frequency Coupling Metrics. *Brain Connect* 2, 155–163. doi:10.1089/brain.2012.0085.

Boëx, C., de Balthasar, C., Kós, M.-I., and Pelizzone, M. (2003). Electrical field interactions in different cochlear implant systems. *J Acoust Soc Am* 114, 2049–2057. doi:10.1121/1.1610451.

Bouthour, W., Mégevand, P., Donoghue, J., Lüscher, C., Birbaumer, N., and Krack, P. (2019). Biomarkers for closed-loop deep brain stimulation in Parkinson disease and beyond. *Nat Rev Neurol* 15, 343–352. doi:10.1038/s41582-019-0166-4.

Briaire, J. J., and Frijns, J. H. M. (2005). Unraveling the electrically evoked compound action potential. *Hear Res* 205, 143–156. doi:10.1016/j.heares.2005.03.020.

Brittain, J.-S., and Brown, P. (2014). Oscillations and the basal ganglia: Motor control and beyond. *Neuroimage* 85, 637–647. doi:10.1016/j.neuroimage.2013.05.084.

Brodsky, M. A., Anderson, S., Murchison, C., Seier, M., Wilhelm, J., Vederman, A., and Burchiel, K. J. (2017). Clinical outcomes of asleep vs awake deep brain stimulation for Parkinson disease. *Neurology* 89, 1944–1950. doi:10.1212/WNL.0000000000004630.

Brown, C. J., and Abbas, P. J. (1990). Electrically evoked whole-nerve action potentials: Parametric data from the cat. *J Acoust Soc Am* 88, 2205–2210. doi:10.1121/1.400117.

Brown, P. (2003). Oscillatory nature of human basal ganglia activity: Relationship to the pathophysiology of Parkinson's disease. *Mov Disord* 18, 357–363. doi:10.1002/mds.10358.

Brown, P., Mazzone, P., Oliviero, A., Altibrandi, M. G., Pilato, F., Tonali, P. A., and Di Lazzaro, V. (2004). Effects of stimulation of the subthalamic area on oscillatory pallidal activity in Parkinson's disease. *Exp Neurol* 188, 480–490. doi:10.1016/j.expneurol.2004.05.009.

Brown, P., Oliviero, A., Mazzone, P., Insola, A., Tonali, P., and Di Lazzaro, V. (2001). Dopamine dependency of oscillations between subthalamic nucleus and pallidum in Parkinson's disease. *J Neurosci* 21, 1033–1038. doi:21/3/1033 [pii].

Brown, P., and Williams, D. (2005). Basal ganglia local field potential activity: Character and functional significance in the human. *Clin Neurophysiol* 116, 2510–2519. doi:10.1016/j.clinph.2005.05.009.

Buzsáki, G. (2004). Large-scale recording of neuronal ensembles. *Nat Neurosci* 7, 446–451. doi:10.1038/nn1233.

Buzsáki, G. (2006). *Rhythms of the Brain*. Oxford University Press doi:10.1093/acprof:oso/9780195301069.001.0001.

Buzsáki, G., Anastassiou, C. A., and Koch, C. (2012). The origin of extracellular fields and currents -- EEG, ECoG, LFP and spikes. *Nat Rev Neurosci* 13, 407–420. doi:10.1038/nrn3241.

Camara, C., Isasi, P., Warwick, K., Ruiz, V., Aziz, T., Stein, J., and Bakštein, E. (2015). Resting tremor classification and detection in Parkinson's disease patients. *Biomed Signal Process Control* 16, 88–97. doi:10.1016/j.bspc.2014.09.006.

Campbell, B. A., Machado, A. G., and Baker, K. B. (2019). *Electrophysiologic mapping for deep brain stimulation for movement disorders*. 1st ed. Elsevier B.V. doi:10.1016/B978-0-444-64032-1.00022-9.

Canolty, R. T., Edwards, E., Dalal, S. S., Soltani, M., Nagarajan, S. S., Berger, M. S., Barbaro, N. M., Knight, R. T., Kirsch, H. E., Berger, M. S., Barbaro, N. M., and Knight, R. T. (2006). High Gamma Power is Phase-Locked to Theta Oscillations in Human Neocortex. *Science* 313, 1626–1628. doi:10.1126/science.1128115.High.

Canolty, R. T., and Knight, R. T. (2010). The functional role of cross-frequency coupling. *Trends Cogn Sci* 14, 506–515. doi:10.1016/j.tics.2010.09.001.

Cassidy, M., Mazzone, P., Oliviero, A., Insola, A., Tonali, P., Di Lazzaro, V., and Brown, P. (2002). Movement-related changes in synchronization in the human basal ganglia. *Brain* 125, 1235–1246. doi:10.1093/brain/awf135.

Chen, C. C., Pogosyan, A., Zrinzo, L. U., Tisch, S., Limousin, P., Ashkan, K., Yousry, T., Hariz, M. I., and Brown, P. (2006). Intra-operative recordings of local field potentials can help localize the subthalamic nucleus in Parkinson's disease surgery. *Exp Neurol* 198, 214–221. doi:10.1016/j.expneurol.2005.11.019.

Chen, T., Mirzadeh, Z., Chapple, K. M., Lambert, M., Shill, H. A., Moguel-Cobos, G., Tröster, A. I., Dhall, R., and Ponce, F. A. (2018). Clinical outcomes following awake and asleep deep brain stimulation for Parkinson disease. *J Neurosurg* 130, 109–120. doi:10.3171/2017.8.JNS17883.

Cheyne, D., Bells, S., Ferrari, P., Gaetz, W., and Bostan, A. C. (2008). Self-paced movements induce high-frequency gamma oscillations in primary motor cortex. *Neuroimage* 42, 332–342. doi:10.1016/j.neuroimage.2008.04.178.

Cleary, D. R., Raslan, A. M., Rubin, J. E., Bahgat, D., Viswanathan, A., Heinricher, M. M., and Burchiel, K. J. (2013). Deep brain stimulation entrains local neuronal firing in human globus pallidus internus. *J Neurophysiol* 109, 978–987. doi:10.1152/jn.00420.2012.

Cogan, S. F. (2008). Neural Stimulation and Recording Electrodes. *Annu Rev Biomed Eng* 10, 275–309. doi:10.1146/annurev.bioeng.10.061807.160518.

Cohen, M. X. (2008). Assessing transient cross-frequency coupling in EEG data. *J Neurosci Methods* 168, 494–499.

doi:10.1016/j.jneumeth.2007.10.012.

Cole, S. R., van der Meij, R., Peterson, E. J., de Hemptinne, C., Starr, P. A., and Voytek, B. (2017). Nonsinusoidal Beta Oscillations Reflect Cortical Pathophysiology in Parkinson's Disease. *J Neurosci* 37, 4830–4840. doi:10.1523/JNEUROSCI.2208-16.2017.

Collins, K. L., Lehmann, E. M., and Patil, P. G. (2010). Deep brain stimulation for movement disorders. *Neurobiol Dis* 38, 338–345. doi:10.1016/j.nbd.2009.11.019.

Connolly, A. T., Kaemmerer, W. F., Dani, S., Stanslaski, S. R., Panken, E., Johnson, M. D., and Denison, T. (2015). Guiding Deep Brain Stimulation Contact Selection Using Local Field Potentials Sensed by a Chronically Implanted Device in Parkinson ' s Disease Patients *. 22–24.

Creutzfeldt, O. D., Watanabe, S., and Lux, H. D. (1966). Relations between EEG phenomena and potentials of single cortical cells. I. Evoked responses after thalamic and epicortical stimulation. *Electroencephalogr Clin Neurophysiol* 20, 1–18. doi:10.1016/0013-4694(66)90136-2.

de Hemptinne, C., Ryapolova-Webb, E. S., Air, E. L., Garcia, P. A., Miller, K. J., Ojemann, J. G., Ostrem, J. L., Galifianakis, N. B., and Starr, P. A. (2013). Exaggerated phase-amplitude coupling in the primary motor cortex in Parkinson disease. *Proc Natl Acad Sci U S A* 110, 4780–5. doi:10.1073/pnas.1214546110.

de Hemptinne, C., Swann, N. C., Ostrem, J. L., Ryapolova-Webb, E. S., San Luciano, M., Galifianakis, N. B., and Starr, P. a (2015). Therapeutic deep

brain stimulation reduces cortical phase-amplitude coupling in Parkinson's disease. *Nat Neurosci* 18, 779–786. doi:10.1038/nn.3997.

DeLong, M. R., and Wichmann, T. (2007). Circuits and Circuit Disorders of the Basal Ganglia. *Arch Neurol* 64, 20. doi:10.1001/archneur.64.1.20.

deSouza, R.-M., Moro, E., Lang, A. E., and Schapira, A. H. V. (2013). Timing of deep brain stimulation in Parkinson disease: A need for reappraisal? *Ann Neurol* 73, 565–575. doi:10.1002/ana.23890.

Deuschl, G., Schade-Brittinger, C., Krack, P., Volkmann, J., Schäfer, H., Bötzel, K., Daniels, C., Deutschländer, A., Dillmann, U., Eisner, W., Gruber, D., Hamel, W., Herzog, J., Hilker, R., Klebe, S., Kloß, M., Koy, J., … Voges, J. (2006). A Randomized Trial of Deep-Brain Stimulation for Parkinson's Disease. *N Engl J Med* 355, 896–908. doi:10.1056/NEJMoa060281.

Dostrovsky, J. O., Levy, R., Wu, J. P., Hutchison, W. D., Tasker, R. R., and Lozano, A. M. (2000). Microstimulation-Induced Inhibition of Neuronal Firing in Human Globus Pallidus. *J Neurophysiol* 84, 570–574. doi:10.1152/jn.2000.84.1.570.

Duda, R. O., Hart, P. E., and Stork, D. G. (2000). *Pattern Classification*. 2nd ed. Wiley-Interscience.

Eisinger, R. S., Cernera, S., Gittis, A., Gunduz, A., and Okun, M. S. (2019). A review of basal ganglia circuits and physiology: Application to deep brain stimulation. *Parkinsonism Relat Disord* 59, 9–20. doi:10.1016/j.parkreldis.2019.01.009.

Escobar, D., Johnson, L. A., Nebeck, S. D., Zhang, J., Johnson, M. D., Baker, K. B., Molnar, G. F., and Vitek, J. L. (2017). Parkinsonism and Vigilance: Alteration in neural oscillatory activity and phase-amplitude coupling in the basal ganglia and motor cortex. *J Neurophysiol* 118, jn.00388.2017. doi:10.1152/jn.00388.2017.

Eusebio, A., Thevathasan, W., Doyle Gaynor, L., Pogosyan, A., Bye, E., Foltynie, T., Zrinzo, L., Ashkan, K., Aziz, T., and Brown, P. (2011). Deep brain stimulation can suppress pathological synchronisation in parkinsonian patients. *J Neurol Neurosurg Psychiatry* 82, 569–573. doi:10.1136/jnnp.2010.217489.

Fahn, S. (2003). Description of Parkinson's disease as a clinical syndrome. *Ann N Y Acad Sci* 991, 1–14. doi:10.1111/j.1749-6632.2003.tb07458.x.

Filali, M., Hutchison, W. D., Palter, V. N., Lozano, A. M., and Dostrovsky, J. O. (2004). Stimulation-induced inhibition of neuronal firing in human subthalamic nucleus. *Exp Brain Res* 156, 274–281. doi:10.1007/s00221-003-1784-y.

Foffani, G., Ardolino, G., Meda, B., Egidi, M., Rampini, P., Caputo, E., Baselli, G., and Priori, A. (2005). Altered subthalamo-pallidal synchronisation in parkinsonian dyskinesias. *J Neurol Neurosurg Psychiatry* 76, 426–8. doi:10.1136/jnnp.2004.043547.

Foffani, G., Priori, A., Egidi, M., Rampini, P., Tamma, F., Caputo, E., Moxon, K. A., Cerutti, S., and Barbieri, S. (2003). 300-Hz subthalamic oscillations in Parkinson's disease. *Brain* 126, 2153–2163. doi:10.1093/brain/awg229.

Garcia, L., D'Alessandro, G., Bioulac, B., and Hammond, C. (2005a). High-frequency stimulation in Parkinson's disease: more or less? *Trends Neurosci* 28, 209–216. doi:10.1016/j.tins.2005.02.005.

Garcia, L., D'Alessandro, G., Fernagut, P., Bioulac, B., and Hammond, C. (2005b). Impact of High-Frequency Stimulation Parameters on the Pattern of Discharge of Subthalamic Neurons. *J Neurophysiol* 94, 3662–3669. doi:10.1152/jn.00496.2005.

Gatev, P., Darbin, O., and Wichmann, T. (2006). Oscillations in the basal ganglia under normal conditions and in movement disorders. *Mov Disord* 21, 1566–1577. doi:10.1002/mds.21033.

Giannicola, G., Rosa, M., Marceglia, S., Scelzo, E., Rossi, L., Servello, D., Menghetti, C., Pacchetti, C., Zangaglia, R., Locatelli, M., Caputo, E., Cogiamanian, F., Ardolino, G., Barbieri, S., and Priori, A. (2013). The Effects of Levodopa and Deep Brain Stimulation on Subthalamic Local Field Low-Frequency Oscillations in Parkinson's Disease. *Neurosignals* 21, 89–98. doi:10.1159/000336543.

Giannicola, G., Rosa, M., Servello, D., Menghetti, C., Carrabba, G., Pacchetti, C., Zangaglia, R., Cogiamanian, F., Scelzo, E., Marceglia, S., Rossi, L., and Priori, A. (2012). Subthalamic local field potentials after seven-year deep brain stimulation in Parkinson's disease. *Exp Neurol* 237, 312–317. doi:10.1016/j.expneurol.2012.06.012.

Gilmour, T. P., Lieu, C. A., Nolt, M. J., Piallat, B., Deogaonkar, M., and Subramanian, T. (2011). The effects of chronic levodopa treatments on

the neuronal firing properties of the subthalamic nucleus and substantia nigra reticulata in hemiparkinsonian rhesus monkeys. *Exp Neurol* 228, 53–58. doi:10.1016/j.expneurol.2010.12.001.

Gmel, G. E., Obradovic, M., Gorman, R. B., Single, P. S., Parker, J. L., Hamilton, T. J., Chenery, H. J., Coyne, T., and Silburn, P. A. (2015). A new biomarker for subthalamic deep brain stimulation for patients with advanced Parkinson's disease - A pilot study. *J Neural Eng* 12. doi:10.1088/1741-2560/12/6/066013.

Goetz, C. G. (2011). The History of Parkinson's Disease: Early Clinical Descriptions and Neurological Therapies. *Cold Spring Harb Perspect Med* 1, a008862–a008862. doi:10.1101/cshperspect.a008862.

Goetz, C. G., Poewe, W., Rascol, O., and Sampaio, C. (2005). Evidence-based medical review update: Pharmacological and surgical treatments of Parkinson's disease: 2001 to 2004. *Mov Disord* 20, 523–539. doi:10.1002/mds.20464.

Gourisankar, A., Eisenstein, S. A., Trapp, N. T., Koller, J. M., Campbell, M. C., Ushe, M., Perlmutter, J. S., Hershey, T., and Black, K. J. (2018). Mapping movement, mood, motivation and mentation in the subthalamic nucleus. *R Soc Open Sci* 5, 171177. doi:10.1098/rsos.171177.

Granziera, C., Pollo, C., Russmann, H., Staedler, C., Ghika, J., Villemure, J. G., Burkhard, P. R., and Vingerhoets, F. J. G. (2008). Sub-acute delayed failure of subthalamic DBS in Parkinson's disease: The role of micro-lesion effect. *Park Relat Disord* 14, 109–113.

doi:10.1016/j.parkreldis.2007.06.013.

Grill, W. M., Snyder, A. N., and Miocinovic, S. (2004). Deep brain stimulation creates an informational lesion of the stimulated nucleus. *Neuroreport* 15, 1137–1140. doi:10.1097/00001756-200405190-00011.

Groiss, S. J., Wojtecki, L., Südmeyer, M., and Schnitzler, a (2009). Deep brain stimulation in Parkinson's disease. *Ther Adv Neurol Disord* 2, 20–28. doi:10.1177/1756285609339382.

Gross, R. E., Krack, P., Rodriguez-Oroz, M. C., Rezai, A. R., and Benabid, A.-L. (2006). Electrophysiological mapping for the implantation of deep brain stimulators for Parkinson's disease and tremor. *Mov Disord* 21, S259–S283. doi:10.1002/mds.20960.

Guehl, D., Cuny, E., Benazzouz, A., Rougier, A., Tison, F., Machado, S., Grabot, D., Gross, C., Bioulac, B., and Burbaud, P. (2006). Side-effects of subthalamic stimulation in Parkinson's disease: clinical evolution and predictive factors. *Eur J Neurol* 13, 963–971. doi:10.1111/j.1468-1331.2006.01405.x.

Gunduz, A., Foote, K. D., and Okun, M. S. (2017). Reengineering deep brain stimulation for movement disorders: Emerging technologies. *Curr Opin Biomed Eng* 4, 97–105. doi:10.1016/j.cobme.2017.09.001.

Guo, Y., Rubin, J. E., McIntyre, C. C., Vitek, J. L., and Terman, D. (2008). Thalamocortical Relay Fidelity Varies Across Subthalamic Nucleus Deep Brain Stimulation Protocols in a Data-Driven Computational Model. *J Neurophysiol* 99, 1477–1492. doi:10.1152/jn.01080.2007.

Hammond, C., Bergman, H., and Brown, P. (2007). Pathological synchronization in Parkinson's disease: networks, models and treatments. *Trends Neurosci* 30, 357–364. doi:10.1016/j.tins.2007.05.004.

Hariz, M. (2012). Twenty-five years of deep brain stimulation: Celebrations and apprehensions. *Mov Disord* 27, 930–933. doi:10.1002/mds.25007.

Hariz, M. (2014). Deep brain stimulation: new techniques. *Parkinsonism Relat Disord* 20, S192–S196. doi:10.1016/S1353-8020(13)70045-2.

Harris, K. D., Quiroga, R. Q., Freeman, J., and Smith, S. L. (2016). Improving data quality in neuronal population recordings. *Nat Neurosci* 19, 1165–1174. doi:10.1038/nn.4365.

Hashimoto, T., Elder, C. M., Okun, M. S., Patrick, S. K., and Vitek, J. L. (2003). Stimulation of the Subthalamic Nucleus Changes the Firing Pattern of Pallidal Neurons. *J Neurosci* 23, 1916–1923. doi:10.1523/JNEUROSCI.23-05-01916.2003.

Hell, F., Palleis, C., Mehrkens, J. H., Koeglsperger, T., and Bötzel, K. (2019). Deep brain stimulation programming 2.0: Future perspectives for target identification and adaptive closed loop stimulation. *Front Neurol* 10, 1–11. doi:10.3389/fneur.2019.00314.

Herzog, J., Fietzek, U., Hamel, W., Morsnowski, A., Steigerwald, F., Schrader, B., Weinert, D., Pfister, G., Müller, D., Mehdorn, H. M., Deuschl, G., and Volkmann, J. (2004). Most effective stimulation site in subthalamic deep brain stimulation for Parkinson's disease. *Mov Disord* 19, 1050–1054. doi:10.1002/mds.20056.

Hickey, P., and Stacy, M. (2016). Deep brain stimulation: A paradigm shifting approach to treat Parkinson's disease. *Front Neurosci* 10, 1–11. doi:10.3389/fnins.2016.00173.

Hill, D. N., Mehta, S. B., and Kleinfeld, D. (2011). Quality Metrics to Accompany Spike Sorting of Extracellular Signals. *J Neurosci* 31, 8699–8705. doi:10.1523/JNEUROSCI.0971-11.2011.

Hirschmann, J., Butz, M., Hartmann, C. J., Hoogenboom, N., Özkurt, T. E., Vesper, J., Wojtecki, L., and Schnitzler, A. (2016). Parkinsonian Rest Tremor Is Associated With Modulations of Subthalamic High-Frequency Oscillations. *Mov Disord* 31, 1551–1559. doi:10.1002/mds.26663.

Ho, A. L., Ali, R., Connolly, I. D., Henderson, J. M., Dhall, R., Stein, S. C., and Halpern, C. H. (2018). Awake versus asleep deep brain stimulation for Parkinson's disease: a critical comparison and meta-analysis. *J Neurol Neurosurg Psychiatry* 89, 687–691. doi:10.1136/jnnp-2016-314500.

Hoang, K. B., Cassar, I. R., Grill, W. M., and Turner, D. A. (2017). Biomarkers and stimulation algorithms for adaptive brain stimulation. *Front Neurosci* 11. doi:10.3389/fnins.2017.00564.

Hoang, K. B., and Turner, D. A. (2019). The Emerging Role of Biomarkers in Adaptive Modulation of Clinical Brain Stimulation. *Neurosurgery* 85, E430–E439. doi:10.1093/neuros/nyz096.

Holdefer, R. N., Cohen, B. A., and Greene, K. A. (2010). Intraoperative local field recording for deep brain stimulation in Parkinson's disease and essential tremor. *Mov Disord* 25, 2067–2075. doi:10.1002/mds.23232.

Horn, A., and Kühn, A. A. (2015). Lead-DBS: A toolbox for deep brain stimulation electrode localizations and visualizations. *Neuroimage* 107, 127–135. doi:10.1016/j.neuroimage.2014.12.002.

Horn, A., Neumann, W.-J., Degen, K., Schneider, G.-H., and Kühn, A. A. (2017). Toward an electrophysiological "sweet spot" for deep brain stimulation in the subthalamic nucleus. *Hum Brain Mapp* 3390, 3377–3390. doi:10.1002/hbm.23594.

Hornykiewicz, O. (2006). "The discovery of dopamine deficiency in the parkinsonian brain," in *Parkinson's Disease and Related Disorders* (Vienna: Springer Vienna), 9–15. doi:10.1007/978-3-211-45295-0_3.

Hua, S. E., Lenz, F. A., Zirh, T. A., Reich, S. G., and Dougherty, P. M. (1998). Thalamic neuronal activity correlated with essential tremor. *J Neurol Neurosurg Psychiatry* 64, 273–276. doi:10.1136/jnnp.64.2.273.

Humphrey, D. R., and Schmidt, E. M. (1990). "Extracellular Single-Unit Recording Methods," in *Neurophysiological Techniques: Applications to Neural Systems*, eds. A. A. Boulton, G. B. Baker, and C. H. Vanderwolf (Totowa, NJ: Humana Press), 1–64. doi:10.1385/0-89603-185-3:1.

Hutchison, W. D., Allan, R. J., Opitz, H., Levy, R., Dostrovsky, J. O., Lang, A. E., and Lozano, A. M. (1998). Neurophysiological identification of the subthalamic nucleus in surgery for Parkinson's disease. *Ann Neurol* 44, 622–628. doi:10.1002/ana.410440407.

Ince, N. F., Gupte, A., Wichmann, T., Ashe, J., Henry, T., Bebler, M., Eberly, L., and Abosch, A. (2010). Selection of optimal programming contacts

based on local field potential recordings from subthalamic nucleus in patients with Parkinson's disease. *Neurosurgery* 67, 390–397. doi:10.1227/01.NEU.0000372091.64824.63.

Jankovic, J. (2001). Parkinson's disease therapy: treatment of early and late disease. *Chin Med J (Engl)* 114, 227–34. Available at: http://www.ncbi.nlm.nih.gov/pubmed/11780303.

Jankovic, J. (2008). Parkinson's disease: clinical features and diagnosis. *J Neurol Neurosurg Psychiatry* 79, 368–376. doi:10.1136/jnnp.2007.131045.

Johnson, L. A., Nebeck, S. D., Muralidharan, A., Johnson, M. D., Baker, K. B., and Vitek, J. L. (2016). Closed-Loop Deep Brain Stimulation Effects on Parkinsonian Motor Symptoms in a Non-Human Primate – Is Beta Enough? *Brain Stimul* 9, 892–896. doi:10.1016/j.brs.2016.06.051.

Johnson, M. D., Miocinovic, S., McIntyre, C. C., and Vitek, J. L. (2008). Mechanisms and targets of deep brain stimulation in movement disorders. *Neurotherapeutics* 5, 294–308. doi:10.1016/j.nurt.2008.01.010.

Kaku, H., Ozturk, M., Viswanathan, A., Jimenez-Shahed, J., Sheth, S., and Ince, N. F. (2019). Grouping Neuronal Spiking Patterns in the Subthalamic Nucleus of Parkinsonian Patients. in *2019 41st Annual International Conference of the IEEE Engineering in Medicine and Biology Society (EMBC)* (IEEE), 4221–4224. doi:10.1109/EMBC.2019.8857418.

Kaku, H., Ozturk, M., Viswanathan, A., Shahed, J., Sheth, S. A., Kumar, S., and Ince, N. F. (2020). Unsupervised clustering reveals spatially varying

single neuronal firing patterns in the subthalamic nucleus of patients with Parkinson's disease. *Clin Park Relat Disord* 3, 100032. doi:10.1016/j.prdoa.2019.100032.

Kane, A., Hutchison, W. D., Hodaie, M., Lozano, A. M., and Dostrovsky, J. O. (2009). Dopamine-dependent high-frequency oscillatory activity in thalamus and subthalamic nucleus of patients with Parkinson's disease. *Neuroreport* 20, 1549–1553. doi:10.1097/WNR.0b013e32833282c8.

Kent, A. R., Swan, B. D., Brocker, D. T., Turner, D. A., Gross, R. E., and Grill, W. M. (2015). Measurement of Evoked Potentials During Thalamic Deep Brain Stimulation. *Brain Stimul* 8, 42–56. doi:10.1016/j.brs.2014.09.017.

Kolb, R., Abosch, A., Felsen, G., and Thompson, J. A. (2017). Use of intraoperative local field potential spectral analysis to differentiate basal ganglia structures in Parkinson's disease patients. *Physiol Rep* 5, 1–14. doi:10.14814/phy2.13322.

Krack, P., Batir, A., Van Blercom, N., Chabardes, S., Fraix, V., Ardouin, C., Koudsie, A., Limousin, P. D., Benazzouz, A., LeBas, J. F., Benabid, A.-L., and Pollak, P. (2003). Five-Year Follow-up of Bilateral Stimulation of the Subthalamic Nucleus in Advanced Parkinson's Disease. *N Engl J Med* 349, 1925–1934. doi:10.1056/NEJMoa035275.

Krack, P., Kumar, R., Ardouin, C., Dowsey, P. L., McVicker, J. M., Benabid, A.-L., and Pollak, P. (2001). Mirthful laughter induced by subthalamic nucleus stimulation. *Mov Disord* 16, 867–875. doi:10.1002/mds.1174.

Kühn, A. A., Kempf, F., Brucke, C., Gaynor Doyle, L., Martinez-Torres, I.,

Pogosyan, A., Trottenberg, T., Kupsch, A., Schneider, G.-H., Hariz, M. I., Vandenberghe, W., Nuttin, B., and Brown, P. (2008). High-Frequency Stimulation of the Subthalamic Nucleus Suppresses Oscillatory Activity in Patients with Parkinson's Disease in Parallel with Improvement in Motor Performance. *J Neurosci* 28, 6165–6173. doi:10.1523/JNEUROSCI.0282-08.2008.

Kühn, A. A., Kupsch, A., Schneider, G. H., and Brown, P. (2006). Reduction in subthalamic 8-35 Hz oscillatory activity correlates with clinical improvement in Parkinson's disease. *Eur J Neurosci* 23, 1956–1960. doi:10.1111/j.1460-9568.2006.04717.x.

Kühn, A. A., Trottenberg, T., Kivi, A., Kupsch, A., Schneider, G. H., and Brown, P. (2005). The relationship between local field potential and neuronal discharge in the subthalamic nucleus of patients with Parkinson's disease. *Exp Neurol* 194, 212–220. doi:10.1016/j.expneurol.2005.02.010.

Kühn, A. A., Williams, D., Kupsch, A., Limousin, P., Hariz, M., Schneider, G., Yarrow, K., and Brown, P. (2004). Event-related beta desynchronization in human subthalamic nucleus correlates with motor performance. *Brain* 127, 735–746. doi:10.1093/brain/awh106.

Lakatos, P., Karmos, G., Mehta, A. D., Ulbert, I., and Schroeder, C. E. (2008). Entrainment of Neuronal Attentional Selection. *Science (80-)* 320, 23–25. doi:10.1126/science.1154735.

Lee, D., Dallapiazza, R., De Vloo, P., and Lozano, A. (2018). Current surgical

treatments for Parkinson's disease and potential therapeutic targets. *Neural Regen Res* 13, 1342–1345. doi:10.4103/1673-5374.235220.

Lempka, S. F., and McIntyre, C. C. (2013). Theoretical Analysis of the Local Field Potential in Deep Brain Stimulation Applications. *PLoS One* 8, e59839. doi:10.1371/journal.pone.0059839.

Lenz, F. A., Dostrovsky, J. O., Kwan, H. C., Tasker, R. R., Yamashiro, K., and Murphy, J. T. (1988). Methods for microstimulation and recording of single neurons and evoked potentials in the human central nervous system. *J Neurosurg* 68, 630–634. doi:10.3171/jns.1988.68.4.0630.

Leventhal, D. K., Gage, G. J., Schmidt, R., Pettibone, J. R., Case, A. C., and Berke, J. D. (2012). Basal ganglia beta oscillations accompany cue utilization. *Neuron* 73, 523–536. doi:10.1016/j.neuron.2011.11.032.

Levy, R., Ashby, P., Hutchison, W. D., Lang, A. E., Lozano, A. M., and Dostrovsky, J. O. (2002). Dependence of subthalamic nucleus oscillations on movement and dopamine in Parkinson's disease. *Brain* 125, 1196–1209. doi:10.1093/brain/awf128.

Levy, R., Hutchison, W. D., Lozano, A. M., and Dostrovsky, J. O. (2000). High-frequency synchronization of neuronal activity in the subthalamic nucleus of parkinsonian patients with limb tremor. *J Neurosci* 20, 7766–7775. doi:20/20/7766 [pii].

Limousin, P., Krack, P., Pollak, P., Benazzouz, A., Ardouin, C., Hoffmann, D., and Benabid, A.-L. (1998). Electrical Stimulation of the Subthalamic Nucleus in Advanced Parkinson's Disease. *N Engl J Med* 339, 1105–

1111. doi:10.1056/NEJM199810153391603.

Limousin, P., Pollak, P., Benazzouz, A., Hoffmann, D., Le Bas, J.-F., Perret, J. E., Benabid, A.-L., and Broussolle, E. (1995). Effect on parkinsonian signs and symptoms of bilateral subthalamic nucleus stimulation. *Lancet* 345, 91–95. doi:10.1016/S0140-6736(95)90062-4.

Lindén, H., Tetzlaff, T., Potjans, T. C., Pettersen, K. H., Grün, S., Diesmann, M., and Einevoll, G. T. (2011). Modeling the Spatial Reach of the LFP. *Neuron* 72, 859–872. doi:10.1016/j.neuron.2011.11.006.

Little, S., and Brown, P. (2012). What brain signals are suitable for feedback control of deep brain stimulation in Parkinson's disease? *Ann N Y Acad Sci* 1265, 9–24. doi:10.1111/j.1749-6632.2012.06650.x.

Little, S., Pogosyan, A., Neal, S., Zavala, B., Zrinzo, L., Hariz, M., Foltynie, T., Limousin, P., Ashkan, K., Fitzgerald, J., Green, A. L., Aziz, T. Z., and Brown, P. (2013). Adaptive deep brain stimulation in advanced Parkinson disease. *Ann Neurol*, 449–457. doi:10.1002/ana.23951.

Litvak, V., Eusebio, A., Jha, A., Oostenveld, R., Barnes, G., Foltynie, T., Limousin, P., Zrinzo, L., Hariz, M. I., Friston, K., and Brown, P. (2012). Movement-related changes in local and long-range synchronization in parkinson's disease revealed by simultaneous magnetoencephalography and intracranial recordings. *J Neurosci* 32, 10541–10553. doi:10.1523/JNEUROSCI.0767-12.2012.

Liu, Z., He, S., and Li, L. (2020). General Anesthesia versus Local Anesthesia for Deep Brain Stimulation in Parkinson's Disease: A Meta-Analysis.

Stereotact Funct Neurosurg, 1–10. doi:10.1159/000505079.

Lopez-Azcarate, J., Tainta, M., Rodriguez-Oroz, M. C., Valencia, M., Gonzalez, R., Guridi, J., Iriarte, J., Obeso, J. A., Artieda, J., and Alegre, M. (2010). Coupling between beta and high-frequency activity in the human subthalamic nucleus may be a pathophysiological mechanism in Parkinson's disease. *J Neurosci* 30, 6667–6677. doi:10.1523/JNEUROSCI.5459-09.2010.

Lozano-Soldevilla, D., ter Huurne, N., and Oostenveld, R. (2016). Neuronal Oscillations with Non-sinusoidal Morphology Produce Spurious Phase-to-Amplitude Coupling and Directionality. *Front Comput Neurosci* 10, 1–17. doi:10.3389/fncom.2016.00087.

Lu, C. W., Malaga, K. A., Chou, K. L., Chestek, C. A., and Patil, P. G. (2019). High density microelectrode recording predicts span of therapeutic tissue activation volumes in subthalamic deep brain stimulation for Parkinson disease. *Brain Stimul*. doi:10.1016/j.brs.2019.11.013.

Machado, A., Rezai, A. R., Kopell, B. H., Gross, R. E., Sharan, A. D., and Benabid, A.-L. (2006). Deep brain stimulation for Parkinson's disease: Surgical technique and perioperative management. *Mov Disord* 21, S247–S258. doi:10.1002/mds.20959.

Magnin, M., Jetzer, U., Morel, A., and Jeanmonod, D. (2001). Microelectrode recording and macrostimulation in thalamic and subthalamic MRI guided stereotactic surgery. *Neurophysiol Clin* 31, 230–238. doi:10.1016/S0987-7053(01)00261-1.

Mahlknecht, P., Limousin, P., and Foltynie, T. (2015). Deep brain stimulation for movement disorders: update on recent discoveries and outlook on future developments. *J Neurol* 262, 2583–2595. doi:10.1007/s00415-015-7790-8.

Marceglia, S., Foffani, G., Bianchi, A. M., Baselli, G., Tamma, F., Egidi, M., and Priori, A. (2006). Dopamine-dependent non-linear correlation between subthalamic rhythms in Parkinson's disease. *J Physiol* 571, 579–591. doi:10.1113/jphysiol.2005.100271.

Marceglia, S., Mrakic-Sposta, S., Tommasi, G., Bartolomei, L., Foresti, C., Valzania, F., Galati, S., Stefani, A., Tamma, F., and Priori, A. (2010). Multicenter study report: electrophysiological monitoring procedures for subthalamic deep brain stimulation surgery in Parkinson's disease. *Neurol Sci* 31, 449–457. doi:10.1007/s10072-010-0254-0.

Massano, J., and Bhatia, K. P. (2012). Clinical Approach to Parkinson's Disease: Features, Diagnosis, and Principles of Management. *Cold Spring Harb Perspect Med* 2, a008870–a008870. doi:10.1101/cshperspect.a008870.

Matsuoka, A. J., Rubinstein, J. T., Abbas, P. J., and Miller, C. A. (2001). The effects of interpulse interval on stochastic properties of electrical stimulation: models and measurements. *IEEE Trans Biomed Eng* 48, 416–424. doi:10.1109/10.915706.

McConnell, G. C., So, R. Q., Hilliard, J. D., Lopomo, P., and Grill, W. M. (2012). Effective Deep Brain Stimulation Suppresses Low-Frequency

Network Oscillations in the Basal Ganglia by Regularizing Neural Firing Patterns. *J Neurosci* 32, 15657–15668. doi:10.1523/JNEUROSCI.2824-12.2012.

McIntyre, C. C., and Grill, W. M. (2001). Finite element analysis of the current-density and electric field generated by metal microelectrodes. *Ann Biomed Eng* 29, 227–235. doi:10.1114/1.1352640.

McIntyre, C. C., Grill, W. M., Sherman, D. L., and Thakor, N. V. (2004a). Cellular Effects of Deep Brain Stimulation: Model-Based Analysis of Activation and Inhibition. *J Neurophysiol* 91, 1457–1469. doi:10.1152/jn.00989.2003.

McIntyre, C. C., and Hahn, P. J. (2010). Network perspectives on the mechanisms of deep brain stimulation. *Neurobiol Dis* 38, 329–337. doi:10.1016/j.nbd.2009.09.022.

McIntyre, C. C., Savasta, M., Kerkerian-Le Goff, L., and Vitek, J. L. (2004b). Uncovering the mechanism(s) of action of deep brain stimulation: activation, inhibition, or both. *Clin Neurophysiol* 115, 1239–1248. doi:10.1016/j.clinph.2003.12.024.

Meidahl, A. C., Moll, C. K. E., van Wijk, B. C. M., Gulberti, A., Tinkhauser, G., Westphal, M., Engel, A. K., Hamel, W., Brown, P., and Sharott, A. (2019). Synchronised spiking activity underlies phase amplitude coupling in the subthalamic nucleus of Parkinson's disease patients. *Neurobiol Dis* 127, 101–113. doi:10.1016/j.nbd.2019.02.005.

Meidahl, A. C., Tinkhauser, G., Herz, D. M., Cagnan, H., Debarros, J., and

Brown, P. (2017). Adaptive Deep Brain Stimulation for Movement Disorders: The Long Road to Clinical Therapy. *Mov Disord* 32, 810–819. doi:10.1002/mds.27022.

Meissner, W., Leblois, A., Hansel, D., Bioulac, B., Gross, C. E., Benazzouz, A., and Boraud, T. (2005). Subthalamic high frequency stimulation resets subthalamic firing and reduces abnormal oscillations. *Brain* 128, 2372–2382. doi:10.1093/brain/awh616.

Miller, C. A., Abbas, P. J., Rubinstein, J. T., Robinson, B. K., Matsuoka, A. J., and Woodworth, G. (1998). Electrically evoked compound action potentials of guinea pig and cat: responses to monopolar, monophasic stimulation. *Hear Res* 119, 142–154. doi:10.1016/S0378-5955(98)00046-X.

Miller, C. A., Brown, C. J., Abbas, P. J., and Chi, S.-L. (2008). The clinical application of potentials evoked from the peripheral auditory system. *Hear Res* 242, 184–197. doi:10.1016/j.heares.2008.04.005.

Miller, K. J., Hermes, D., Honey, C. J., Hebb, A. O., Ramsey, N. F., Knight, R. T., Ojemann, J. G., and Fetz, E. E. (2012). Human Motor Cortical Activity Is Selectively Phase-Entrained on Underlying Rhythms. *PLoS Comput Biol* 8. doi:10.1371/journal.pcbi.1002655.

Miocinovic, S., Somayajula, S., Chitnis, S., and Vitek, J. L. (2013). History, Applications, and Mechanisms of Deep Brain Stimulation. *JAMA Neurol* 70, 163. doi:10.1001/2013.jamaneurol.45.

Miyagi, Y., Okamoto, T., Morioka, T., Tobimatsu, S., Nakanishi, Y., Aihara, K.,

Hashiguchi, K., Murakami, N., Yoshida, F., Samura, K., Nagata, S., and Sasaki, T. (2009). Spectral Analysis of Field Potential Recordings by Deep Brain Stimulation Electrode for Localization of Subthalamic Nucleus in Patients with Parkinson’s Disease. *Stereotact Funct Neurosurg* 87, 211–218. doi:10.1159/000225974.

Moffitt, M. A., and McIntyre, C. C. (2005). Model-based analysis of cortical recording with silicon microelectrodes. *Clin Neurophysiol* 116, 2240–2250. doi:10.1016/j.clinph.2005.05.018.

Montgomery, E. B. (2006). Effects of GPi stimulation on human thalamic neuronal activity. *Clin Neurophysiol* 117, 2691–2702. doi:10.1016/j.clinph.2006.08.011.

Nambu, A. (2011). Somatotopic Organization of the Primate Basal Ganglia. *Front Neuroanat* 5, 1–9. doi:10.3389/fnana.2011.00026.

Novak, P., Daniluk, S., Ellias, S. A., and Nazzaro, J. M. (2007). Detection of the subthalamic nucleus in microelectrographic recordings in Parkinson disease using the high-frequency (> 500 Hz) neuronal background. *J Neurosurg* 106, 175–179. doi:10.3171/jns.2007.106.1.175.

Novak, P., Przybyszewski, A. W., Barborica, A., Ravin, P., Margolin, L., and Pilitsis, J. G. (2011). Localization of the subthalamic nucleus in Parkinson disease using multiunit activity. *J Neurol Sci* 310, 44–49. doi:10.1016/j.jns.2011.07.027.

Obeso, J. A., Rodríguez-Oroz, M. C., Benitez-Temino, B., Blesa, F. J., Guridi, J., Marin, C., and Rodriguez, M. (2008). Functional organization of the

basal ganglia: Therapeutic implications for Parkinson's disease. *Mov Disord* 23, S548–S559. doi:10.1002/mds.22062.

Odekerken, V. J. J., van Laar, T., Staal, M. J., Mosch, A., Hoffmann, C. F. E., Nijssen, P. C. G., Beute, G. N., van Vugt, J. P. P., Lenders, M. W. P. M., Contarino, M. F., Mink, M. S. J., Bour, L. J., van den Munckhof, P., Schmand, B. A., de Haan, R. J., Schuurman, P. R., and de Bie, R. M. A. (2013). Subthalamic nucleus versus globus pallidus bilateral deep brain stimulation for advanced Parkinson's disease (NSTAPS study): A randomised controlled trial. *Lancet Neurol* 12, 37–44. doi:10.1016/S1474-4422(12)70264-8.

Okun, M. S., Green, J., Saben, R., Gross, R., Foote, K. D., and Vitek, J. L. (2003). Mood changes with deep brain stimulation of STN and GPi: results of a pilot study. *J Neurol Neurosurg Psychiatry* 74, 1584–6. doi:10.1136/jnnp.74.11.1584.

Okun, M. S., Tagliati, M., Pourfar, M., Fernandez, H. H., Rodriguez, R. L., Alterman, R. L., and Foote, K. D. (2005). Management of Referred Deep Brain Stimulation Failures. *Arch Neurol* 62, 1250. doi:10.1001/archneur.62.8.noc40425.

Osorio, I., Frei, M. G., Manly, B. F. J., Sunderam, S., Bhavaraju, N. C., and Wilkinson, S. B. (2001). An Introduction to Contingent (Closed-Loop) Brain Electrical Stimulation for Seizure Blockage, to Ultra-short-term Clinical Trials, and to Multidimensional Statistical Analysis of Therapeutic Efficacy. *J Clin Neurophysiol* 18, 533–544. doi:10.1097/00004691-

200111000-00003.

Oswal, A., Beudel, M., Zrinzo, L., Limousin, P., Hariz, M., Foltynie, T., Litvak, V., and Brown, P. (2016). Deep brain stimulation modulates synchrony within spatially and spectrally distinct resting state networks in Parkinson's disease. *Brain* 139, 1482–1496. doi:10.1093/brain/aww048.

Oswal, A., Brown, P., and Litvak, V. (2013). Synchronized neural oscillations and the pathophysiology of Parkinson's disease. *Curr Opin Neurol* 26, 662–670. doi:10.1097/WCO.0000000000000034.

Özkurt, T. E., Butz, M., Homburger, M., Elben, S., Vesper, J., Wojtecki, L., and Schnitzler, A. (2011). High frequency oscillations in the subthalamic nucleus: A neurophysiological marker of the motor state in Parkinson's disease. *Exp Neurol* 229, 324–331. doi:10.1016/j.expneurol.2011.02.015.

Ozturk, M., Abosch, A., Francis, D., Wu, J., Jimenez-Shahed, J., and Ince, N. F. (2019). Distinct subthalamic coupling in the ON state describes motor performance in Parkinson's disease. *Mov Disord*. doi:10.1002/mds.27800.

Ozturk, M., Kaku, H., Jimenez-Shahed, J., Viswanathan, A., Sheth, S. A., Kumar, S., and Ince, N. F. (2020a). Subthalamic Single Cell and Oscillatory Neural Dynamics of a Dyskinetic Medicated Patient With Parkinson's Disease. *Front Neurosci* 14, 1–8. doi:10.3389/fnins.2020.00391.

Ozturk, M., Telkes, I., Viswanathan, A., Jimenez-shahed, J., Tarakad, A., Kumar, S., Sheth, S. A., and Ince, N. F. (2020b). Randomized, double-blind assessment of LFP versus SUA guidance in STN-DBS lead

implantation : A Pilot Study. *Front Neurosci* [Accepted]. doi:10.3389/fnins.2020.00611.

Parastarfeizabadi, M., and Kouzani, A. Z. (2017). Advances in closed-loop deep brain stimulation devices. *J Neuroeng Rehabil* 14, 79. doi:10.1186/s12984-017-0295-1.

Parker, J. L., Obradovic, M., Hesam Shariati, N., Gorman, R. B., Karantonis, D. M., Single, P. S., Laird-Wah, J., Bickerstaff, M., and Cousins, M. J. (2020). Evoked Compound Action Potentials Reveal Spinal Cord Dorsal Column Neuroanatomy. *Neuromodulation Technol Neural Interface* 23, 82–95. doi:10.1111/ner.12968.

Parkinson's Foundation, Understanding Parkinson's, Statistics (2020). [Accessed April 1, 2020]. Available at: https://www.parkinson.org/Understanding-Parkinsons/Statistics.

Parkinson, J. (2002). An Essay on the Shaking Palsy. *J Neuropsychiatry Clin Neurosci* 14, 223–236. doi:10.1176/jnp.14.2.223.

Patel, N. K., Khan, S., and Gill, S. S. (2008). Comparison of Atlas- and Magnetic-Resonance-Imaging-Based Stereotactic Targeting of the Subthalamic Nucleus in the Surgical Treatment of Parkinson’s Disease. *Stereotact Funct Neurosurg* 86, 153–161. doi:10.1159/000120427.

Penny, W. D., Duzel, E., Miller, K. J., and Ojemann, J. G. (2008). Testing for nested oscillation. *J Neurosci Methods* 174, 50–61. doi:10.1016/j.jneumeth.2008.06.035.

Pettersen, K. H., Lindén, H., Dale, A. M., and Einevoll, G. T. (2012). "Extracellular spikes and CSD," in *Handbook of Neural Activity Measurement*, eds. R. Brette and A. Destexhe (Cambridge: Cambridge University Press), 92–135. doi:10.1017/CBO9780511979958.004.

Pinzon-Morales, R. D., Orozco-Gutierrez, A. A., and Castellanos-Dominguez, G. (2011). Novel signal-dependent filter bank method for identification of multiple basal ganglia nuclei in Parkinsonian patients. *J Neural Eng* 8, 036026. doi:10.1088/1741-2560/8/3/036026.

Plonsey, R., and Barr, R. C. (2007). *Bioelectricity: a quantitative approach*. Springer Science & Business Media.

Priori, A., Ardolino, G., Marceglia, S., Mrakic-Sposta, S., Locatelli, M., Tamma, F., Rossi, L., and Foffani, G. (2006). Low-frequency subthalamic oscillations increase after deep brain stimulation in Parkinson's disease. *Brain Res Bull* 71, 149–154. doi:10.1016/j.brainresbull.2006.08.015.

Priori, A., Foffani, G., Pesenti, A., Bianchi, A., Chiesa, V., Baselli, G., Caputo, E., Tamma, F., Rampini, P., Egidi, M., Locatelli, M., Barbieri, S., and Scarlato, G. (2002). Movement-related modulation of neural activity in human basal ganglia and its L-DOPA dependency: Recordings from deep brain stimulation electrodes in patients with Parkinson's disease. *Neurol Sci* 23, 101–102. doi:10.1007/s100720200089.

Priori, A., Foffani, G., Pesenti, A., Tamma, F., Bianchi, A. M., Pellegrini, M., Locatelli, M., Moxon, K. A., and Villani, R. M. (2004). Rhythm-specific pharmacological modulation of subthalamic activity in Parkinson's

disease. *Exp Neurol* 189, 369–379. doi:10.1016/j.expneurol.2004.06.001.

Priori, A., Foffani, G., Rossi, L., and Marceglia, S. (2013). Adaptive deep brain stimulation (aDBS) controlled by local field potential oscillations. *Exp Neurol* 245, 77–86. doi:10.1016/j.expneurol.2012.09.013.

Przybyszewski, A. W., Ravin, P., Pilitsis, J. G., Szymanski, A., Barborica, A., and Novak, P. (2016). Multi-parametric analysis assists in STN localization in Parkinson's patients. *J Neurol Sci* 366, 37–43. doi:10.1016/j.jns.2016.04.043.

R.D., H. (1990). Estimation of surviving spiral ganglion cells in the deaf rat using the electrically evoked auditory brainstem response. *Hear Res* 49, 155–168. Available at: http://www.embase.com/search/results?subaction=viewrecord&from=export&id=L20370259%5Cnhttp://sfx.library.uu.nl/utrecht?sid=EMBASE&issn=03785955&id=doi:&atitle=Estimation+of+surviving+spiral+ganglion+cells+in+the+deaf+rat+using+the+electrically+evoked+audi.

Ray, N. J., Jenkinson, N., Wang, S., Holland, P., Brittain, J. S., Joint, C., Stein, J. F., and Aziz, T. (2008). Local field potential beta activity in the subthalamic nucleus of patients with Parkinson's disease is associated with improvements in bradykinesia after dopamine and deep brain stimulation. *Exp Neurol* 213, 108–113. doi:10.1016/j.expneurol.2008.05.008.

Reese, R., Leblois, A., Steigerwald, F., Pötter-Nerger, M., Herzog, J., Mehdorn, H. M., Deuschl, G., Meissner, W. G., and Volkmann, J. (2011).

Subthalamic deep brain stimulation increases pallidal firing rate and regularity. *Exp Neurol* 229, 517–521. doi:10.1016/j.expneurol.2011.01.020.

Richardson, R. M., Ostrem, J. L., and Starr, P. A. (2009). Surgical repositioning of misplaced subthalamic electrodes in Parkinson's disease: Location of effective and ineffective leads. *Stereotact Funct Neurosurg* 87, 297–303. doi:10.1159/000230692.

Rodriguez-Oroz, M. C., Jahanshahi, M., Krack, P., Litvan, I., Macias, R., Bezard, E., and Obeso, J. A. (2009). Initial clinical manifestations of Parkinson's disease: features and pathophysiological mechanisms. *Lancet Neurol* 8, 1128–1139. doi:10.1016/S1474-4422(09)70293-5.

Rodriguez-Oroz, M. C., López-Azcárate, J., Garcia-Garcia, D., Alegre, M., Toledo, J., Valencia, M., Guridi, J., Artieda, J., and Obeso, J. A. (2011). Involvement of the subthalamic nucleus in impulse control disorders associated with Parkinson's disease. *Brain* 134, 36–49. doi:10.1093/brain/awq301.

Rodriguez-Oroz, M. C., Rodriguez, M., Guridi, J., Mewes, K., Chockkman, V., Vitek, J., DeLong, M. R., and Obeso, J. A. (2001). The subthalamic nucleus in Parkinson's disease: somatotopic organization and physiological characteristics. *Brain* 124, 1777–90. doi:10.1093/brain/124.9.1777.

Rosa, M., Giannicola, G., Servello, D., Marceglia, S., Pacchetti, C., Porta, M., Sassi, M., Scelzo, E., Barbieri, S., and Priori, A. (2011). Subthalamic

Local Field Beta Oscillations during Ongoing Deep Brain Stimulation in Parkinson's Disease in Hyperacute and Chronic Phases. *Neurosignals* 19, 151–162. doi:10.1159/000328508.

Rosa, M., Marceglia, S., Servello, D., Foffani, G., Rossi, L., Sassi, M., Mrakic-Sposta, S., Zangaglia, R., Pacchetti, C., Porta, M., and Priori, A. (2010). Time dependent subthalamic local field potential changes after DBS surgery in Parkinson's disease. *Exp Neurol* 222, 184–190. doi:10.1016/j.expneurol.2009.12.013.

Rouse, A. G., Stanslaski, S. R., Cong, P., Jensen, R. M., Afshar, P., Ullestad, D., Gupta, R., Molnar, G. F., Moran, D. W., and Denison, T. J. (2011). A chronic generalized bi-directional brain–machine interface. *J Neural Eng* 8, 036018. doi:10.1088/1741-2560/8/3/036018.

Rubin, J. E., and Terman, D. (2004). High Frequency Stimulation of the Subthalamic Nucleus Eliminates Pathological Thalamic Rhythmicity in a Computational Model. *J Comput Neurosci* 16, 211–235. doi:10.1023/B:JCNS.0000025686.47117.67.

Rubinstein, J. T. (2004). An introduction to the biophysics of the electrically evoked compound action potential. *Int J Audiol* 43 Suppl 1, S3-9.

Saenger, V. M., Kahan, J., Foltynie, T., Friston, K., Aziz, T. Z., Green, A. L., van Hartevelt, T. J., Cabral, J., Stevner, A. B. A., Fernandes, H. M., Mancini, L., Thornton, J., Yousry, T., Limousin, P., Zrinzo, L., Hariz, M., Marques, P., … Deco, G. (2017). Uncovering the underlying mechanisms and whole-brain dynamics of deep brain stimulation for Parkinson's

disease. *Sci Rep* 7, 9882. doi:10.1038/s41598-017-10003-y.

Schiefer, T. K., Matsumoto, J. Y., and Lee, K. H. (2011). Moving Forward: Advances in the Treatment of Movement Disorders with Deep Brain Stimulation. *Front Integr Neurosci* 5, 1–16. doi:10.3389/fnint.2011.00069.

Schneider, S. A., and Deuschl, G. (2015). Medical and Surgical Treatment of Tremors. *Neurol Clin* 33, 57–75. doi:10.1016/j.ncl.2014.09.005.

Sharott, A., Gulberti, A., Zittel, S., Tudor Jones, A. A., Fickel, U., Munchau, A., Koppen, J. A., Gerloff, C., Westphal, M., Buhmann, C., Hamel, W., Engel, A. K., and Moll, C. K. E. (2014). Activity Parameters of Subthalamic Nucleus Neurons Selectively Predict Motor Symptom Severity in Parkinson's Disease. *J Neurosci* 34, 6273–6285. doi:10.1523/jneurosci.1803-13.2014.

Shreve, L. A., Velisar, A., Malekmohammadi, M., Koop, M. M., Trager, M., Quinn, E. J., Hill, B. C., Blumenfeld, Z., Kilbane, C., Mantovani, A., Henderson, J. M., and Bronte-Stewart, H. (2017). Subthalamic oscillations and phase amplitude coupling are greater in the more affected hemisphere in Parkinson's disease. *Clin Neurophysiol* 128, 128–137. doi:10.1016/j.clinph.2016.10.095.

Sinclair, N. C., McDermott, H. J., Bulluss, K. J., Fallon, J. B., Perera, T., Xu, S. S., Brown, P., and Thevathasan, W. (2018). Subthalamic nucleus deep brain stimulation evokes resonant neural activity. *Ann Neurol* 83, 1027–1031. doi:10.1002/ana.25234.

Sinclair, N. C., McDermott, H. J., Fallon, J. B., Perera, T., Brown, P., Bulluss,

K. J., and Thevathasan, W. (2019). Deep brain stimulation for Parkinson's disease modulates high-frequency evoked and spontaneous neural activity. *Neurobiol Dis* 130, 104522. doi:10.1016/j.nbd.2019.104522.

Soares, J., Kliem, M. A., Betarbet, R., Greenamyre, J. T., Yamamoto, B., and Wichmann, T. (2004). Role of External Pallidal Segment in Primate Parkinsonism: Comparison of the Effects of 1-Methyl-4-Phenyl-1,2,3,6-Tetrahydropyridine-Induced Parkinsonism and Lesions of the External Pallidal Segment. *J Neurosci* 24, 6417–6426. doi:10.1523/jneurosci.0836-04.2004.

Spildooren, J., Vercruysse, S., Desloovere, K., Vandenberghe, W., Kerckhofs, E., and Nieuwboer, A. (2010). Freezing of gait in Parkinson's disease: The impact of dual-tasking and turning. *Mov Disord* 25, 2563–2570. doi:10.1002/mds.23327.

Stanslaski, S., Afshar, P., Cong, P., Giftakis, J., Stypulkowski, P., Carlson, D., Linde, D., Ullestad, D., Avestruz, A.-T., and Denison, T. (2012). Design and Validation of a Fully Implantable, Chronic, Closed-Loop Neuromodulation Device With Concurrent Sensing and Stimulation. *IEEE Trans Neural Syst Rehabil Eng* 20, 410–421. doi:10.1109/TNSRE.2012.2183617.

Stanslaski, S., Cong, P., Carlson, D., Santa, W., Jensen, R., Molnar, G., Marks, W. J., Shafquat, A., and Denison, T. (2009). An implantable Bi-directional brain-machine interface system for chronic neuroprosthesis research. in *2009 Annual International Conference of the IEEE*

Engineering in Medicine and Biology Society (IEEE), 5494–5497. doi:10.1109/IEMBS.2009.5334562.

Starr, P. A., Theodosopoulos, P. V, and Turner, R. (2003). Surgery of the subthalamic nucleus: use of movement-related neuronal activity for surgical navigation. *Neurosurgery* 53, 1146–9; discussion 1149. doi:10.1227/01.neu.0000088803.79153.05.

Stefani, A., Fedele, E., Vitek, J., Pierantozzi, M., Galati, S., Marzetti, S., Peppe, A., Bassi, M. S., Bernardi, G., and Stanzione, P. (2011). The clinical efficacy of L-DOPA and STN-DBS share a common marker: Reduced GABA content in the motor thalamus. *Cell Death Dis* 2, 1–9. doi:10.1038/cddis.2011.35.

Sterio, D., Zonenshayn, M., Mogilner, A. Y., Rezai, A. R., Kiprovski, K., Kelly, P. J., and Beric, A. (2002). Neurophysiological Refinement of Subthalamic Nucleus Targeting. *Neurosurgery* 50, 58–69. doi:10.1097/00006123-200201000-00012.

Strauss, I., Kalia, S. K., and Lozano, A. M. (2014). Where are we with surgical therapies for Parkinson's disease? *Parkinsonism Relat Disord* 20, S187–S191. doi:10.1016/S1353-8020(13)70044-0.

Stypulkowski, P. H., Giftakis, J. E., and Billstrom, T. M. (2011). Development of a Large Animal Model for Investigation of Deep Brain Stimulation for Epilepsy. *Stereotact Funct Neurosurg* 89, 111–122. doi:10.1159/000323343.

Sun, F. T., and Morrell, M. J. (2014). Closed-loop Neurostimulation: The

Clinical Experience. *Neurotherapeutics* 11, 553–563. doi:10.1007/s13311-014-0280-3.

Swann, N. C., de Hemptinne, C., Miocinovic, S., Qasim, S., Wang, S. S., Ziman, N., Ostrem, J. L., San Luciano, M., Galifianakis, N. B., and Starr, P. A. (2016). Gamma Oscillations in the Hyperkinetic State Detected with Chronic Human Brain Recordings in Parkinson's Disease. *J Neurosci* 36, 6445–6458. doi:10.1523/JNEUROSCI.1128-16.2016.

Tavares, A. L. T., Jefferis, G. S. X. E., Koop, M., Hill, B. C., Hastie, T., Heit, G., and Bronte-Stewart, H. (2005). Quantitative measurements of alternating finger tapping in Parkinson's disease correlate with UPDRS motor disability and reveal the improvement in fine motor control from medication and deep brain stimulation. *Mov Disord* 20, 1286–1298. doi:10.1002/mds.20556.

Telkes, I., Jimenez-Shahed, J., Viswanathan, A., Abosch, A., and Ince, N. F. (2016). Prediction of STN-DBS electrode implantation track in Parkinson's disease by using local field potentials. *Front Neurosci* 10, 1–16. doi:10.3389/fnins.2016.00198.

Telkes, I., Viswanathan, A., Jimenez-Shahed, J., Abosch, A., Ozturk, M., Gupte, A., Jankovic, J., and Ince, N. F. (2018). Local field potentials of subthalamic nucleus contain electrophysiological footprints of motor subtypes of Parkinson's disease. *Proc Natl Acad Sci* 115, 201810589. doi:10.1073/pnas.1810589115.

Temel, Y., Blokland, A., Steinbusch, H. W. M., and Visser-Vandewalle, V.

(2005). The functional role of the subthalamic nucleus in cognitive and limbic circuits. *Prog Neurobiol* 76, 393–413. doi:10.1016/j.pneurobio.2005.09.005.

Terman, D., Rubin, J. E., Yew, A. C., and Wilson, C. J. (2002). Activity Patterns in a Model for the Subthalamopallidal Network of the Basal Ganglia. *J Neurosci* 22, 2963–2976. doi:10.1523/JNEUROSCI.22-07-02963.2002.

Thenganatt, M. A., and Jankovic, J. (2014). Parkinson disease subtypes. *JAMA Neurol* 71, 499–504. doi:10.1001/jamaneurol.2013.6233.

Theodosopoulos, P. V., Marks, W. J., Christine, C., and Starr, P. A. (2003). Locations of movement-related cells in the human subthalamic nucleus in Parkinson's disease. *Mov Disord* 18, 791–798. doi:10.1002/mds.10446.

Thompson, J. A., Lanctin, D., Ince, N. F., and Abosch, A. (2014). Clinical implications of local field potentials for understanding and treating movement disorders. *Stereotact Funct Neurosurg* 92, 251–263. doi:10.1159/000364913.

Thompson, J. A., Oukal, S., Bergman, H., Ojemann, S., Hebb, A. O., Hanrahan, S., Israel, Z., and Abosch, A. (2018a). Semi-automated application for estimating subthalamic nucleus boundaries and optimal target selection for deep brain stimulation implantation surgery. *J Neurosurg* 130, 1–10. doi:10.3171/2017.12.JNS171964.

Thompson, J. A., Tekriwal, A., Felsen, G., Ozturk, M., Telkes, I., Wu, J., Ince, N. F., and Abosch, A. (2018b). Sleep patterns in Parkinson's disease:

direct recordings from the subthalamic nucleus. *J Neurol Neurosurg Psychiatry* 89, 95–104. doi:10.1136/jnnp-2017-316115.

Uhlhaas, P. J., and Singer, W. (2006). Neural Synchrony in Brain Disorders: Relevance for Cognitive Dysfunctions and Pathophysiology. *Neuron* 52, 155–168. doi:10.1016/j.neuron.2006.09.020.

Urrestarazu, E., Iriarte, J., Alegre, M., Clavero, P., Rodríguez-Oroz, M. C., Guridi, J., Obeso, J. A., and Artieda, J. (2009). Beta activity in the subthalamic nucleus during sleep in patients with Parkinson's disease. *Mov Disord* 24, 254–260. doi:10.1002/mds.22351.

Valsky, D., Marmor-Levin, O., Deffains, M., Eitan, R., Blackwell, K. T., Bergman, H., and Israel, Z. (2017). Stop! border ahead: Automatic detection of subthalamic exit during deep brain stimulation surgery. *Mov Disord* 32, 70–79. doi:10.1002/mds.26806.

van Wijk, B. C. M., Beudel, M., Jha, A., Oswal, A., Foltynie, T., Hariz, M. I., Limousin, P., Zrinzo, L., Aziz, T. Z., Green, A. L., Brown, P., and Litvak, V. (2016). Subthalamic nucleus phase-amplitude coupling correlates with motor impairment in Parkinson's disease. *Clin Neurophysiol* 127, 2010–2019. doi:10.1016/j.clinph.2016.01.015.

van Wijk, B. C. M., Pogosyan, A., Hariz, M. I., Akram, H., Foltynie, T., Limousin, P., Horn, A., Ewert, S., Brown, P., and Litvak, V. (2017). Localization of beta and high-frequency oscillations within the subthalamic nucleus region. *NeuroImage Clin* 16, 175–183. doi:10.1016/j.nicl.2017.07.018.

Vitek, J. L., Zhang, J., Hashimoto, T., Russo, G. S., and Baker, K. B. (2012). External pallidal stimulation improves parkinsonian motor signs and modulates neuronal activity throughout the basal ganglia thalamic network. *Exp Neurol* 233, 581–586. doi:10.1016/j.expneurol.2011.09.031.

Walter, B. L., and Vitek, J. L. (2004). Surgical treatment for Parkinson's disease. *Lancet Neurol* 3, 719–728. doi:10.1016/S1474-4422(04)00934-2.

Wang, J., Hirschmann, J., Elben, S., Hartmann, C. J., Vesper, J., Wojtecki, L., and Schnitzler, A. (2014). High-frequency oscillations in Parkinson's disease: Spatial distribution and clinical relevance. *Mov Disord* 29, 1265–1272. doi:10.1002/mds.25962.

Wang, J., Ponce, F. A., Tao, J., Yu, H., Liu, J., Wang, Y., Luan, G., and Ou, S. (2019). Comparison of Awake and Asleep Deep Brain Stimulation for Parkinson's Disease: A Detailed Analysis Through Literature Review. *Neuromodulation Technol Neural Interface* 2019, ner.13061. doi:10.1111/ner.13061.

Weinberger, M., Mahant, N., Hutchison, W. D., Lozano, A. M., Moro, E., Hodaie, M., Lang, A. E., and Dostrovsky, J. O. (2006). Beta Oscillatory Activity in the Subthalamic Nucleus and Its Relation to Dopaminergic Response in Parkinson's Disease. *J Neurophysiol* 96, 3248–3256. doi:10.1152/jn.00697.2006.

Welter, M.-L., Houeto, J.-L., Bonnet, A.-M., Bejjani, P.-B., Mesnage, V., Dormont, D., Navarro, S., Cornu, P., Agid, Y., and Pidoux, B. (2004). Effects of High-Frequency Stimulation on Subthalamic Neuronal Activity in

Parkinsonian Patients. *Arch Neurol* 61, 89. doi:10.1001/archneur.61.1.89.

Westen, A. A., Dekker, D. M. T., Briaire, J. J., and Frijns, J. H. M. (2011). Stimulus level effects on neural excitation and eCAP amplitude. *Hear Res* 280, 166–176. doi:10.1016/j.heares.2011.05.014.

Wichmann, T., Bergman, H., Starr, P. A., DeLong, M. R., Watts, R. L., and Subramanian, T. (1999). Comparison of MPTP-induced changes in spontaneous neuronal discharge in the internal pallidal segment and in the substantia nigra pars reticulata in primates. *Exp Brain Res* 125, 397–409. doi:10.1007/s002210050696.

Wichmann, T., and Delong, M. R. (1996). Functional and pathophysiological models of the basal ganglia. *Curr Opin Neurobiol* 6, 751–758. doi:10.1016/S0959-4388(96)80024-9.

Wichmann, T., and DeLong, M. R. (2006). “Basal ganglia discharge abnormalities in Parkinson’s disease,” in *Parkinson’s Disease and Related Disorders* (Vienna: Springer Vienna), 21–25. doi:10.1007/978-3-211-45295-0_5.

Williams, D., Kühn, A., Kupsch, A., Tijssen, M., van Bruggen, G., Speelman, H., Hotton, G., Loukas, C., and Brown, P. (2005). The relationship between oscillatory activity and motor reaction time in the parkinsonian subthalamic nucleus. *Eur J Neurosci* 21, 249–258. doi:10.1111/j.1460-9568.2004.03817.x.

Williams, J. C., Rennaker, R. L., and Kipke, D. R. (1999). Long-term neural recording characteristics of wire microelectrode arrays implanted in

cerebral cortex. *Brain Res Protoc* 4, 303–313. doi:10.1016/S1385-299X(99)00034-3.

Williams, N. R., Foote, K. D., and Okun, M. S. (2014). STN vs. GPi Deep Brain Stimulation: Translating the Rematch into Clinical Practice. *Mov Disord Clin Pract* 1, 24–35. doi:10.1002/mdc3.12004.

Wingeier, B., Tcheng, T., Koop, M. M., Hill, B. C., Heit, G., and Bronte-Stewart, H. (2006). Intra-operative STN DBS attenuates the prominent beta rhythm in the STN in Parkinson's disease. *Exp Neurol* 197, 244–251. doi:10.1016/j.expneurol.2005.09.016.

Wojtecki, L., Nickel, J., Timmermann, L., Maarouf, M., Südmeyer, M., Schneider, F., Seitz, R. J., Voges, J., Sturm, V., and Schnitzler, A. (2007). Pathological crying induced by deep brain stimulation. *Mov Disord* 22, 1314–1316. doi:10.1002/mds.21266.

Wolfinger, R., and Chang, M. (1995). Comparing the SAS ® GLM and MIXED Procedures for Repeated Measures. *Sas* 1995, 1–11.

Wong, J. K., Cauraugh, J. H., Ho, K. W. D., Broderick, M., Ramirez-Zamora, A., Almeida, L., Wagle Shukla, A., Wilson, C. A., de Bie, R. M., Weaver, F. M., Kang, N., and Okun, M. S. (2019). STN vs. GPi deep brain stimulation for tremor suppression in Parkinson disease: A systematic review and meta-analysis. *Parkinsonism Relat Disord* 58, 56–62. doi:10.1016/j.parkreldis.2018.08.017.

Wong, S., Baltuch, G. H., Jaggi, J. L., and Danish, S. F. (2009). Functional localization and visualization of the subthalamic nucleus from

microelectrode recordings acquired during DBS surgery with unsupervised machine learning. *J Neural Eng* 6, 026006. doi:10.1088/1741-2560/6/2/026006.

Xu, W., Russo, G. S., Hashimoto, T., Zhang, J., and Vitek, J. L. (2008). Subthalamic Nucleus Stimulation Modulates Thalamic Neuronal Activity. *J Neurosci* 28, 11916–11924. doi:10.1523/JNEUROSCI.2027-08.2008.

Yanagisawa, T., Yamashita, O., Hirata, M., Kishima, H., Saitoh, Y., Goto, T., Yoshimine, T., and Kamitani, Y. (2012). Regulation of Motor Representation by Phase-Amplitude Coupling in the Sensorimotor Cortex. *J Neurosci* 32, 15467–15475. doi:10.1523/JNEUROSCI.2929-12.2012.

Yang, A. I., Vanegas, N., Lungu, C., and Zaghloul, K. A. (2014). Beta-Coupled High-Frequency Activity and Beta-Locked Neuronal Spiking in the Subthalamic Nucleus of Parkinson's Disease. *J Neurosci* 34, 12816–12827. doi:10.1523/JNEUROSCI.1895-14.2014.

Yoshida, F., Martinez-Torres, I., Pogosyan, A., Holl, E., Petersen, E., Chen, C. C., Foltynie, T., Limousin, P., Zrinzo, L. U., Hariz, M. I., and Brown, P. (2010). Value of subthalamic nucleus local field potentials recordings in predicting stimulation parameters for deep brain stimulation in Parkinson's disease. *J Neurol Neurosurg Psychiatry* 81, 885–889. doi:10.1136/jnnp.2009.190918.

Zaidel, A., Spivak, A., Grieb, B., Bergman, H., and Israel, Z. (2010). Subthalamic span of β oscillations predicts deep brain stimulation efficacy for patients with Parkinson's disease. *Brain* 133, 2007–2021.

doi:10.1093/brain/awq144.

Zaidel, A., Spivak, A., Shpigelman, L., Bergman, H., and Israel, Z. (2009). Delimiting subterritories of the human subthalamic nucleus by means of microelectrode recordings and a Hidden Markov Model. *Mov Disord* 24, 1785–1793. doi:10.1002/mds.22674.

Zhang, S., Zhou, P., Jiang, S., Wang, W., and Li, P. (2016). Interleaving subthalamic nucleus deep brain stimulation to avoid side effects while achieving satisfactory motor benefits in Parkinson disease: A report of 12 cases. *Med (United States)* 95, e5575. doi:10.1097/MD.0000000000005575.

Zhou, A., Johnson, B. C., and Muller, R. (2018). Toward true closed-loop neuromodulation: artifact-free recording during stimulation. *Curr Opin Neurobiol* 50, 119–127. doi:10.1016/j.conb.2018.01.012.

Zhuang, Q. X., Li, G. Y., Li, B., Zhang, C. Z., Zhang, X. Y., Xi, K., Li, H. Z., Wang, J. J., and Zhu, J. N. (2018). Regularizing firing patterns of rat subthalamic neurons ameliorates parkinsonian motor deficits. *J Clin Invest* 128, 5413–5427. doi:10.1172/JCI99986.

Zonenshayn, M., Rezai, A. R., Mogilner, A. Y., Beric, A., Sterio, D., and Kelly, P. J. (2000). Comparison of anatomic and neurophysiological methods for subthalamic nucleus targeting. *Neurosurgery* 47, 282–294. doi:10.1097/00006123-200008000-00005.